Radboud University Nijmegen


Faculty of Science

# Shadow Tolerance Optimisation of Thin-Film Solar Modules

Internship Graduation Project at TNO Solliance

Thesis MSc Mathematics

*Author:*
Nikki Jaspers

*Supervisor Solliance:*
Baris Dai, MSc

*Supervisor University:*
dr. Wieb Bosma



March 11, 2020

# Preface

For the last six and a half months I've been doing an internship at TNO Solliance in Eindhoven. This internship is my graduation project for the Master Mathematics at the Radboud University. During this project I researched the effect of partial shading on thin-film solar modules. This thesis lying before you is the result of that research. The target audience for this thesis is colleague Mathematics students, which is why in the first chapter basic principles from electrical engineering and photovolaic technology are explained.

A large amount of my time went to developing a model in MATLAB that can simulate the electrical behaviour of a solar module. The rest of my time went to literature research, verifying the MATLAB model, and generating actual results with the model. The research question - Which electrical interconnection between solar cells can best be used to get the most shadow tolerant design? - was mostly answered, though the answer is complicated and not straight-forward. As a nice side result in my opinion, the developed MATLAB model could be used in future projects to get more insight on the electrical behaviour of various types of solar modules.

With my theoretical mathematics background, it was very interesting to have a change of scenery and work in a company. I found it motivating that I was working in a field that impacts real-life solar energy applications, especially considering current climate change issues.

I would like to thank both my supervisors, Baris Dai (Solliance) and Wieb Bosma (Radboud University), for their guidance and support during this internship graduation project. I also wish to thank dr. Hans Kraaijevanger (Radboud University) for helping me out with the numerical methods going into my model, and Henk Steijvers (Solliance) for helping me with the model verification experiment. Furthermore, I would like to give special thanks to my parents, siblings and friends who were always there for me when I needed them, and supported me greatly throughout my studies.

Finally thanks to you, the reader, for showing an interest in my work and I hope you enjoy reading it.

Nikki Jaspers

Nijmegen, February 25, 2020

# Abstract

Photovoltaic (PV) modules consist of electrically interconnected solar cells. PV modules usually have a series-parallel (SP) connection topology. It is known that under partial shading conditions mismatching between the cells occur, which can drastically reduce the power output of a PV module. Research has shown that for traditional silicon PV modules, other configurations, like the total-cross-tied (TCT) configuration, can be less susceptible to power losses under partial shading. Since thin-film modules have the potential to be integrated in various building elements and multi-functional surfaces, non-uniform irradiance is to be expected more often. This makes researching shadow tolerant electrical designs for thin-film solar arrays worthwile. In this research, a generic MATLAB code was developed to simulate the electrical behaviour of a PV module for multiple interconnection topologies and for any type of cell, type of bypass diode, module size and shading pattern. A bypass diode is an electrical component included in PV modules, that prevents the solar cells from being damaged by mismatching effects. The goal of this study is to discover which out of the two configurations SP and TCT, constitutes the most shadow tolerant thin-film PV module.

It was shown that the designed model has a sufficient degree of precision, by means of a verification experiment in which fifteen different shading patterns were tested for four CIGS modules. Thereafter, the MATLAB model was used to calculate current-voltage curves and maximum power points of TCT and SP modules for various modules sizes and shading patterns. The properties of CIGS cells were used for modelling the solar cell components of the modules, and the bypass diodes were modelled as Schottky diodes. Analysis of the resulting data indicates that neither of the configurations generally has the largest maximum power output. However, it was found in the simulated scenarios that if TCT is the best configuration, the power gain compared to SP can be very large: up to about 200%. Whereas, if SP was the best configuration in a certain shading scenario, then the power loss of TCT compared to SP is limited to 20%. On this basis, it is recommended to use a TCT configuration if no additional information about expected shading patterns is available. To determine which configuration is optimal for specific situations, further development would be necessary to combine the designed model with a tool that predicts shading patterns over time.

# Contents

**Preface** i

**Abstract** ii

**Introduction** 2

**1 Background** 4
- 1.1 Photovoltaic technology . . . 4
- 1.2 Electrical circuits . . . 4
- 1.3 Circuit components . . . 5
  - 1.3.1 Diode . . . 5
  - 1.3.2 Current source . . . 8

**2 Photovoltaic cell** 9
- 2.1 Single diode model . . . 9
- 2.2 Lambert $W$ function . . . 13
- 2.3 Maximum power point . . . 15
- 2.4 Determining model parameters . . . 17
  - 2.4.1 Cell temperature . . . 17
  - 2.4.2 Short circuit current . . . 18
  - 2.4.3 Open circuit voltage . . . 18
  - 2.4.4 Reverse saturation current . . . 19
  - 2.4.5 Photogenerated current . . . 19
  - 2.4.6 Shunt resistance, series resistance and the ideality factor . . . 20
- 2.5 Effect of temperature and solar irradiance . . . 22

**3 Photovoltaic module** 25
- 3.1 Homogeneous module . . . 25
  - 3.1.1 Parallel cells . . . 25
  - 3.1.2 Cells in series . . . 26
  - 3.1.3 Series-parallel and total-cross-tied configuration . . . 26
- 3.2 Partial shading and mismatching . . . 27
- 3.3 Bypass diodes . . . 29
- 3.4 Special shading patterns . . . 32
  - 3.4.1 Semi-homogeneous shade . . . 32
  - 3.4.2 Shading equivalencies . . . 34
- 3.5 System of equations . . . 34

**4 MATLAB model** 38
- 4.1 Structure of the model . . . 38
- 4.2 Solving the system of equations . . . 39
  - 4.2.1 Jacobian matrix of the system of equations . . . 40
  - 4.2.2 Euler's method . . . 41
- 4.3 Computing time . . . 42

**5 Verification of the model** 43
- 5.1 The PV modules and shading patterns . . . 43
- 5.2 Solar simulator and irradiance . . . 44
- 5.3 Cell temperature and efficiency . . . 46
- 5.4 Cell ideality factor and resistances . . . 48
- 5.5 Determining bypass diode parameters . . . 49

5.6 Results . . . 49
5.7 Electroluminescence measurements . . . 52

**6 Findings** **54**
6.1 Effect of bypass diodes . . . 54
6.1.1 Modules with and without bypass diodes . . . 54
6.1.2 Individual cell operating points . . . 55
6.1.3 Other bypass diodes . . . 57
6.2 Random patterns . . . 58
6.3 Impact of module dimensions . . . 61
6.4 More patterns . . . 64

**Conclusion** **66**

**Discussion and outlook** **66**

**References** **67**

**Appendices** **68**
I Best Research-Cell Efficiencies Chart . . . 69
II Datasheet MiaSolé CIGS Solar Cell . . . 70
III Shading patterns 12x4 . . . 72
IV Shading patterns 24x4 . . . 74
V Results verification experiment . . . 76
VI Effect of bypass diodes: results . . . 81
VII More patterns . . . 83

# Introduction

With increasing awareness about carbon emissions and global warming, research related to renewable energy becomes more and more important. Solar energy is one of those renewable energy resources, and in particular thin-film solar techniques show promising prospects for the future. At Solliance Solar Research, the goal is to further develop production processes and systems for thin-film solar technologies until they can be scaled up to an economically viable level. Thin-film solar cells that are worked on at Solliance include perovskite cells and CIGS cells.

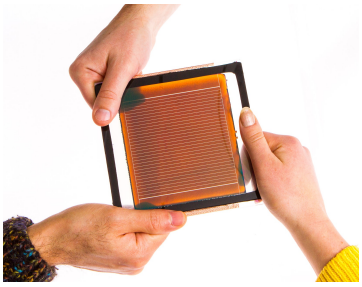

Figure 1: Semi-transparent perovskite thin-film cell[1]

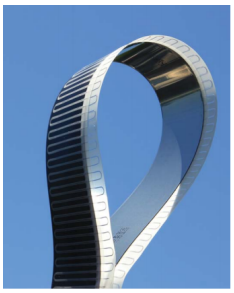

Figure 2: Flexible CIGS thin-film cell (Appendix II)

Solliance Solar Research was founded in 2010 and is a joint venture between the Dutch TNO, the Belgian imec and ECN (the Energy research Centre of the Netherlands, that became a part of TNO in 2018). Together with industrial and academic partners, Solliance Solar Research plays a leading role in the worldwide research and development of thin-film solar technology. Solliance has a strong focus on developing technologies for adaptable, flexible and semi-transparant thin-film solar applications. The vision for the future is massive application of thin-film solar technologies in infrastructure, building materials and transport to create multi-functional use of available area.[2]

However, integration of solar thin-film in a wide variety of applications can pose some extra challenges. In practice, 3D applications of thin-film solar modules can have non-uniform solar irradiance due to self-shadowing, or varying surface angles with respect to the sun. In addition, integration of solar modules to create multi-functional surfaces will be mostly called for in urban areas. But then partial shadowing caused by surrounding structures is to be expected. These situations decrease the power output of solar modules considerably.

Solar cell performance depends of course on the solar irradiance, but also on other ambient conditions like the temperature. Solar modules are formed by connecting solar cells in series and/or parallel. Due to fluctuations in solar irradiance and temperature, the maximum power output of a solar module varies. The output voltage, and with that the output current and power, of a solar module is a function of the load. By controlling the output voltage at the load, it is possible to have the solar module operate at its maximum power output. When the ambient conditions on the cells are homogeneous this maximum power point is well predictable. However, the behaviour of a solar module under non-uniform irradiance, i.e., partial shade, changes drastically. In addition to a global maximum power point there may occur multiple local maximum power points under partial shading conditions, which is a problem for maximum power point trackers. On top of that, calculating the module's electrical behaviour becomes much more complicated as the module no longer behaves like a scaled up version of a single solar cell. The module turns into a system of complicated interactions between

non-linear circuit components that all behave differently. Since the cells are affecting each other, some cells may be forced to operate at a voltage level exceeding a certain breakdown voltage. This can damage the solar module permanently, and therefore bypass diodes are incorporated to protect the cells. Bypass diodes add yet another challenge to predict the solar module's behaviour, as they are one more non-linear circuit component that complicate interactions in the module. Furthermore, the type and number of bypass diodes also affects the solar module behaviour.

In case of non-uniform conditions, the choice of interconnection topology for the solar module has an impact on the maximum power output. There are multiple interconnection topologies, like total-cross-tied (TCT), series-parallel (SP), bridge-linked (BL), and honey-comb (HC). These configurations have been tested under partial shading conditions for crystalline silicon modules[3], but no such research was found for thin-film solar modules. At Solliance, a number of measurements was done to compare TCT and SP configurations under partial shading and it was observed that the TCT configuration can have promising results for thin-film CIGS solar cells. That was the motivation for setting up this research project.

The objective of this research is to develop a model that predicts solar module behaviour for various partial shading scenarios, and moreover, to compare the interconnection topologies SP and TCT for thin-film solar modules to find the most shadow tolerant design.

# 1 Background

Before we can get to the actual research question, let's start with an underlying theoretical framework about photovoltaics and electrical circuits. In this chapter we present basic concepts and principles of physics that can be found in educational physics books like Jewett and Serway [4] (chapter 4).

## 1.1 Photovoltaic technology

Photovoltaic technology is a technology that converts photonic energy into electricity using solar cells. An example of a photonic energy source is of course the sun. Over the last decades photovoltaic technology has gained in popularity, with many commercially available photovoltaic (PV) applications today. The solar cell, also called PV cell throughout this report, contains a material that absorbs sunlight. In this material the photons excite electrons to a higher energy state. These electrons then move into an external circuit, where the electrons' energy will be used up by a load and the electrons return to the solar cell. The material in solar cells that is used for this energy conversion is generally a p-n junction semiconductor. [5]

There are a number of solar cell types, of which the most widely used and oldest one is crystalline silicon. In current research, these cells have conversion efficiencies between 21.2% and 27.6%. [6] A newer type of solar cells, are the thin-film cells. These are, as the name suggests, thinner cells, sometimes flexible and (semi-)transparent, which renders them suitable for a wide variety of applications. Another advantage of thin-film cells is that they have a lower cost and need less material compared with silicon based solar cells. [7] Among the thin-film solar cells there are different types based on materials that are used in the cell: a-Si thin-film solar cells, c-Si solar cells, CdTe solar cells, CIS & CIGS solar cells and perovskite solar cells. [7] The efficiency of CIGS thin-film solar cells can be up to 23.4%, and perovskite cells currently have research-cell efficiencies up to 25.2% (see Appendix I). [6] So these thin-film technologies can compete with the silicon PV cells. A disadvantage of perovskite cells is the short lifespan, but perovskite cells are rapidly developing and Solliance, and partners, recently managed to make a more stable version of these cells. [1]

Another upcoming development is multi-junction solar cells. These are stacks of individual solar cells, which absorb different wavelengths of incoming sunlight due to the different materials in each layer. The layers together create a more efficient cell than cells with a single semiconductor layer. In theory the efficiency of a multi-junction with perovskite cells can even become 73% [8]. The production time and costs are however larger than for single-junction cells. [9]

## 1.2 Electrical circuits

Electric current $I$ is the net flow of electric charge. The moving charged particles (electrons and ions) that constitute this flow are called the charge carriers. The convention is that the direction of the current is the same direction as the flow of positive charge carriers. So in a circuit the direction of the current is from the plus terminal of the power source outwards. Voltage is the difference in electrical potential between two points. These two points are indicated by a plus and minus sign.

An electrical circuit consists of connected components. To calculate the voltage and current in parts of the circuit, Kirchoff's circuit laws are used. The first law, Kirchoff's current law, states that sum of the currents in a circuit junction equals 0, where incoming currents are positive and outgoing currents are negative. Kirchhoff's second law, the voltage law, states that in all closed loops of a circuit the directed sum of the voltages equals zero.

A third law that will be relevant is Ohm's law: $V = IR$. This law states that the current $I$ flowing through a conductor between two points is directly proportional to the potential difference $V$ across those points. The proportionality constant is $R$, the resistance. Note that not all electrical components obey this linearity property. For example, the diode is one of those non-ohmic, or nonlinear, semiconductors.

As a corollary of the voltage law, two electric components connected in parallel have the same voltage (in opposite direction within their loop) but can have different current. Similarly, from the current law we can derive that two components in series have the same current but can have different voltages. See the examples below.

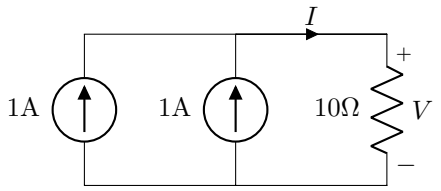


Two current sources of 1A in parallel with a resistor $R = 10\Omega$. As a consequence $I = 2\text{A}$ and $V = IR = 20\text{V}$.

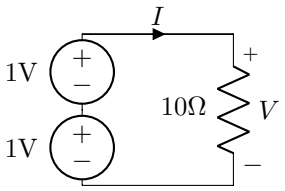


Two voltage sources of 1V in series with a resistor $R = 10\Omega$. As a consequence $V = 2\text{V}$ and $I = V/R = 0,2\text{A}$.

A circuit that is not connected is called an open circuit. In this case there is no net flow of charge carriers, so the current is zero. The voltage over the end points of the circuit is called $V_{\text{oc}}$: the open circuit voltage. A short circuit is a circuit with a connection allowing current from a power source to flow freely between two points, where there should be a resistor or load. The voltage level is zero and the current is called $I_{\text{sc}}$, the short circuit current.

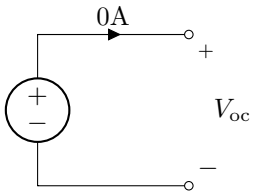


Open circuit with a voltage source.

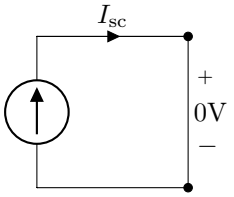


Closed circuit with a current source.

## 1.3 Circuit components

A solar photovoltaic cell can be modelled with an electrical circuit. The following components occur in this circuit:

diode

current source

resistor

### 1.3.1 Diode

A diode is an electronic component that (ideally) conducts current in only one direction. A diode is formed by a so-called p-n junction. A p-n junction, also called a semiconductor

junction, is formed by the boundary surface between two layers of material. One layer is the p-type and the other is the n-type. In the negative- or n-type layer the majority charge carriers are electrons. A charge carrier is a charged particle that can freely move around in the material. The n-type layer also contains positively charged atoms that donated an electron, but those are fixed. The net charge of the layer is zero, so the 'n' relates to the charge of the majority charge carriers.

In the p-type (positive-type) layer the majority charge carriers are holes. A hole is the lack of an electron in an atom where one could exist in the atom lattice. The p-type layer also has a net charge of zero: the holes are offset by fixed negatively charged atoms that accepted an electron.

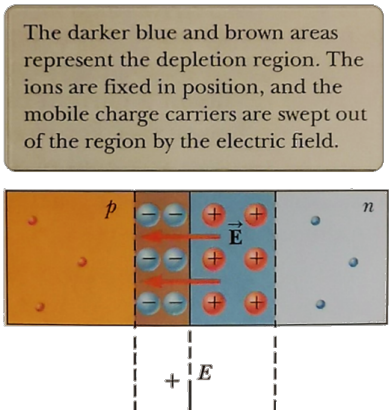


Figure 3: Representation of a p-n junction.[4]

In each layer there is also a minority of some charge carriers that are oppositely charged from the majority charge carriers. This is basically an impurity in the material. For instance, the n-type layer, also contains some holes in lesser amount. Those are the minority charge carriers.

At the p-n junction, where the two layers touch, there is interaction between the holes and electrons. Electrons fill up the holes, and what is left are the fixed positively charged atoms and the negatively charged atoms. Because the charged atoms are situated next to each other, the net charge at the p-n junction is still zero. The zone around the p-n junction where this happens is called the depletion zone. The depletion zone basically acts as an insulator. So the thinner the depletion zone, the higher the conductivity of the diode. The thickness of the depletion zone, and therefore the conductivity, depends on the external voltage that is applied.

If there is a positive voltage applied to the p-layer, it will pull electrons from the n-layer and repel holes from the p-type layer. Both carriers are moving towards the p-n junction and the depletion zone becomes thinner. The conductivity of the diode increases as the voltage increases, and this state is called the *forward bias*. Schematically a diode in forward bias looks like this:

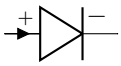


The opposite situation, where negative voltage is applied to the p-type and positive voltage is applied to the n-type, is called *reverse bias*. The negative voltage on the n-side will pull the electrons away from the p-n junction, and the positive voltage on the p-side does the same for the holes. The depletion zone becomes thicker and ideally the current is totally blocked. However, due to the minority charge carriers there is a small current, called the reverse saturation current $I_0$. Note that $I_0$ is the size of the reverse saturation current, so it is a positive value, but the direction is opposite from current under forward bias. If the diode is in reverse bias, we also say that the current is in block direction, which schematically looks like this:

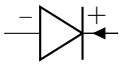

In an ideal situation the diode behaves as a switch that conducts the current completely in forward bias (positive voltage), and conducts no current in reverse bias (negative voltage). However, in reality the I-V curve of a diode looks different: the current doesn't suddenly change from zero at negative voltages to infinity at positive voltages. Instead, the diode has an exponential I-V curve where for negative voltages the current is slightly negative (limited by horizontal asymptote $-I_0$), for no voltage there is of course no current, and for positive voltages the current is in positive direction. This I-V characteristic is described with the Shockley diode equation,

$$I = I_0 \left( \exp\left( \frac{qV}{nkT} \right) - 1 \right), \tag{1.1}$$

where $k$ is the Boltzmann constant, $q$ is the elementary charge (charge of an electron), $T$ is the temperature of the diode in Kelvin, $I_0$ is the reverse saturation current and $n$ is what is called the ideality factor. The diode current is $I$, and $V$ is the voltage across the diode.

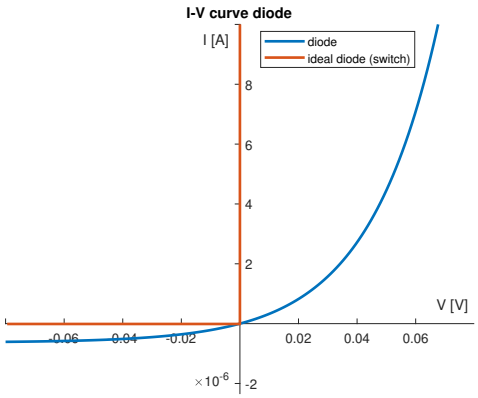


Figure 4: I-V curve of a switch compared with a diode based on the Shockley diode equation with $I_0 \approx 6 \cdot 10^{-7}$, $T = 278\text{K}$, $n = 1$.

We see that $I$ and $V$ are not directly proportional, i.e., a diode is not an ohmic conductor. In this equation we can also see that, indeed, under reverse bias (i.e., $V$ is negative) the current of the diode approaches the reverse saturation current: as $V \to -\infty$ we have $I \to -I_0$. The parameter $n$ is the diode ideality factor. This unitless factor depends on the quality of the diode and is a value between 1 and 2. In an ideal situation recombination of an electron and a hole does not occur at the p-n junction of a semiconductor. In that case the ideality factor is 1. However, in reality there is a recombination in depletion regions and this can increase the ideality factor up to 2. The factor depends on the material of the semiconductor and is also not really a constant. The ideality factor varies with the current level; it decreases from 2 at low currents to 1 at high currents, but might also go up to 2 again at high current levels depending on carrier concentrations in the device.[10,11,12]

The Shockley diode equation lacks in describing some properties about the diode. Firstly, for negative voltages exceeding a certain reverse voltage, called the *breakdown voltage* $V_{\text{br}}$, reverse current starts to flow freely. This might cause a breakdown of the diode. Also, there is a maximum forward current that the diode can withstand before it heats up too much. Lastly, there is a slightly steeper jump in the current just before

zero, though this is negligible since we're talking about such small currents around zero. An actual diode I-V characteristic looks more like in Figure 5, but we can estimate the region between breakdown voltage and maximum forward current with the Shockley equation.

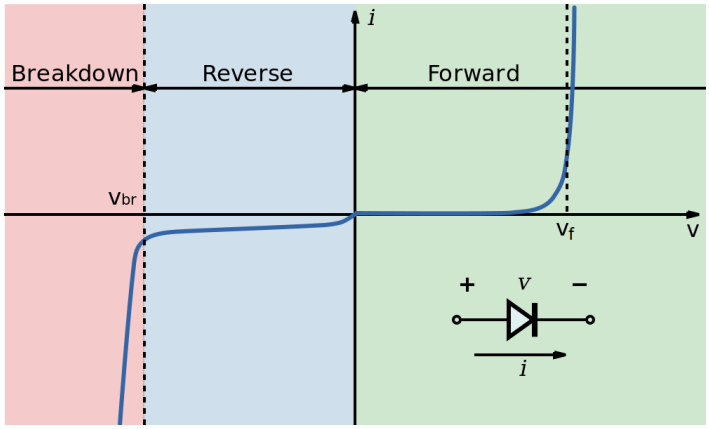


Figure 5: I-V curve diode. $V_{br}$ is the breakdown voltage and $V_f$ is the forward voltage: the threshold voltage at which point the forward current is considered to start flowing. [13]

### 1.3.2 Current source

As suppliers of electricity, the most known are voltage sources. Examples of voltage sources are a battery or the power supply of a wall outlet. A voltage source delivers a fixed voltage and generates variable current. On the other hand we have a current source. A current source generates a fixed current and has a variable voltage. A photovoltaic cell can be modelled with the help of a current source. However, the current is not exactly fixed like for a general current source. Fluctuation in the current of a photocell is caused by shifting ambient conditions like temperature and irradiance. So the solar cell is a current source in the sense that it generates a fixed current for fixed ambient conditions.

# 2 Photovoltaic cell

The electrical behaviour of a photovoltaic (PV) cell can be illustrated with an I-V curve. This is a graph that shows the relation between the output voltage (V) and output current (I) of a cell. The photovoltaic cell generates current, which is influenced by the level of sunlight on the cell, however, the amount of output current can not be directly controlled. On the other hand, the operation point (I,V) is determined by the load that is connected to the PV cell or module.

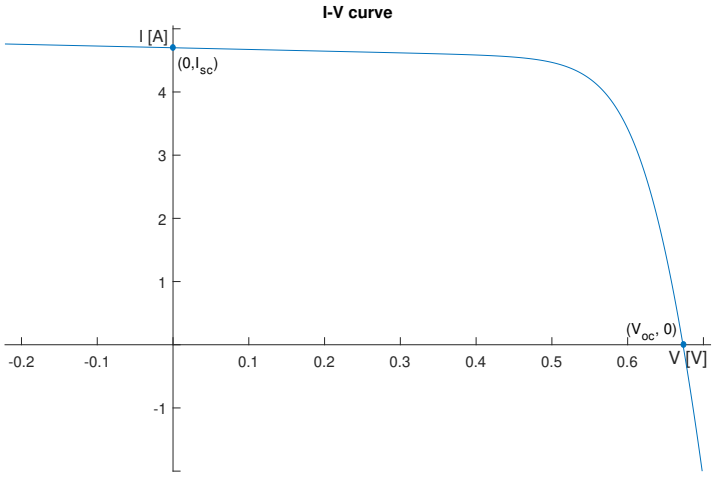


Figure 6: Simulated I-V curve of a MiaSolé CIGS cell (Appendix II) at an irradiance of 1000W/m$^2$ and cell temperature of 25°C.

Overall, the shape of the I-V curve is generally the same for all solar cells. However, the slopes of the approximately linear pieces before and after the 'knee' of the curve can vary depending on the resistances in the cell. More about the effects of the resistances later will be discussed later.

## 2.1 Single diode model

In order to be able to evaluate the performance of photovoltaic cells and modules under various ambient conditions, a PV model will be useful. The photovoltaic cell can be modelled with an electrical circuit. This is called an equivalent circuit model. The most widely used equivalent circuit model of a photocell is the single diode model.

There are more elaborate models like a double diode model and even a multi-dimension diode model. Models like this can achieve lower modelling errors than the single diode model, especially for thin-film PV technologies.[14] The disadvantage is, however, that these models have higher computation costs and need more preliminary data to find all the unknown parameters. Whereas the single diode model can predict the cell behaviour by just using the information provided by the PV cell manufacturer without needing to measure additional data. This makes the single diode model most suited for our objective; making a model of PV modules where theoretical ambient conditions and PV cell properties can easily be put in.

In the single diode model[15,16] there is a current source and a diode connected in parallel.

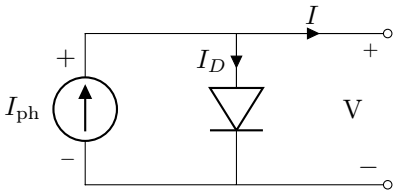


Figure 7: Single diode model of an ideal photocell.

Because of the diode, a nonlinear component, we know that the current-voltage relation of the PV cell will behave nonlinearly. $I_{\text{ph}}$ is the photogenerated current and $I_D$ is the current through the diode. We can calculate $I$ according to Kirchoff's current law as $I = I_{\text{ph}} - I_D$. Now we remember that $I_D = I_0 \left( \exp(\frac{qV_D}{nkT}) - 1 \right)$ and since $V_D = V$, we get the following equation.

$$I = I_{\text{ph}} - I_0 \left( \exp(\frac{qV}{nkT}) - 1 \right) \tag{2.1}$$

However, the single diode model above is an ideal depiction of a photocell. In reality, the photocell does not behave like this because there are some resistances.

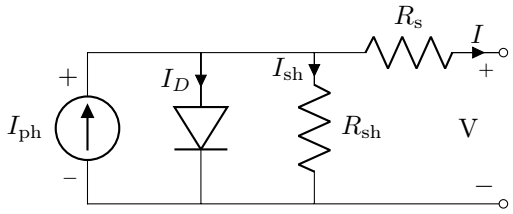


Figure 8: Single diode model of a photocell.

Parameter $R_{\text{sh}}$ is the shunt resistance. A shunt is a microscopic defect in the solar cell which provides an alternative path for the current between the contacts on the front and the back surfaces. The shunt resistance is preferable as high as possible, since a low resistance would mean that the current prefers to travel through the shunt. $R_{\text{s}}$ is the series resistance, which is caused by resistance in the cell and within the contacts, and by interaction between the semiconductor layer and the metal contacts. We assume $R_{\text{s}}$ and $R_{\text{sh}}$ are known constant properties of the photocell for now.

By Kirchoff's current law we get that $I = I_{\text{ph}} - I_D - I_{\text{sh}}$. By Ohm's law we know that $I_{\text{sh}} = V_{\text{sh}}/R_{\text{sh}}$. With Kirchoff's voltage law and by Ohm's law we can derive $V_{\text{sh}} = V + V_{\text{s}} = V + IR_{\text{s}}$. Note that $V_D = V_{\text{sh}}$, so $I_D = I_0 \left( \exp(\frac{qV_{\text{sh}}}{nkT}) - 1 \right)$. We get the following equations:

$$I_{\text{sh}} = \frac{V + IR_{\text{s}}}{R_{\text{sh}}} \quad \text{and} \quad I_D = I_0 \left( \exp(\frac{q(V + IR_{\text{s}})}{nkT}) - 1 \right).$$

Now we can derive the following I-V characteristic for a photovoltaic cell.

$$I = I_{\text{ph}} - I_0 \left( \exp(\frac{q\,(V + IR_{\text{s}})}{nkT}) - 1 \right) - \frac{V + IR_{\text{s}}}{R_{\text{sh}}} \tag{2.2}$$

Note that for $R_{\text{sh}} \to \infty$ and $R_{\text{s}} \to 0$ the Equation 2.2 equals 2.1. This makes sense since in an ideal cell there are no defects in the layers so the shunt resistance is infinitely

large. Also, the wiring would have no resistance which means the series resistance is zero, and the ideality factor would be 1 for a perfect semiconductor layer.

Below we can see the effects of the three parameters $R_{\text{sh}}$, $R_{\text{s}}$ and $n$ on the I-V curve compared to an ideal PV cell. In Figure 9, only the ideality factor is varied. We see that the higher the ideality factor, the softer the 'knee' of the curve. In Figure 10, the shunt resistance is varied. We can see that for higher values of $R_{\text{sh}}$ ($R_{\text{sh}} > 100$ in this case) the I-V curve nearly coincides with the ideal I-V curve. In Figure 11 we see the effect of varying the series resistance. For smaller values of $R_{\text{s}}$ ($R_{\text{s}} < 0.001$ in this case) the I-V curves also rapidly converges to the ideal I-V curve. In the figures we can see that the slope around the short circuit point is mainly influenced by the shunt resistance, while the slope around the open circuit point is mainly influenced by both the series resistance and the ideality factor.

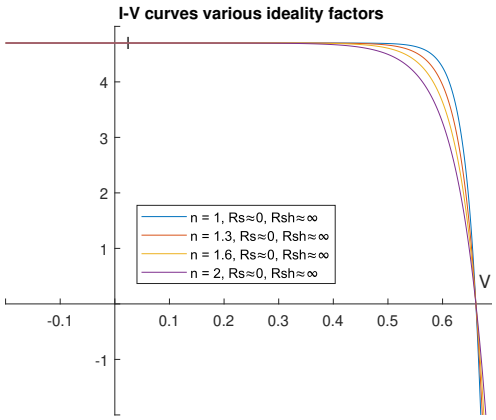


Figure 9: Simulated behaviour of a CIGS cell for varying ideality factors and constant series resistance and shunt resistance

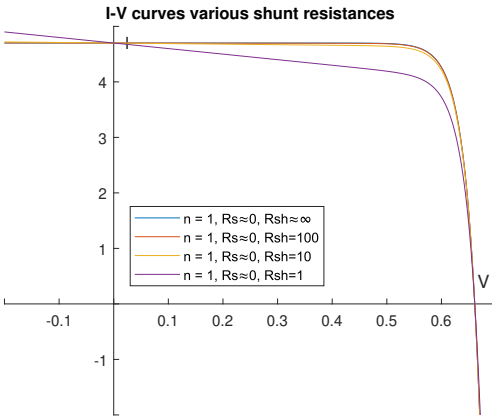


Figure 10: Simulated behaviour of a CIGS cell for varying shunt resistances and constant series resistance and ideality factor

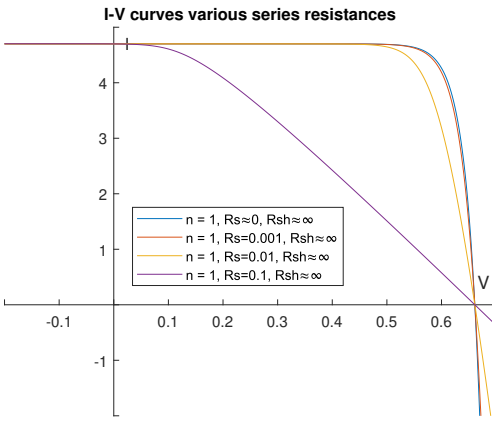


Figure 11: Simulated behaviour of a CIGS cell for varying series resistances and constant shunt resistance and ideality factor

It is important to note here that the cells in the figures are modelled as CIGS cells at standard test conditions (more about these conditions later). So the other parameters of the I-V characteristic, $I_0$ and $I_{\text{ph}}$, are based on the choice of $R_{\text{sh}}$ and $R_{\text{s}}$. They are calculated, this method will be shown later on, such that all curves go through the same open and short circuit points as provided by the datasheet in Appendix II. This means that $I_0$ and $I_{\text{ph}}$ have different values for the different choices of $R_{\text{s}}, R_{\text{sh}}$ and $n$. If we were to assume that $I_0$ and $I_{\text{ph}}$ are the same for all cells, then the figures would show shifts in open circuit voltages and short circuit currents for the varying resistances and ideality factors. This can be seen in the figure below where we set $I_0 = 10^{-7}$A, $I_{\text{ph}} = 5$A and cell temperature $T = 25°$C.

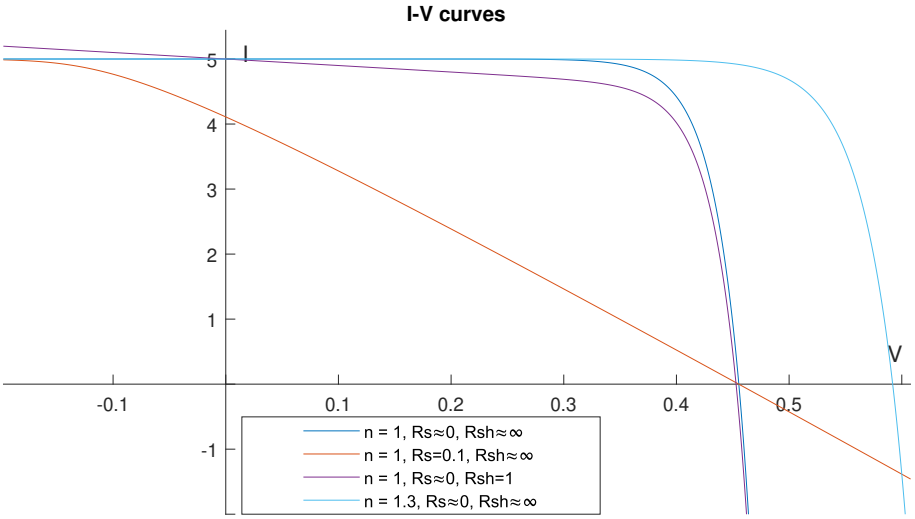

Equation 2.2 is a nonlinear implicit function and $I$ can not be written in terms of elementary functions. Let us instead write this equation as the solution curve at 0 of a function in the two variables $V$ and $I$. We define the function $F_{\text{cell}}$ and get the *I-V curve* for $F_{\text{cell}} = 0$.

**Definition 2.1.**

$$F_{\text{cell}}(V, I) = I_{\text{ph}} - I_0 \left( \exp(\frac{q\,(V + IR_{\text{s}})}{nkT}) - 1 \right) - \frac{V + IR_{\text{s}}}{R_{\text{sh}}} - I$$

To solve the I-V curve at a certain voltage $V$, $F_{\text{cell}}(V, I) = 0$ needs to be solved with a numeric method like `fzero`, which finds the zero of a function in one variable, in MATLAB. However, this is not a very fast method. So when this method is used for calculating many $(V, I)$-points for multiple cells, then the program's computing time quickly increases. Instead we can rewrite the I-V characteristic with the help of the Lambert $W$ function, which can be solved more efficiently.

## 2.2 Lambert $W$ function

The Lambert $W$ function is the inverse of the function $\mathbb{C} \to \mathbb{C}$, $z \mapsto ze^z$, so $z = W(ze^z)$. The Lambert $W$ function can not be expressed in terms of elementary functions. Let $f : \mathbb{R} \to \mathbb{R}$, $x \mapsto xe^x$, then $f^{-1}$ is the Lambert $W$ function restricted to the real numbers.

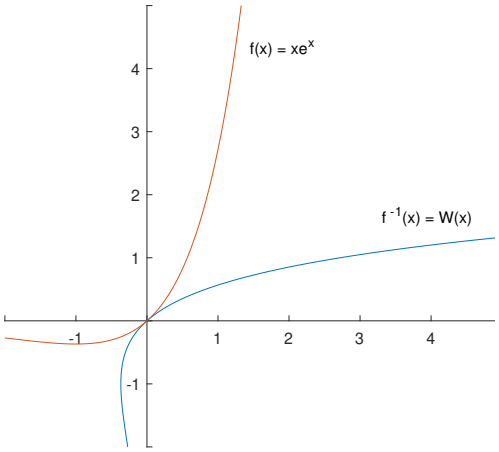


Figure 12: The Lambert $W$ function and its inverse

Since $f'(x) = xe^x + e^x$, we see that the minimum of $f$ is $(-1, -1/e)$. Also, $f$ is injective on $[0, \infty)$. *Proof.* Suppose $x, y \geq 0$, and $f(x) = f(y)$ and let $y \geq x$ w.l.o.g. Then we get that $x/y = e^{y-x}$. Since $y - x \geq 0$ we know that $x/y = e^{y-x} \geq 1$. So $x \geq y$ which implies $x = y$. □
We have a strict minimum in $(-\infty, 0)$, so the continuous function $f$ is not injective on this domain. Moreover, we know that $f(x) < 0$ for $x < 0$ and $f(x) \to 0$ as $x \to -\infty$. We can conclude that the Lambert $W$ function is multi-valued on $[-1/e, 0)$ and single-valued on $[0, \infty)$. Also note that since $f$ is a (single-valued) function, the Lambert $W$ function is injective.

The Lambert $W$ function is usually mentioned as consisting of two branches: the principle branch $W_0$, which is the part for $W(x) \geq -1$, and the lower branch $W_{-1}$, which

is the part for $W(x) \leq -1$. Note that the $W_0$ branch is a strictly increasing function, because $xe^x$ is strictly increasing for $x > -1$.

With the help of the Lambert $W$ function we can rewrite the I-V characteristic of a cell (see Equation 2.2). As a result we can get the output current of cell, $\mathcal{I}_{\text{cell}}$, as a function of the voltage $V$. Define $c = \dfrac{q}{nkT}$ and $d = \dfrac{R_{\text{s}}R_{\text{sh}}}{R_{\text{s}} + R_{\text{sh}}}$.

$$\mathcal{I}_{\text{cell}}(V) = \frac{R_{\text{sh}}}{R_{\text{s}} + R_{\text{sh}}}(I_{\text{ph}} + I_0 - \frac{V}{R_{\text{sh}}}) - \frac{1}{cR_{\text{s}}} W\left(cdI_0 e^{cd(V/R_{\text{s}} + I_{\text{ph}} + I_0)}\right) \tag{2.3}$$

*Proof.* From Equation 2.2 we get

$$\begin{aligned}
& I = I_{\text{ph}} - I_0 \exp\left(cV + cR_{\text{s}}I\right) + I_0 - \frac{V}{R_{\text{sh}}} - \frac{R_{\text{s}}}{R_{\text{sh}}} I \\
\Rightarrow \quad & \frac{R_{\text{sh}} + R_{\text{s}}}{R_{\text{sh}}} I + \frac{V}{R_{\text{sh}}} - I_{\text{ph}} - I_0 = -I_0 \exp\left(cV + cR_{\text{s}}I\right) \\
\Rightarrow \quad & \frac{1}{cd}\left(cR_{\text{s}}I + cd(\frac{V}{R_{\text{sh}}} - I_{\text{ph}} - I_0)\right) = -I_0 \exp\left(cV + cR_{\text{s}}I\right)
\end{aligned}$$

Now let's say $\alpha = cR_{\text{s}}I$ and $\beta = cd(\dfrac{V}{R_{\text{sh}}} - I_{\text{ph}} - I_0)$, just for notational clarity. We get

$$\begin{aligned}
& -(\alpha + \beta) = cdI_0 e^{cV + \alpha} \\
\Rightarrow \quad & -(\alpha + \beta) e^{-(\alpha+\beta)} = cdI_0 e^{cV + \alpha - (\alpha+\beta)} \\
\Rightarrow \quad & -(\alpha + \beta) e^{-(\alpha+\beta)} = cdI_0 e^{cV - \beta}
\end{aligned}$$

Note that the right-hand side of the last equation is no longer dependent on $I$. Because $z = W(ze^z)$, we now know that $-(\alpha + \beta) = W\left(-(\alpha + \beta)e^{-(\alpha+\beta)}\right) = W\left(cdI_0 e^{cV - \beta}\right)$. So

$$\begin{aligned}
& -\left(cR_{\text{s}}I + cd(\frac{V}{R_{\text{sh}}} - I_{\text{ph}} - I_0)\right) = W\left(cdI_0 \exp\left(cV - cd(\frac{V}{R_{\text{sh}}} - I_{\text{ph}} - I_0)\right)\right) \\
\Rightarrow \quad & I = \frac{d}{R_{\text{s}}}(I_{\text{ph}} + I_0 - \frac{V}{R_{\text{sh}}}) \\
& \quad - \frac{1}{cR_{\text{s}}} W\left(cdI_0 \exp\left(cd\left((\frac{R_{\text{s}} + R_{\text{sh}}}{R_{\text{s}}R_{\text{sh}}} - \frac{1}{R_{\text{sh}}})V + I_{\text{ph}} + I_0\right)\right)\right) \\
\Rightarrow \quad & I = \frac{R_{\text{sh}}}{R_{\text{s}} + R_{\text{sh}}}(I_{\text{ph}} + I_0 - \frac{V}{R_{\text{sh}}}) - \frac{1}{cR_{\text{s}}} W\left(cdI_0 e^{cd(V/R_{\text{s}} + I_{\text{ph}} + I_0)}\right)
\end{aligned}$$

□

Note that for a solar cell we always have $c \geq 0$ (since $T \geq 0$K, $n \geq 0$), $d \geq 0$ (since $R_{\text{s}}, R_{\text{sh}} \geq 0$) and $I_0 \geq 0$. So the argument of $W$ in Equation 2.3 is always greater than or equal to zero, i.e. ,always lies on the $W_0$ branch. Since $W(x)$ is single-valued for $x \geq 0$, this means that $\mathcal{I}_{\text{cell}}$ is always single-valued, i.e., is a function on $\mathbb{R}$. Note also that $\mathcal{I}_{\text{cell}}$ is a strictly decreasing function because $-1/cR_{\text{s}} < 0$, the argument of $W$ in $\mathcal{I}_{\text{cell}}$ is a strictly increasing function of $V$, and the $W_0$ branch is a strictly increasing function as seen in the previous section.

With the Lambert $W$ function we can also write the voltage of a cell, $\mathcal{V}_{\text{cell}}$, as a function of it's total current $I$.

$$\mathcal{V}_{\text{cell}}(I) = R_{\text{sh}}(I_{\text{ph}} + I_0) - (R_{\text{sh}} + R_{\text{s}})I - \frac{1}{c} W\left(cR_{\text{sh}}I_0 e^{cR_{\text{sh}}(I_{\text{ph}} + I_0 - I)}\right) \tag{2.4}$$

*Proof.* We rewrite Eq. 2.2to

$$\begin{aligned} & \frac{V}{R_{\text{sh}}} = I_{\text{ph}} - I_0 \exp(cV + cIR_{\text{s}}) + I_0 - \frac{R_{\text{s}}}{R_{\text{sh}}} I - I \\ \Rightarrow \quad & cV = cR_{\text{sh}} \left(I_{\text{ph}} + I_0 - I\right) - cR_{\text{s}} I - cR_{\text{sh}} I_0 \exp\left(cV + cIR_{\text{s}}\right) \\ \Rightarrow \quad & -cV + \beta = cR_{\text{sh}} I_0 \exp\left(cV + cIR_{\text{s}}\right) \end{aligned}$$

where $\beta = cR_{\text{sh}} \left(I_{\text{ph}} + I_0 - I\right) - cR_{\text{s}} I$. So

$$\begin{aligned} & (-cV + \beta) e^{-cV+\beta} = cR_{\text{sh}} I_0 e^{cIR_{\text{s}}+\beta} \\ \Rightarrow \quad & -cV + \beta = W\left(cR_{\text{sh}} I_0 e^{cIR_{\text{s}}+\beta}\right) \\ \Rightarrow \quad & V = R_{\text{sh}}(I_{\text{ph}} + I_0 - I) - R_{\text{s}} I - \frac{1}{c} W\left(cR_{\text{sh}} I_0 e^{cR_{\text{sh}}(I_{\text{ph}}+I_0-I)}\right) \end{aligned}$$

□

Since $c, R_{\text{sh}}, I_0 \geq 0$ we know that the argument of $W$ in Equation 2.4 is larger than or equal to 0. So $\mathcal{V}_{\text{cell}}$ is also a function on $\mathbb{R}$. In other words we now know that it's inverse, $\mathcal{V}_{\text{cell}}$, is an injective function. Note that we know that $\mathcal{V}_{\text{cell}}$ and $\mathcal{I}_{\text{cell}}$ are inverses because they are both derived from Eq. 2.2, even though this is not immediately visible in the definitions of $\mathcal{V}_{\text{cell}}$ and $\mathcal{I}_{\text{cell}}$. Since $\mathcal{V}_{\text{cell}}$ is the inverse of $\mathcal{I}_{\text{cell}}$, we know that it is also a strictly decreasing function.

## 2.3 Maximum power point

Power is current times voltage (the unit is Watt $[W = V \cdot A]$). The output voltage over the cell is fixed by the load that is connected to the solar cell or solar module, which in term determines the output current. So the power output of the cell is also controlled by the voltage of the load. There is an operating point where the power output (P) is maximal. This is clarified by the P-V curve as seen in the following figure. Ideally, all solar cells operate always at this *maximum power point* (MPP).

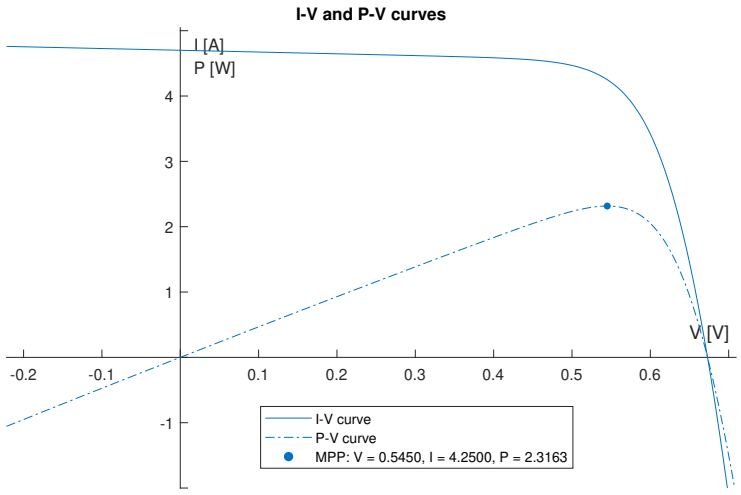


Figure 13: Simulated I-V and P-V curves of a CIGS cell (Appendix II) at STC.

At the open circuit operating point the current is 0A, and at the short circuit point the voltage is 0V. Consequently, at these points there is no power production. If $V > V_{\text{oc}}$ the P-V curve drops below zero, i.e., the solar cell consumes power. If $V < 0$ the solar cell is in reverse bias. In this case the solar cell also consumes power. When the solar cell consumes too much power, it might heat up and cause defects, called hot spots, in the cell.

At the maximum power point we have that the derivative of power with respect to voltage is zero. So for the voltage value at the MPP, $V_{\text{MPP}}$, we have $\frac{dP}{dV}\big|_{V=V_{\text{MPP}}} = 0$. We can write power output as a function of voltage with Equation 2.3:
$P_{\text{cell}}(V) = \mathcal{I}_{\text{cell}}(V) \cdot V$. We get that

$$\frac{dP_{\text{cell}}}{dV} = \frac{d\mathcal{I}_{\text{cell}}}{dV} \cdot V + \mathcal{I}_{\text{cell}}(V). \tag{2.5}$$

Let's define $\chi(V) = cdI_0 \exp\left(cd(V/R_{\text{s}} + I_{\text{ph}} + I_0)\right)$, then $\chi'(V) = \frac{cd}{R_{\text{s}}}\chi(V)$. So

$$\begin{aligned} \mathcal{I}_{\text{cell}}(V) &= \frac{R_{\text{sh}}}{R_{\text{s}} + R_{\text{sh}}}(I_{\text{ph}} + I_0 - \frac{V}{R_{\text{sh}}}) - \frac{1}{cR_{\text{s}}} W\left(\chi(V)\right) \\ \Rightarrow \quad \frac{d\mathcal{I}_{\text{cell}}}{dV} &= -\frac{1}{R_{\text{s}} + R_{\text{sh}}} - \frac{1}{cR_{\text{s}}} W'\left(\chi(V)\right) \cdot \frac{cd}{R_{\text{s}}}\chi(V) \end{aligned} \tag{2.6}$$

For calculating the derivative of Lambert $W$ let $y = W(x)$. Then, since $y = W(ye^y)$ and $W$ injective, we have $x = ye^y$. So

$$\begin{aligned} 1 &= \frac{dW(ye^y)}{dy} = \frac{dW(x)}{dx} \cdot \frac{dx}{dy} \\ \Rightarrow \quad 1 &= W'(x)(ye^y + e^y) = W'(x)\frac{(1+y)ye^y}{y} = W'(x)\frac{(1+W(x))\,x}{W(x)} \end{aligned}$$

We know that $W(x) = -1$ for $x = -1/e$, so

$$W'(x) = \frac{W(x)}{(1+W(x))x}, \qquad \text{for } x \notin \{-1/e, 0\} \tag{2.7}$$

Now let's combine (2.6) and (2.7).

$$\begin{aligned} \frac{d\mathcal{I}_{\text{cell}}}{dV} &= -\frac{1}{R_{\text{s}} + R_{\text{sh}}} - \frac{1}{cR_{\text{s}}} \frac{W\left(\chi(V)\right)}{(1 + W\left(\chi(V)\right))\chi(V)} \cdot \frac{cd}{R_{\text{s}}}\chi(V) \\ \Rightarrow \quad \frac{d\mathcal{I}_{\text{cell}}}{dV} &= -\frac{1}{R_{\text{s}} + R_{\text{sh}}} - \frac{R_{\text{sh}}}{(R_{\text{s}} + R_{\text{sh}})R_{\text{s}}} \cdot \frac{W\left(\chi(V)\right)}{1 + W\left(\chi(V)\right)} \\ \Rightarrow \quad \frac{d\mathcal{I}_{\text{cell}}}{dV} &= -\frac{R_{\text{s}} + R_{\text{s}}W\left(\chi(V)\right) + R_{\text{sh}}W\left(\chi(V)\right)}{(R_{\text{s}} + R_{\text{sh}})R_{\text{s}}(1 + W\left(\chi(V)\right))} \\ \Rightarrow \quad \frac{d\mathcal{I}_{\text{cell}}}{dV} &= -\frac{(R_{\text{s}} + R_{\text{sh}})(1 + W\left(\chi(V)\right)) - R_{\text{sh}}}{R_{\text{s}}(R_{\text{s}} + R_{\text{sh}})(1 + W\left(\chi(V)\right))} \end{aligned}$$

Note that always $\chi(V) \geq 0$ for a solar cell, so $W(\chi(V)) \neq -1$. We get the final equation:

$$\mathcal{I}'_{\text{cell}}(V) = \frac{d}{R_{\text{s}}^2} \cdot \frac{1}{1 + W\left(\chi(V)\right)} - \frac{1}{R_{\text{s}}} \tag{2.8}$$

where $\chi(V) = cdI_0 e^{cd(V/R_{\text{s}} + I_{\text{ph}} + I_0)}$.

Combining this with (2.5) gives the following equation for the derivative of the output power.

$$\mathcal{P}'_{\text{cell}}(V) = \frac{d}{R_{\text{s}}^2} \cdot \frac{V}{1 + W\left(\chi(V)\right)} - \left(\frac{1}{R_{\text{s}}} + \frac{1}{R_{\text{s}} + R_{\text{sh}}}\right) V - \frac{1}{cR_{\text{s}}} W\left(\chi(V)\right) + \frac{d}{R_{\text{s}}}(I_{\text{ph}} + I_0) \tag{2.9}$$

where $\chi(V) = cdI_0 e^{cd(V/R_s + I_{ph} + I_0)}$.

Finally, to find the maximum power point of a PV cell we can solve $P'_{cell}(V_{MPP}) = 0$ numerically.

## 2.4 Determining model parameters

There are five unknown parameters in the photovoltaic cell: $I_0, I_{ph}, R_{sh}, R_s, n$. The temperature $T$ also needs to be calculated, because the $T$ in the I-V equations refers to the *temperature of the cell*. This is not the same as the ambient temperature. Known properties of the cell are some temperature coefficients, $K_I$ and $K_V$, and the nominal operating cell temperature NOCT. Also known are the short circuit current and open circuit voltage for standard test conditions, resp. $I_{sc,\ ref}$ and $V_{oc,\ ref}$. The consensus is that standard test conditions (STC) are:
- a solar irradiance, $G_{ref}$, of 1000W/m$^2$
- a *cell temperature* of $T_{ref} = 25°$C and
- no wind.

In most locations, the standard test conditions are not representative of the average operating conditions. The cell temperature of fully illuminated modules is usually much higher than 25°C, unless the weather is really cold, and the solar irradiance less than 1000 W/m$^2$.[17]

All these known properties have values that can be found on the manufacturer's datasheet of the PV cell. Besides that the manufacturer provides the voltage and current at the nominal power point ($V_{MPP,\ ref}$ and $I_{MPP,\ ref}$). The nominal power point is the maximum power point for standard test conditions (STC).

These known values can be used to determine the single diode model parameters. For example, the datasheet of a CIGS photocell provided by the manufacturer MiaSolé can be seen in Appendix II.

### 2.4.1 Cell temperature

The temperature $T$ used in the model (Eq. 2.2, 2.3) is the cell temperature (in Kelvin). However, most of the time only the ambient temperature (temperature of the surrounding air) of the cell is measured, and not the temperature of the cell itself. These two values are not the same. The cell temperature depends on the irradiance, ambient temperature and the NOCT. The NOCT is the nominal operating cell temperature [in °C], a property provided by the solar photovoltaic cell manufacturer. The NOCT is the cell temperature measured for nominal operating conditions (not to be confused with standard test conditions) which are:
- an irradiance of 800 W/m$^2$ on the cell surface
- an ambiant temperature of 20°C
- a wind velocity of 1 m/s
- open back side mounting.

We can approximate the cell temperature with the following expression[18]:

$$T = T_{amb} + \frac{\text{NOCT} - 20°\text{C}}{800\text{W/m}^2} \cdot G \tag{2.10}$$

where $G$ is the solar irradiance in W/m$^2$. Note that if $T_{amb}$ is provided in degrees Celsius, then $T$ calculated as above is also in Celsius. So then we need to convert $T$ to Kelvin for use in the I-V equations.

### 2.4.2 Short circuit current

The given value $I_{\text{sc, ref}}$ is the reference short circuit current. This is the short circuit current of the cell for standard test conditions.

The short circuit current is dependent on irradiance, and on temperature as well. So we can write the short circuit current as $I_{\text{sc}}(T, G)$. The dependence of the short circuit current on temperature is approximately linear. The relation with the temperature is given by the temperature coefficient of the short circuit current: $K_I$. The given temperature coefficient is usually obtained at the standard irradiance: 1000 W/m$^2$. If the given coefficient is a relative temperature coefficient, i.e., the coefficient is in %/°C, then it represents $\frac{1}{I_{\text{sc}}}\frac{dI_{\text{sc}}}{dT}\Big|_{I_{\text{sc}}=I_{\text{sc,ref}}} \cdot 100\%$. So we can calculate the short circuit current at a temperature $T$, and for standard irradiance, as

$$I_{\text{sc}}(T, G_{\text{ref}}) = I_{\text{sc,ref}}\left(1 + \frac{K_I}{100\%}(T - T_{\text{ref}})\right).$$

The relative temperature coefficient for short circuit current of thin-film solar cells is positive and usually quite small: order of $10^{-3}$ - $10^{-1}$. Sometimes, the given temperature coefficient is absolute, i.e., in A/°C, and then we have

$$I_{\text{sc}}(T, G_{\text{ref}}) = I_{\text{sc,ref}} + K_I(T - T_{\text{ref}}).$$

The short circuit current is approximately directly proportional to the irradiance and can be estimated with $I_{\text{sc}}(T, G) = G/G_{\text{ref}} \cdot I_{\text{sc}}(T, G_{\text{ref}})$. We get the equation for short circuit current:

$$I_{\text{sc}}(T, G) = I_{\text{sc,ref}}\left(1 + \frac{K_I}{100\%}(T - T_{\text{ref}})\right)\frac{G}{G_{\text{ref}}} \tag{2.11}$$

Note that since the $K_I$ is usually very small for thin-film solar cells, we can conclude that the short circuit current of thin-film solar cells is mostly influenced by the irradiance level.[19,20,21]

### 2.4.3 Open circuit voltage

The given value $V_{\text{oc, ref}}$ is the open circuit voltage for STC. The open circuit also has a linear correlation with the temperature. For given relative temperature coefficient $K_V$ and for standard irradiance, we can calculate the open circuit voltage as

$$V_{\text{oc},G_{\text{ref}}}(T) = V_{\text{oc,ref}}\left(1 + \frac{K_V}{100\%}(T - T_{\text{ref}})\right). \tag{2.12}$$

Again, if the given temperature coefficient is absolute, so in V/°C, then we use

$$V_{\text{oc},G_{\text{ref}}}(T) = V_{\text{oc,ref}} + K_V(T - T_{\text{ref}}).$$

The open circuit voltage of a solar cell decreases with higher temperature so the temperature coefficient of the open circuit voltage is negative.

The open circuit voltage also depends on irradiance, however this dependency is not linear, and the temperature coefficient of the short circuit current varies for different levels of irradiance. The given temperature coefficient is only for the standard irradiance. Therefore it is not possible to calculate $V_{\text{oc}}$ at an irradiance that is not 1000 W/m$^2$, with the given temperature coefficient. Instead, we calculate the open circuit voltage with $\mathcal{V}_{\text{cell}}(0)$ and only use the temperature coefficient of the open circuit voltage for calculating $I_0$, as we will see next.[19,20,21,22]

### 2.4.4 Reverse saturation current

The reverse saturation current does not vary with irradiance, but does depend heavily on the cell temperature. The reverse saturation current may be expressed as

$$I_0 = I_{0,ref} \left(\frac{T}{T_{\text{ref}}}\right)^3 \exp\left(qE_g\left(\frac{1}{T_{\text{ref}}} - \frac{1}{T}\right)\right),$$

where $E_g$ is the band gap energy of the semiconductor material and $I_{0,ref}$ is the reverse saturation current at reference temperature, which can be approximately obtained as $I_{0,ref} = \dfrac{I_{\text{sc,ref}}}{\exp\left(qV_{\text{oc,ref}}/nkT_{\text{ref}} - 1\right)}$.[23,24,16,25]

However, the reverse saturation current can be obtained more accurately and without needing to know the band gap energy. Since the reverse saturation current does not vary with irradiance, as we can see in the formulas above, we can calculate the reverse saturation current at $G_{\text{ref}}$. We get the following two equations by respectively substituting the open circuit, and short circuit values at standard irradiance in Equation 2.2.

$$0 = I_{\text{ph}}(T, G_{\text{ref}}) - I_0(T)\left(\exp(\frac{qV_{\text{oc}}(T)}{nkT}) - 1\right) - \frac{V_{\text{oc}}(T)}{R_{\text{sh}}}$$
$$I_{\text{sc}}(T) = I_{\text{ph}}(T, G_{\text{ref}}) - I_0(T)\left(\exp(\frac{qR_{\text{s}}I_{\text{sc}}(T)}{nkT}) - 1\right) - \frac{R_{\text{s}}I_{\text{sc}}(T)}{R_{\text{sh}}}$$

where $V_{\text{oc}}(T) = V_{\text{oc},G_{\text{ref}}}(T)$ and $I_{\text{sc}}(T) = I_{\text{sc}}(T, G_{\text{ref}})$.
Combining the two equations we get

$$\left(1 + \frac{R_{\text{s}}}{R_{\text{sh}}}\right) I_{\text{sc}}(T) = -I_0(T)\left(\exp(\frac{qR_{\text{s}}I_{\text{sc}}(T)}{nkT}) - \exp(\frac{qV_{\text{oc}}(T)}{nkT})\right) + \frac{V_{\text{oc}}(T)}{R_{\text{sh}}}$$
$$\Rightarrow \quad I_0(T) = \frac{\frac{R_{\text{s}}+R_{\text{sh}}}{R_{\text{sh}}} I_{\text{sc}}(T) - \frac{V_{\text{oc}}(T)}{R_{\text{sh}}}}{\exp(\frac{qV_{\text{oc}}(T)}{nkT}) - \exp(\frac{qR_{\text{s}}I_{\text{sc}}(T)}{nkT})}$$

With equation (2.11) and (2.12) we obtain the expression for the reverse saturation current at cell temperature $T$:

$$I_0(T) = \frac{(R_{\text{s}} + R_{\text{sh}})I_{\text{sc}}(T) - V_{\text{oc}}(T)}{R_{\text{sh}}e^{q/nkT}\left(e^{V_{\text{oc}}(T)} - e^{R_{\text{s}}I_{\text{sc}}(T)}\right)}, \text{ where} \tag{2.13}$$
$$V_{\text{oc}}(T) = V_{\text{oc,ref}}(1 + \frac{K_V}{100\%}(T - T_{\text{ref}})), \text{ and}$$
$$I_{\text{sc}}(T) = I_{\text{sc,ref}}(1 + \frac{K_I}{100\%}(T - T_{\text{ref}})).$$

Note that the reverse saturation current is the size of a current and does not contain any information of the direction of the current. Therefore, the reverse saturation current can not be negative. This means that if $(R_{\text{s}} + R_{\text{sh}})I_{\text{sc}}(T) < V_{\text{oc}}(T)$ or $V_{\text{oc}}(T) < R_{\text{s}}I_{\text{sc}}$, the values of $R_{\text{s}}$ and/or $R_{\text{sh}}$ are not realistic. The value of $R_{\text{s}}$ might be too high and the value of $R_{\text{sh}}$ too low.

### 2.4.5 Photogenerated current

The photogenerated current can be calculated with the previously obtained parameters. Consider the I-V characteristic at the short circuit current:

$$I_{\text{sc}} = I_{\text{ph}} - I_0(e^{qI_{\text{sc}}R_{\text{s}}/nkT} - 1) - \frac{I_{\text{sc}}R_{\text{s}}}{R_{\text{sh}}}$$

We get

$$I_{\text{ph}}(T,G) = \frac{R_{\text{sh}} + R_{\text{s}}}{R_{\text{sh}}} I_{\text{sc}}(T,G) + I_0(T)(e^{qI_{\text{sc}}(T,G)R_{\text{s}}/nkT} - 1) \tag{2.14}$$

We see that $I_{\text{ph}}$ depends on irradiance and temperature, since $I_0$ and $I_{\text{sc}}$ depend on irradiance and temperature.

### 2.4.6 Shunt resistance, series resistance and the ideality factor

In the calculations of the reverse saturation current and photogenerated current above we see that they depend on the shunt resistance, series resistance and ideality factor. This means that we have five unknown properties: $I_0, I_{\text{ph}}, R_{\text{sh}}, R_{\text{s}}$ and $n$, and only three known datapoints that they depend on: $(V_{\text{oc}}, 0)$, $(0, I_{\text{sc}})$ and $(V_{\text{MPP}}, I_{\text{MPP}})$ for STC. In addition we also know that $\left.\frac{dP}{dV}\right|_{V=V_{\text{MPP}}} = 0$. That gives us four equations to find five unknown variables, which means we can't find the unique values unless we have more data points. Ideally we get more data points and fit the unknowns of I-V curve to those data points, however, for the purpose of our model we don't want to require measuring of the PV cells beforehand.

As we saw in chapter 1, the ideality factor $n$ is a value between 1 and 2, but it is not really a constant and it depends on complex recombination processes in the semiconductor material. As a result, it is really complicated to determine the ideality factor. In literature[15,16,21,26], we mostly see two methods. The first is assuming a constant ideality factor based on the PV technology, see the table below. These factors are purely empirically determined and are an approximation.

| Technology | $n$ |
|---|---|
| Si-mono | 1.2 |
| Si-poly | 1.3 |
| a-Si:H | 1.8 |
| CdTe | 1.5 |
| CIS | 1.5 |
| GaAs | 1.3 |

Table 1: Ideality factor $n$ dependence on PV technology[16]

Then with the ideality factor fixed, we can determine the resistances by solving the following system of equations:

$$\begin{cases} \mathcal{I}_{\text{cell}}(V_{\text{MPP, ref}}) = I_{\text{MPP, ref}} \\ P'_{\text{cell}}(V_{\text{MPP, ref}}) = 0 \end{cases}$$

where we substitute $I_0 = I_0(T_{\text{ref}})$ and $I_{\text{ph}} = I_{\text{ph}}(T_{\text{ref}}, G_{\text{ref}})$ from equation (2.13) and (2.14), in the equations of $\mathcal{I}_{\text{cell}}$, Equation 2.3, and of $P'_{\text{cell}}$, Equation 2.9.

The second method is to fit the ideality factor, together with the shunt resistance and series resistance to given data of the PV cell. Using this method is justified, as the model is just a means of simulating the behaviour of a cell as good as possible. This method can improve the model's accuracy, but as said before we have too little data supplied by the manufacturer to determine $n$, $R_{\text{sh}}$ and $R_{\text{s}}$ uniquely. Since we know that $n$ is a value between 1 and 2 it is possible to fit $R_{\text{sh}}$ and $R_{\text{s}}$ for fixed values of $n$ and then pick 'the best' set of values. This is done by solving the abovementioned system of equations multiple times for $n$ ranging from 1 with small increments (0.01) up to 2. Then we minimize the norm of the residual from the system of equations of all the

possible $(n, R_{\text{sh}}, R_{\text{s}})$ combinations, i.e., we pick the values for which the nominal power point deviates least from the given nominal power point.

If we use both methods for the CIGS cell from Appendix II, we get the following I-V curves.

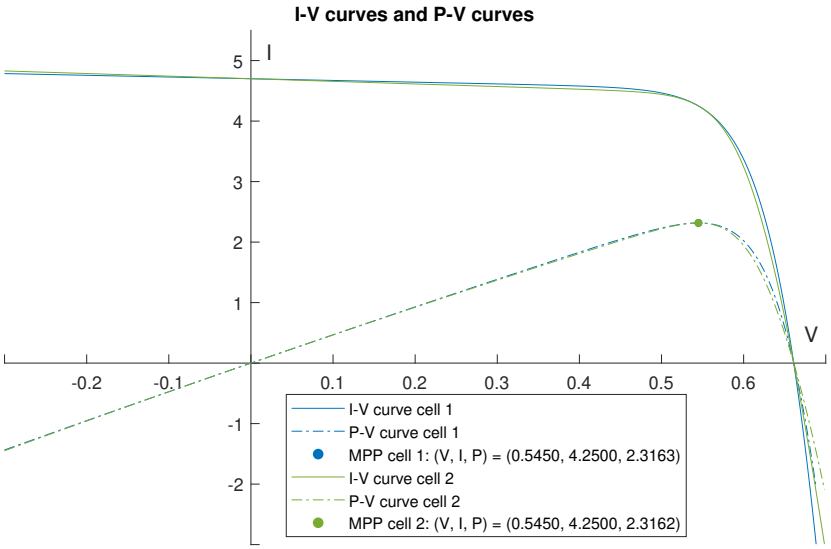


Figure 14: For cell 1 the method of predetermining $n = 1.5$ is used. The corresponding resistances for this cell are $R_{\text{s}} = 0.0026, R_{\text{sh}} = 3.52$. Cell 2 is determined with the fitting method and has $n = 1.07, R_{\text{s}} = 0.0078, R_{\text{sh}} = 2.32$.

As we can see both methods give a nominal power point that is within the range of precision of the given nominal power point, and both I-V curves go through the correct open circuit and closed circuit points. The shape of the I-V curves however, are different because, mathematically, with different $n$ belong different resistances.

A problem with the fitting method is that there are multiple choices of the parameters that cause only small deviations from the given nominal power point. Since the nominal power point isn't given with great precision, this means that the choice of $n, R_{\text{sh}}, R_{\text{s}}$ is a bit arbitrary and imprecise. For example, if the increments for ranging $n$ are 0.1 instead, then the fitting method gives us a cell with $n = 1.0, R_{\text{s}} = 0.0087, R_{\text{sh}} = 2.19$. These are different values compared with the fitting method from the figure above, while the nominal power points, up to the given precision, are the same. So the fitting method is only useful when there is nothing known about the value of $n$ or when there is at least one more data point.

With an extra data point around the short circuit point we have a third method to get the three unknown parameters: first determine the shunt resistance, and then determine the two other parameters with the system of equations from before. As we saw in figures 9, 10 and 11, the slope around the short circuit point is mostly influenced by only the shunt resistance. With some estimations we can show the shunt resistance is approximately minus the inverse of the I-V curve slope around $(0, I_{\text{sc}})$.[12,16,26] Let's

substitute $V = 0$ in Equation 2.3. We get

$$I_{\text{sc}} = \mathcal{I}_{\text{cell}}(0) = \frac{R_{\text{sh}}}{R_{\text{s}} + R_{\text{sh}}}(I_{\text{ph}} + I_0) - \frac{1}{cR_{\text{s}}} W\left(\chi(0)\right)$$
$$\Rightarrow \quad W\left(\chi(0)\right) = cR_{\text{s}}\left(\frac{R_{\text{sh}}}{R_{\text{s}} + R_{\text{sh}}}(I_{\text{ph}} + I_0) - I_{\text{sc, ref}}\right)$$

Since $T \sim 10^2$ (cell temperature in Kelvin), $q/k \sim 10^4$, $n \sim 10^0$, we have $c = q/(nkT) \sim 10^2$. Moreover, we can assume that the series resistance is approximately at most of order $10^{-2}$ (at least for the thin-film solar cells), so at most $cR_{\text{s}} \sim 10^0$. Also, for a general functioning solar cell (not a very low shunt or very high series resistance), we have that $R_{\text{sh}}/(R_{\text{sh}} + R_{\text{s}}) \approx 1$, $I_{\text{sc}} \approx I_{\text{ph}}$ and $I_0 \approx 0$. Therefore, we get that $W\left(\chi(0)\right) \approx 0$. Now let's calculate $\mathcal{I}'_{\text{cell}}(0)$ with Equation 2.8: $\mathcal{I}'_{\text{cell}}(0) \approx \frac{d}{R_{\text{s}}^2} - \frac{1}{R_{\text{s}}} = \frac{R_{\text{sh}} - (R_{\text{s}} + R_{\text{sh}})}{R_{\text{s}}(R_{\text{s}} + R_{\text{sh}})} = -\frac{1}{R_{\text{s}} + R_{\text{sh}}} \approx -1/R_{\text{sh}}$. So if we have an extra data point around the short circuit point, we approximate $R_{\text{sh}}$ by $-\Delta V/\Delta I$ and then calculate $R_{\text{s}}$ and $n$ with the system of equations as shown before.

A final note is that while in most studies $n$, $R_{\text{s}}$ and $R_{\text{sh}}$ are determined as constants, in reality the ideality factor and resistances vary with temperature and irradiance changes. Assuming these parameters to be constant, might cause errors in the model, especially for studying the behaviour of PV modules under shadow and mismatch conditions. Unfortunately, the temperature and irradiance relation with the ideality factor and resistances is nonlinear and there are no formulas known to directly calculate this relation analytically.[26,27] As a result determining the temperature and irradiance influence on these parameter either requires additional measuring[28] or requires a more complicated model (with neural networks)[27] that isn't in the scope of this research. Therefore we ignore the effect of temperature and irradiance on $R_{\text{s}}$, $R_{\text{sh}}$ and $n$ in this model, keeping in mind that this might cause some inaccuracies.

## 2.5 Effect of temperature and solar irradiance

Because the temperature and irradiance influence multiple model parameters in different ways, the effect of these ambient conditions on the I-V curve isn't immediately clear. For example, based on the I-V characteristic in Equation 2.2 it seems that higher cell temperature would increase the current levels of a cell. But in reality current mostly decreases with increasing temperature because the temperature also effects parameters $I_0$ and $I_{\text{ph}}$. In the figures below the effect of temperature and irradiance becomes clear. The figures are simulation results of MiaSolé CIGS cells with 17% efficiency, using the model that is described in the previous sections.

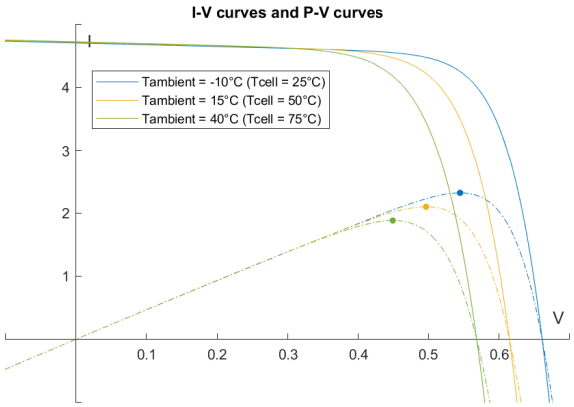


Figure 15: Various ambient temperatures for a constant irradiance of $1000\mathrm{W/m^2}$

An increase in ambient temperature mainly linearly decreases the open circuit voltage which in turn decreases the maximum power point. Also, if we were to zoom in on the short circuit currents in Figure 15 then we can see that a temperature increase slightly increases the short circuit current. This is to be expected by the temperature coefficients found on the data sheet.

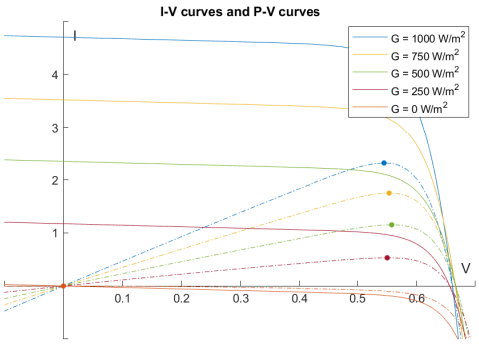


Figure 16: Various solar irradiance levels for a constant ambient temperature of $-10°\mathrm{C}$

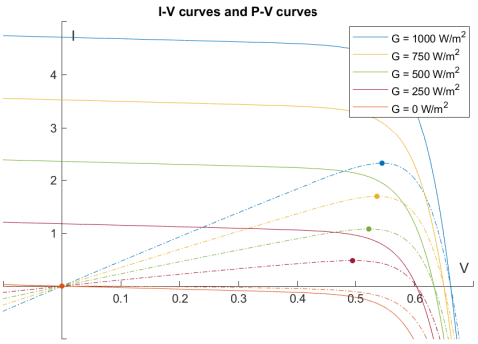


Figure 17: Various solar irradiance levels for a constant cell temperature of $25°\mathrm{C}$

A decrease in irradiance clearly linearly decreases the short circuit current linearly, as we expect by equation (2.11), but the effect on open circuit voltage is unclear in Figure 16. The reason for this is that the cell temperature changes for each level of irradiance, even if the ambient temperature stays the same. In Figure 17 we see that if the cell temperature is kept constant, then a decrease in open circuit voltage is to be expected for a decrease in irradiance.

For future modelling examples and figures we will always use MiaSolé CIGS cells with an efficiency of 17% from Appendix II with fixed ideality $n = 1.5$, unless otherwise mentioned. This type of cell is available at Solliance and will later on be used to verify the model with. When no specific ambient conditions are mentioned, the conditions will

be set at 1000W/m$^2$ and 20°C ambient temperature. Note that these are not standard testing conditions, in that case the ambient temperature would have to be $-10$°C to get a cell temperature of 25°C for the CIGS cells. However, as a more realistic ambient temperature, the temperature of a typical summer day in the Netherlands was picked, which is about 20°C.

# 3 Photovoltaic module

A PV module, also called an array, consists of multiple connected PV cells. Moreover, a module can be built with a number of solar sub-modules. The number of sub-modules, cells per sub-module and the way they are interconnected is up to the designer. The type and size of cells can be picked based on desired application properties. The maximum current and voltage are limited though, by the connected wires and the inverter.

To be able to feed the solar generated electricity into the grid, inverters are used. Inverters can turn the direct current of the PV application into alternating current. Often the inverters have a maximum power point tracker (MPPT) built in, to make sure that the PV modules operate at the maximum power point voltage. In large solar plants multiple PV modules might feed into one inverter. That means that if not all the modules have the same MPP, then there will be some losses in power output. There also exist micro-inverters, they are connected to a single module to ensure each module is operating at its MPP, but these are more expensive.[29] For this research we will focus on partial shading for single PV modules, but the model could also be used to simulate varying ambient conditions on multiple PV modules.

The connection topology of the cells or sub-modules in a PV module is called *the configuration*. The most widely used configuration in PV modules is the series-parallel configuration.

In the electrical circuit representation of a PV module, the solar cell will be represented with the following diagram.

This is a simplified depiction of the single diode model circuit, with the positive terminal at the top of the 'envelope'. These envelopes can in addition represent an entire module, since a PV module can also consist of smaller sub-modules.

## 3.1 Homogeneous module

When all the cells in a module are the same and temperature and irradiance are uniform, then we will call the module homogeneous. The I-V characteristic of the module will look like the I-V characteristic of a single cell but scaled up horizontally and vertically, based on the number of cells in series and in parallel.

### 3.1.1 Parallel cells

Suppose we interconnect a number, $N_p$, of cells in parallel. We define $V_i$ and $I_i$ as the voltage and current of cell number $i$. Let $V$ be the total voltage over the endpoints of the module and $I$ the output current of module. Below, we see an example with four cells in parallel. Because the cells are connected in parallel, we know that the total

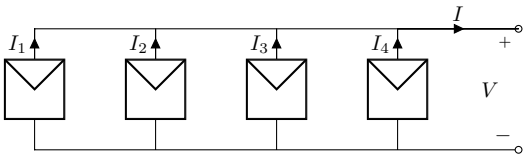


voltage of the module is equal to the voltage of each cell: $V = V_i, \forall i = 1, \ldots, N_p$ and the output current of the module is the sum of all output currents of the cells: $I = \sum_{i=1}^{N_p} I_i$.

Because the voltage over each cell is the same, we get that all the cells have the same output current $\mathcal{I}_{\text{cell}}(V)$. So $I = N_p\mathcal{I}_{\text{cell}}(V)$. On the other hand, we can also write $V$ as a function of $I$: we know all cells have the same output current $I_i = I/N_p$ and $V = V_i$, so $V = \mathcal{V}_{\text{cell}}(I/N_p)$.

### 3.1.2 Cells in series

Suppose we interconnect $N_s$ cells in series to form one 'string'. We define $V_i$ and $I_i$ as the voltage and current of cell number $i$. Let $V$ be the output voltage of the string (voltage over the endpoints of the string) and $I$ the output current of the string. Below, is an example of four cells in series. Since the cells are connected in series, we know that

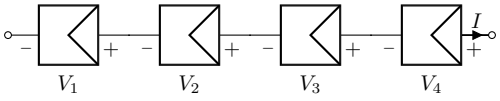


the total current of the string is equal to the current in each cell: $I = I_i, \forall i = 1, \ldots, N_s$, and the total voltage is the sum of all cell voltages: $V = \sum_{i=1}^{N_s} V_i$. We can calculate the current of each cell with $\mathcal{I}_{\text{cell}}(V_i)$. Because we know that all cell currents are equal and $\mathcal{I}_{\text{cell}}$ is an injective function, we get that the voltages of all cells are equal. Hence, $V_i = V_j$, $\forall i, j = 1 \ldots N_s$ and $V = \sum_{i=1}^{N_s} V_i$, so $V_i = V/N_s$ for all $i$. Thereby, $I = \mathcal{I}_{\text{cell}}(V/N_s)$. Note that this only holds because $\mathcal{I}_{\text{cell}}$ is the same function for all the cells, i.e., all parameters in $\mathcal{I}_{\text{cell}}$ are the same for all cells, because they have the same intrinsic and ambient properties. Like before, we can also write $V$ as function of $I$ instead: since we know that $V = N_s V_i$ and $I_i = I$ for all $i$, we get $V = N_s\mathcal{V}_{\text{cell}}(I)$.

Note that *string* is only used to describe a set of cells connected in series. For a set of cells connected in parallel we'll use the term *parallel set*. The term *set* will be used as a collective name to describe both strings and parallel sets.

### 3.1.3 Series-parallel and total-cross-tied configuration

If we create strings with $N_s$ cells connected in series, and then connect $N_p$ of such strings in parallel, then we get a $N_s \times N_p$ series-parallel configuration. This is shown in Figure 18 with $N_s = 2$ and $N_p = 3$. If we connect $N_s$ parallel sets in series and all of those parallel sets consist of $N_p$ cells, then we get the $N_s \times N_p$ parallel-series configuration. This is shown in Figure 19 with $N_s = 2$ and $N_p = 3$.

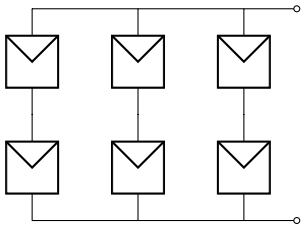

Figure 18: $2 \times 3$ series-parallel configuration

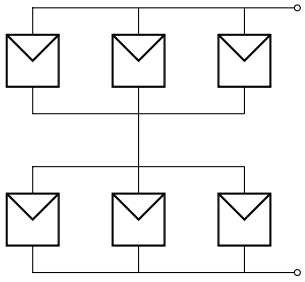

Figure 19: $2 \times 3$ parallel-series configuration

The parallel-series configuration is better known as the total-cross-tied (TCT) configuration. The reason for this is that the circuit of a parallel-series configuration is equivalent to the circuit of series-parallel with cross ties, like in the following figure.

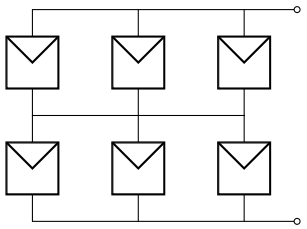

Figure 20: $2 \times 3$ TCT configuration, equivalent to the circuit in Figure 19

Most of the present-day solar modules have a series-parallel (SP) configuration. In a series-parallel configuration, all strings have the same voltage over them, which is the output voltage of the module $V$. Therefore, if all the cells are the same and irradiance and temperature are uniform, then the separate strings all have the output current $\mathcal{I}_{\text{cell}}(V/N_s)$, as seen before. So each string has the same output current and we get that the output current of the module is $I = N_p\mathcal{I}_{\text{cell}}(V/N_s)$.

In the parallel-series, or total-cross-tied, configuration, all the parallel sets are connected in series, so we know that the output current of each set equals the total output current $I$. Therefore, in case of a homogeneous module, we know that the voltage for each string is $\mathcal{V}_{\text{cell}}(I/N_p)$, as seen before. Hence, the voltage over each parallel set is $N_s\mathcal{V}_{\text{cell}}(I/N_p)$, which is also the value for total output voltage $V$ of the module. If we want to write the output current in terms of the output voltage then, using that $\mathcal{V}_{\text{cell}}$ and $\mathcal{I}_{\text{cell}}$ are inverses, we get $\mathcal{V}_{\text{cell}}(I/N_p) = V/N_s \Rightarrow \mathcal{I}_{\text{cell}}(V/N_s) = I/N_p$. So $I = N_p\mathcal{I}_{\text{cell}}(V/N_s)$.

In particular, we get that the open circuit current of a homogeneous module is $N_pI_{\text{sc, cell}}$ and the open circuit voltage is $N_sV_{\text{oc, cell}}$ for both configurations. Also, we get for both configurations that $P = V \cdot N_p\mathcal{I}_{\text{cell}}(V/N_s) = N_sN_p \cdot (V/N_s)\mathcal{I}_{\text{cell}}(V/N_s)$ $= N_sN_p\mathcal{P}_{\text{cell}}(V/N_s)$, i.e., the P-V curve is the singe cell P-V curve scaled with $N_p \cdot N_s$ in $P$-direction and with $N_s$ in $V$-direction. Thereby, $V_{\text{MPP}} = N_sV_{\text{MPP, cell}}$ and $P_{\text{MPP}}$ $= N_sN_pP_{\text{MPP, cell}}$. Moreover, we can conclude that the entire I-V and P-V curves for both configurations are the same. So a rectangular homogeneous module can simply be described with the cell information, number of cells/strings in parallel $N_p$ and number of parallel sets/cells in series $N_s$. In conclusion, for a homogeneous modules the choice of interconnection topology doesn't matter. This changes however when the module is no longer homogeneous, for example because of partial shading on the module.

## 3.2 Partial shading and mismatching

In a homogeneous module each individual cell operates at the same voltage and current as the rest of the cells, and the module's P-V curve is just a scaled up version of the single cell P-V curve. So we know that if the MPPT adjusts the voltage such that the module is operating at its maximum power point, then each cell operates optimally, namely at it's own maximum power point. But in a non-homogeneous module, i.e., a module where the cells have different parameter values, the interconnection between cells causes them to operate at less optimal operating points, even if the module operates at it's MPP. This is because the cells negatively affect each others operating points. This effect is called *mismatching*. Mismatching can cause there to be many local maximum power points in the P-V curve, which causes problems for maximum power point trackers. Also, there can be a lot of power dissipation in mismatched cells and some cells may be forced to operate at a voltage exceeding their breakdown voltage.

Mismatching can be caused by multiple differences in the cell's properties. If the cells have different series resistances for example, this also causes mismatching. This

research focuses on mismatching caused by partial shading on the modules, i.e., the cells are intrinsically the same but there is non-uniform solar irradiance on the module. This means that the irradiance and temperature dependent parameters $T_{\text{cell}}$, $I_{\text{ph}}$ and $I_0$ differ. That being said, the used model developed in this research could also potentially be used to investigate mismatching losses caused by something else (different resistances, having a broken or degraded cell in the module etc.).

The effect of mismatching on the output current and voltage of module is influenced by the interconnection between the cells. In a series string the short-circuit current will be mostly restricted by the short-circuit current of the cell with the lowest output current. Similar mismatch losses can also occur in parallel sets but they are less severe. [12]

We can see this in Figure 21, where we compare mismatching due to partial shading on a string and a parallel set. The figure shows I-V curves of three cells connected both in series and in parallel. Fully illuminated cells have $1000\text{W/m}^2$, and a shaded cell has $0\text{W/m}^2$. Both the series and the parallel set have one shaded cell and two fully illuminated cells. The ambient temperature is set at $20°\text{C}$. Clearly the current is mostly impacted by the cell with the lowest current for the series set, while the parallel set is much less influenced by the shaded cell. This results in a higher maximum power output for the parallel set.

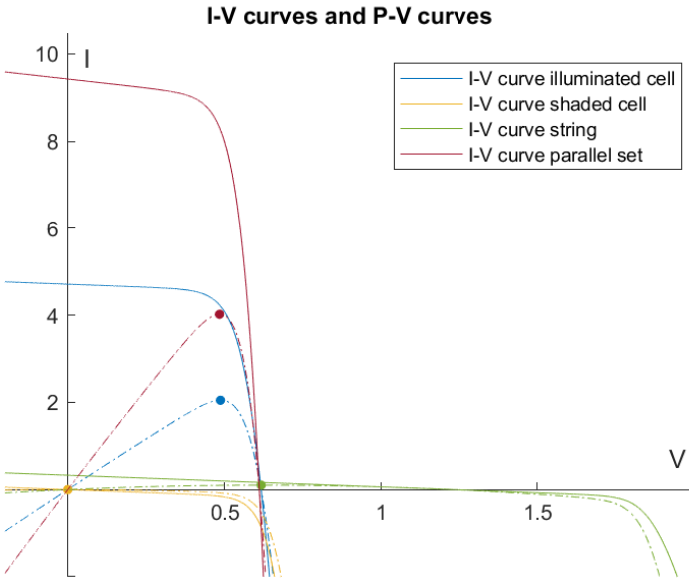


Figure 21: I-V curves of partially shaded parallel and series sets, both have one shaded cell and two fully illuminated cells.

In a parallel set the current of one cell doesn't need to flow through the other cells to reach the positive terminal. So for example the short circuit current of the parallel set in Figure 21 is just twice the short circuit current of the illuminated cell. For a parallel set in general, the voltage over each cell is total voltage over the string $V$, and output current $I$ is the sum of current of each cell. Thus,

$$I = \sum_{i=1}^{N_p} \mathcal{I}_{\text{cell}_i}(V), \tag{3.1}$$

where $\mathcal{I}_{\text{cell}_i}$ is $\mathcal{I}_{\text{cell}}$ as in Equation 2.3 but with parameters specific to the cell $i$, since we connect different cells now. We label these parameters that belong to cell $i$ as $I_{\text{ph}_i}, I_{0_i}, R_{\text{s}_i}, R_{\text{sh}_i}$. Analogously, $\mathcal{V}_{\text{cell}_i}$ is the voltage output as function of current specifically for cell $i$.

So in a parallel set, the limiting factor that is influenced by the other cells is the cell voltage, since all the cells must have the same voltage level. We can see in the figure that for the fully shaded cell the MPP is located at zero voltage, but the power levels for voltages larger than zero and up to the modules open circuit voltage do not decrease by a lot. So the shaded cell's power output at the $V_{\text{MPP}}$ of the fully illuminated cell, is not much lower than the shaded cell's maximum power. Thus, in terms of maximum power output voltages the cells are not really mismatching a lot; at the maximum power point of the parallel set, all the cells are also operating such that the power output is roughly around there individual maximum power.

For a string, the current of one cell has to go through the other cells. The voltage levels of the cells do not directly influence each other, so for example in Figure 21 the open circuit voltage of the string is just twice the open circuit voltage of the illuminated cells. In general we can write:

$$V = \sum_{i=1}^{N_s} \mathcal{V}_{\text{cell}_i}(I). \tag{3.2}$$

The fact that the cells have to have the same current explains the more extreme mismatching for strings. We can see that for current values that are a bit larger than the short circuit current, the voltage of a cell approaches minus infinity rather quickly. So if we want a string to operate at a current that is slightly larger than the short circuit current of the worst cell, then this cell will consume a lot of power because of the large negative voltage. Hence, forcing cells to operate at the same current level has a much more harmful influence on the corresponding voltage, and therefore on the power output of a string. This is why the string is limited by it's worst cell, and why there is no operating point for which all the cells are operating with close to optimal power output.

This effect is the motivation for trying to find more shadow tolerant designs than the widely used series-parallel configuration, since it consists of strings which are very susceptible to partial shading. However, this is not the whole story. In reality bypass diodes are used in modules to reduce mismatch losses and also protect the cells from breaking down due to power dissipation and large negative voltages that exceed breakdown voltages. The bypass diodes also cause the SP configuration to become more tolerant to partial shading.

## 3.3 Bypass diodes

A bypass diode is a non-linear circuit component in PV modules that prevent cells from breaking down. As discussed before, the effects of mismatching can cause some cells to be forced to operate at large negative voltages. When these voltages exceed a certain breakdown voltage, the cell is permanently damaged and this must of course be avoided. Bypass diodes are connected in anti-parallel with a string of cells. Anti-parallel means a parallel connection but with the polarities reversed. So if there is a positive voltage over the string that the bypass diode is in parallel with, then the bypass diode is reverse-biased. Only when the voltage falls below a certain value, namely minus the forward voltage, $-V_f$, of the bypass diode, then current starts flowing through the bypass diode. When the current flows through the diode, there is less current going through the cells, hence the cells are 'bypassed'. The number of cells that should be connected with a bypass diode depends on the forward voltage of the bypass diode and the breakdown

voltages of the cell. If this is chosen correctly, the cells get bypassed before they can reach dangerous negative voltages. As we can see in the following figures, the bypass diode also reduces the loss of power caused by power consumption in cells, especially in strings. Beside the loss of energy yields, power consumption by a cell might also cause the cell to heat up, become a hot-spot and break down. As a general rule a negative power output of a cell is dangerous when it is less than $-2P_{\max}$, where $P_{\max}$ is the maximum power output of the cell.

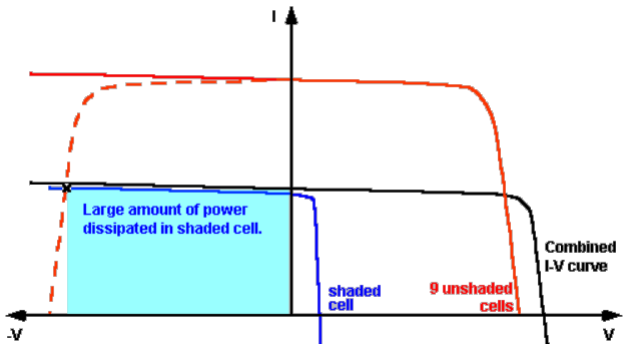


Figure 22: I-V curves of a string of nine unshaded cells, a shaded cell, and the combined string of these cells. The black mark indicates the individual operating point of the shaded cell at the module's $I_{\text{sc}}$. We can see that a large amount of power from the unshaded cells is dissipated in the shaded cell, and the shaded cell is operating at a large negative voltage.[30]

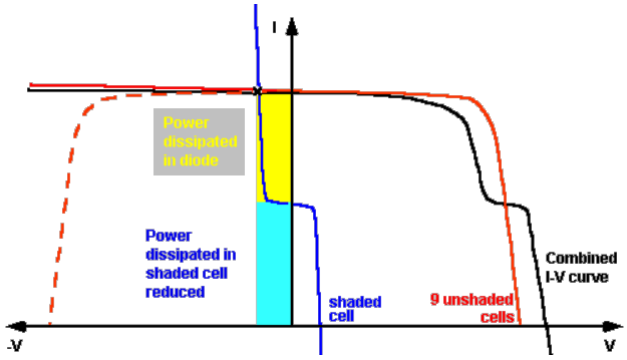


Figure 23: Connecting a bypass diode to the shaded cell limits its reverse voltage. The shaded cell now has much lower reverse voltage and lower power dissipation at the module's $I_{\text{sc}}$. The combined module has much higher current levels than before.[30]

The number of the diodes that are connected to a string of any amount of solar cells, affects the solar array behaviour. In modules made of CIGS cells, every two cells are connected with a Schottky bypass diode. This type of diode has a forward voltage between 0.2V and 0.3V.[31] The breakdown voltage $V_{br}$ of a CIGS cell is $-1.5$V. Although the cell doesn't immediately break at this voltage, it is stable for 60 seconds, it is not adviced to exceed this voltage level.[32] Suppose that there are two CIGS cells connected in series, with one cell shaded, and that string is connected in anti-parallel to a bypass diode (see Figure 24). If the illuminated cell has a voltage of about 0.6V (the open circuit voltage of a MiaSolé CIGS cell is about 0.7V), and the diode is 'turned on', i.e., the voltage over the bypass diode is about $-0.3$V, then the voltage of the shaded cell must be $-0.3 - 0.6 = -0.9$V. So the voltage of the shaded cell does not exceed the

breakdown voltage. Now suppose we connect three cells, of which one shaded, with a bypass diode (see Figure 25). If the illuminated cells operate at 0.6V and the bypass diode operates at $-0.3$V, then the voltage of the shaded cell is $-0.3-0.6-0.6=-1.5$V. So even though there is current bypassed through the diode, the shaded cell operates at a dangerous voltage level. That is why the Schottky diode is suitable to be connected with two CIGS cells and not with more.

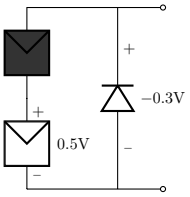


Figure 24: Two CIGS cells with one bypass diode.

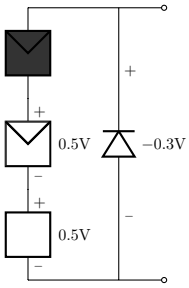


Figure 25: Three CIGS cells with one bypass diode.

For the TCT configuration we don't need to place a bypass diode every two cells but only every two parallel sets. Each cell in the parallel set has the same voltage, thus only entire parallel sets need to be bypassed. Since incorporating bypass diodes can be expensive and labour-intensive, this is a big advantage of the TCT configuration. The resulting SP and TCT modules with bypass diodes will look like the following.

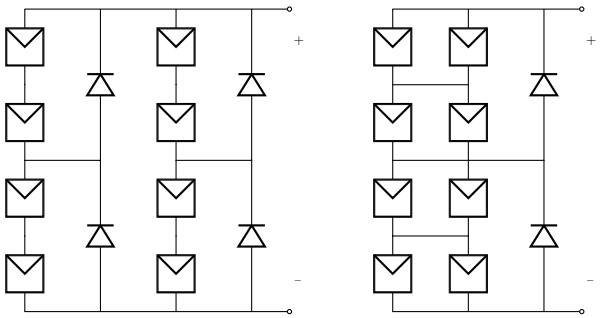


Figure 26: $4 \times 2$ SP and TCT configuration with bypass diodes

If there is an uneven number of cells in the strings or an uneven number of parallel sets, then the last row will get its own bypass diode(s).

We will see later on, in Section 6.1, that including the the bypass diodes can increase the power output of SP by a lot. So where TCT was clearly the better choice before including bypass diodes, with bypass diodes the results aren't that conclusive anymore.

A bypass diode will be modelled as a circuit component with the Shockley diode equation (1.1), but for reversed polarity (because of the anti-parallel connection). Then the diode can be included in the model with a parallel connection to sub-modules. Thus, we define the I-V characteristic of a bypass diode with the following function.

**Definition 3.1.**

$$F_{\mathrm{bd}}(V,I) = I_0\left(\exp(\frac{-qV}{nkT})-1\right) - I$$

Hence, we find the diodes operating points for solving $F_{\text{bd}}(V, I) = 0$.

Usually not much is known about the bypass diode, so we assume the diode's reverse saturation current to be a constant, just as the ideality factor. The temperature of the diode depends on the location of the diode. We don't assume any variations in the diodes temperature, for the changes in irradiance. Temperature can be chosen based on the ambient temperature and location; if the diode is located inside the module it will probably have a temperature close to the module's temperature. Overall, we will model the diode as a more constant component than the PV cells. Finding the $n$ and $I_0$ of the diode, will be based on known specifications like the forward voltage, or a given I-V curve of the diode. But the obtained parameters may vary from the reality when the bypass diodes are connected in a module, because of a different operating temperature, some connection losses due to resistances in wiring, or because given specifications weren't precise. However, the type of diode does affect the modules I-V curve a lot. Therefore, if there are more measurements available, the diode parameters can be fitted to match actual measurements of the module under partial shade.

The Schottky diode used at Solliance is called: Flexible Circuit 201878-001 Flex Schottky Bypass Diode - Thin Film CIGS Solar Qty 100. Some of the specifications are: a maximum reverse voltage of 45V, a maximum forward current of 15A and a leakage current of 0.4mA.

With the Schottky diode connected per two CIGS cell, the maximum reverse current and maximum forward current will clearly be not exceeded. Moreover, we now know that $I_0 = 0.4 \cdot 10^{-3}$A, since leakage current is the same as reverse saturation current. We don't really know the temperature and the ideality factor. However, based on some measurements that we will describe in Section 5.5, the values for the other parameters that came closest to the behaviour of bypass diodes in tested shaded modules are: a diode ideality factor of 1.4 and a temperature of 55 degrees Celsius. From here on out the bypass diodes will be modelled with those parameter values.

## 3.4 Special shading patterns

### 3.4.1 Semi-homogeneous shade

Earlier we saw that the maximum power output for TCT and SP is the same if the irradiance and temperature is uniform. There are more shading scenarios for which TCT and SP have the same maximum power output.

In this section, we will look at TCT modules and SP modules without bypass diodes. We will call a shading pattern a *semi-homogeneous shade* if it either casts a uniform shade on each entire row in a module, i.e., for each row all the cells in that row must have the same irradiance, or if it casts a uniform shade on each entire column in a module, i.e., for each column all the cells in that column must have the same irradiance. See the figure below.

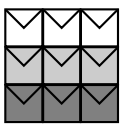

Horizontal
semi-homogeneous shade:
uniform shade per row

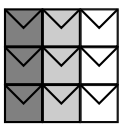

Vertical
semi-homogeneous shade:
uniform shade per column

Note that for a schematic depiction of a module like in this figure, the corresponding TCT and SP modules are connected as they were connected before. This means that

for the SP configuration the columns are connected in series, and then these strings are connected in parallel. For the TCT configuration the rows are connected in parallel and then these parallel sets are connected in series. The positive terminal is always at the top of the module, and the negative terminal is at the bottom.

When there is a horizontally shaped semi-homogeneous shade on a TCT module, then the module is a series connection of homogeneous parallel sets. For a SP module, a horizontal semi-homogeneous shade results in a parallel connection of all the same strings, but the strings themselves might not be homogeneous. For a vertically shaped semi-homogeneous shade this is the other way around: a TCT module consists of the same, possibly non-homogeneous, parallel sets connected in series, and the SP module consists of homogeneous strings connected in parallel. This is clarified by the following picture.

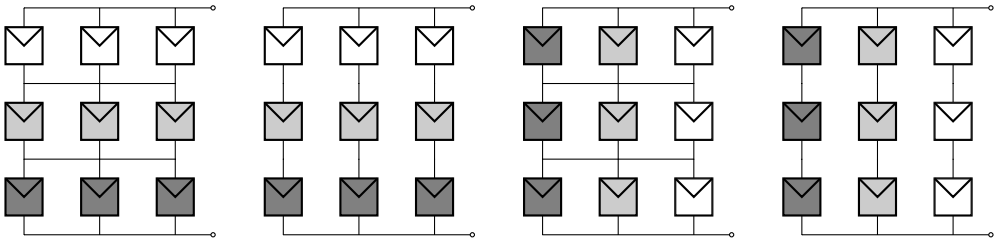

Horizontal semi-homogeneous shade for TCT | Horizontal semi-homogeneous shade for SP | Vertical semi-homogeneous shade for TCT | Vertical semi-homogeneous shade for SP

**Claim 3.1.** We claim that for semi-homogeneous shades, TCT and SP modules have the same I-V curve.

*Proof.* First we need to prove that for a parallel set the output current is an injective function of voltage, and for a string the output voltage is an injective function of current. Let cell $1, 2, \ldots, N_p$ be connected in parallel, and $\nu < \mu$ are two distinct voltage values. Assume that the parallel set has the same current output at both voltages, then by Equation 3.1 we know that $\sum_i \mathcal{I}_{\text{cell}_i}(\nu) = \sum_i \mathcal{I}_{\text{cell}_i}(\mu)$. Hence, $\sum_i \mathcal{I}_{\text{cell}_i}(\nu) - \mathcal{I}_{\text{cell}_i}(\mu) = 0$. But we know that $\mathcal{I}_{\text{cell}}$ is a strictly decreasing function, so $\mathcal{I}_{\text{cell}_i}(\nu) - \mathcal{I}_{\text{cell}_i}(\mu) > 0$ for all $i = 1, \ldots, N_p$. So by contradiction, $\nu$ and $\mu$ have to be the same value and hence the output current of a parallel set is an injective function of the output voltage. In a similar way, using Equation 3.2 and the fact that $\mathcal{V}_{\text{cell}}$ is strictly decreasing, we can prove that the output voltage of a string is an injective function of the output current.

Now assume we have a vertical semi-homogeneous shade on the module.
For SP, each string is homogeneous and each string has the same output voltage $V$. Let the size of the module be $N_s$ x $N_p$. There are $N_p$ strings and since all strings are homogeneous this means there are $N_p$ different cells. For string $S_i$ we have that the total current is $\mathcal{I}_{\text{cell}_i}(V/N_s)$, where $cell_i$ is the cell that makes up string $S_i$. The total output current of the module is $\sum_{i=1}^{N_p} \mathcal{I}_{\text{cell}_i}(V/N_s)$.

For TCT, each parallel set is the same and each parallel set has the same total current. By the fact that for a parallel set the output current is injective as a function of voltage and all parallel sets are the same, we get that all the parallel sets must also have the same total voltage. So the voltage per parallel set is total voltage $V$ of the module divided by the number of parallel sets $N_s$. We get for total current of a parallel set: $\sum_{i=1}^{N_p} \mathcal{I}_{\text{cell}_i}(V/N_s)$. Per construction this is also the total current of the TCT module. Thus, we see that TCT and SP have the same output current as function

of output voltage.
Assume we have a horizontal semi-homogeneous shade on the module.
For TCT, each parallel set is homogeneous and each parallel set has the same output current $I$. We get that for a parallel set $S_i$ the voltage is $\mathcal{V}_{\text{cell}_i}(I/N_p)$, where cell $i$ is the cell that makes up $S_i$. There are $N_s$ parallel sets each of them consisting of one type of the $N_s$ different cells. Thus, the total voltage of the TCT module is $\sum_{i=1}^{N_s} \mathcal{V}_{\text{cell}_i}(I/N_p)$.

For SP, the $N_s$ different cells make up $N_p$ of the same strings. The strings are connected in parallel so all have the same output voltage. By the fact that the output voltage of a string as function of current is injective, and that the strings are all the same, we get that the output current of the strings must also be the same. So the current per string is $I/N_p$, where $I$ is the module's output current. We get that output voltage of a single string is $\sum_{i=1}^{N_s} \mathcal{V}_{\text{cell}_i}(I/N_p)$. Therefore, the output current of the module is $\sum_{i=1}^{N_s} \mathcal{V}_{\text{cell}_i}(I/N_p)$, which is the same as for the TCT configuration. □

### 3.4.2 Shading equivalencies

The order of cells or sub-modules in a set doesn't matter for the output, and therefore some shading patterns turn out to be equivalent. Which patterns are equivalent depends on the topology of the module. In a TCT module the rows are parallel sets, so cells in a row can be interchanged, and the entire rows are connected in series, so entire rows may be interchanged. In a SP module, the columns are strings, so cells in a column can be interchanged, and the entire columns are connected in parallel, so entire columns may be interchanged.

To recap, shading patterns are *TCT-equivalent*, i.e., the same for TCT modules, if one pattern is a permutation of entire rows and/or a permutation of cells inside rows of the other pattern. Shading patterns are *SP-equivalent*, i.e., the same for SP modules, if one pattern is a permutation of entire columns and/or a permutation of cells inside columns of the other pattern. Two shading patterns will be called *equivalent* if they are TCT- and SP-equivalent, which means that two patterns are equivalent if one pattern is a permutation of entire rows and/or entire columns of the other pattern.

For example, in the figures below we have: Figure 27 is TCT-equivalent to Figure 28, SP-equivalent to Figure 29, and equivalent to Figure 30.

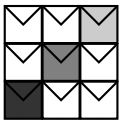

Figure 27

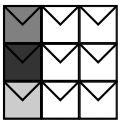

Figure 28

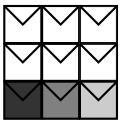

Figure 29

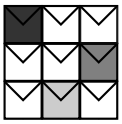

Figure 30

## 3.5 System of equations

In the previous section, we saw the calculation of output voltage or current for modules under semi-homogeneous shading. In this calculation we needed to use that the sub-modules where either all the same or all homogeneous. If this is not the case, we can not formulate the output current or voltage with a single function as we did there. For example, for a TCT module we can calculate the current of each parallel set with Equation 3.1: say that parallel set $S_i$ has output voltage $V_{S_i}$ then the output current is $I_{S_i} = \sum_{j=1}^{N_p} \mathcal{I}_{\text{cell}_i}(V_{S_i})$. The problem is that we don't know what $V_{S_i}$ is, if not all the parallel sets are the same. We only know that the $V_{S_i}$ values add up to be the voltage output of the model. Analogously, we don't directly know the current per string of a SP module, so we don't know the voltages and currents of the cells. As a result,

even for a 2x2 SP or TCT module we can't solve the output current for a given voltage analytically. Instead, in order to solve the I-V curve of a non-homogeneous module we need to formulate a system of equations.

Say we have a module $M$ with $n$ number of base elements. *Base elements* are the PV cells and bypass diodes. Each cell or bypass diode $i$ has a certain unknown voltage $V_i$ and current $I_i$. Note that this gives us $2n$ unknown variables: $V_1, \ldots, V_n, I_1, \ldots, I_n$. We either have a given output voltage, $V_{\text{out}}$, of the module and need to calculate the module's corresponding output current, $I_{\text{out}}$, or vice versa. So in total we have $2n+1$ unknowns, since one of $I_{\text{out}}, V_{\text{out}}$ is given and the other is unknown. For each cell or bypass diode $i$ we have the equation $F_i(V_i, I_i) = 0$. For a PV cell $F_i = F_{\text{cell}_i}$ as in the Definition 2.1, but with parameters $I_{\text{ph}_i}, I_{0_i}, R_{\text{s}_i}, R_{\text{sh}_i}$ specific to this cell $i$. For a bypass diode we have $F_i = F_{\text{bd}}$ as in Definition 3.1, with the parameters specific to the chosen type of bypass diode. This means we get the $n$ equations for all the base elements: $F_i(V_i, I_i) = 0$.

On top of that we have information about the interconnections. A module for the purpose of this research can always be structured as a combination of series and parallel connections. So a module is a set of sets, PV cells, and/or bypass diodes. The sets in a module can in term consist of multiple connected sets again. In other words, a module is a combination of parallel and series connections of smaller sub-modules. At the base, if we keep breaking down the sub-modules into smaller sub-modules, we always end up with sets consisting only of base elements.

**Claim 3.2.** We claim that we can describe all the interconnections in module $M$, with $n-1$ equations of the form $\sum_{i=1}^{n} \gamma_i V_i + \delta_i I_i = 0$, where all $\gamma_i, \delta_i \in \{-1, 0, 1\}$ and either all $\gamma_i$ or all $\delta_i$ are zero.

**Claim 3.3.** Secondly, we claim that the module's output voltage is of the form $\sum_{i=1}^{n} \alpha_i V_i$, and the output current is of the form $\sum_{i=1}^{n} \beta_i I_i$, where $\alpha_i, \beta_i \in \{0, 1\}, \forall i \in \{1, \ldots, n\}$. We proof this inductively.

*Proof.* The smallest sub-modules that we can break the module down to, are strings or parallel sets of only base elements. We see that for this base case the claims holds: Suppose the base elements in such a set are numbered $1 \leq k, k+1, \ldots, k+(m-1) \leq n$, i.e., the set has $m$ base elements. Then if the set is a string, we know $I_k = I_{k+1} = \ldots = I_{k+m-1}$. In other words, we can describe the set's interconnections with $I_{k+1} - I_k = 0, \ldots, I_{k+m-1} - I_k = 0$. If the set is a parallel set then the set's interconnections are described with equations $V_{k+1} - V_k = 0, \ldots, V_{k+m-1} - V_k = 0$. In both cases, this is a system of $m-1$ linear equations of the form $\sum_{i=1}^{n} \gamma_i V_i + \delta_i I_i = 0$, with coefficients $\gamma_i, \delta_i \in \{-1, 0, 1\}$ and where either all the coefficients $\gamma_i$ or all $\delta_i$ are zero (and note that $\gamma_i, \delta_i = 0$ for $i \notin \{k, k+1, \ldots, k+m-1\}$). Also we know that the output current of the set is $I_k$, in case of a series set, or $\sum_{j=k}^{k+m-1} I_j$, in case of a parallel set. And the output voltage is $\sum_{j=k}^{k+m-1} V_j$, in case of a series set, or $V_k$ in case of a parallel set. So the claims 3.2 and 3.3 hold for sets consisting only of base elements.

Now, assume that for sub-modules of module $M$ the claims 3.2 and 3.3 are true. This is the induction hypothesis (IH). Suppose the module $M$ consist of $m$ sub-modules $S_1, \ldots, S_m$. Each submodule $S_k$, $k \in \{1, 2, \ldots, m\}$, has a certain number of base elements, say $n_k$ elements. Let these base elements be given index numbers, and these numbers form the set $N_k \subset \{1, ..., n\}$. By IH we get that the configuration of each submodule $S_k$ can expressed in a system of $n_k - 1$ equations of the form

$\sum_{j\in N_k} \gamma_j V_j + \delta_j I_j$, where $\gamma_j, \delta_j \in \{-1, 0, 1\}$ and either all $\gamma_j$ or all $\delta_j$ are zero. In total this gives us $(n_1-1)+(n_2-1)+\ldots+(n_m-1) = (n_1+n_2+\ldots+n_m)-m = n-m$ equations. These equations describe the configurations for each of the sub-modules internally, but we also have equations for the interconnection between the sub-modules $S_1, \ldots, S_m$. If $M$ is a string of the sub-modules we get the $m-1$ equations $I_{S_2} - I_{S_1} = 0$, $I_{S_3} - I_{S_1} = 0, \ldots, I_{S_m} - I_{S_1} = 0$, and if $M$ is a parallel set then we get the $m-1$ equations $V_{S_2} - V_{S_1} = 0, V_{S_3} - V_{S_1} = 0, \ldots, V_{S_m} - V_{S_1} = 0$. Let's call these equations the connection equations. By IH we know that claim 3.3 holds for all sub-modules, i.e., for all $k \in \{1, 2, \ldots, m\}$ we have $\alpha_j, \beta_j \in \{0, 1\}, j \in N_k$ such that $I_{S_k} = \sum_{j\in N_k} \alpha_j V_j$ and $V_{S_k} = \sum_{j\in N_k} \beta_j I_j$. Substituting this into the connection equations from before and keeping in mind that the sets $\{N_k |\ k = 1, \ldots, m\}$ are disjunct by definition and $\bigcup\{N_k |\ k = 1, \ldots, m\} = \{1, 2, \ldots, n\}$, we get $m-1$ equations of the form $\sum_{i=1}^{n} \gamma_i V_i + \delta_i I_i$, where all $\gamma_i, \delta_i \in \{-1, 0, 1\}$ and either all $\gamma_i$ or all $\delta_i$ are zero. In conclusion, in total we get $(n-m)+(m-1) = n-1$ equations of the form as in claim 3.2 to describe the configuration of $M$.
Finally, note that if the module is a parallel set the total voltage and current are

$$V_M = V_{S_1} = \sum_{j\in N_1} \alpha_j V_j, \text{ where all } \alpha_j \in \{0, 1\}, \text{ and}$$
$$I_M = \sum_{k=1}^{m} I_{S_k} = \sum_{k=1}^{m} \sum_{j\in N_k} \beta_j I_j = \sum_{i=1}^{n} \beta_i I_i, \text{ where all } \beta_i \in \{0, 1\}.$$

Analogously, if $M$ is a series set the total voltage and current for the module are

$$V_M = \sum_{k=1}^{m} V_{S_k} = \sum_{i=1}^{n} \alpha_i V_i, \text{ where all } \alpha_i \in \{0, 1\} \text{ and}$$
$$I_M = I_{S_1} = \sum_{j\in N_1} \beta_j I_j, \text{ where all } \beta_j \in \{0, 1\}.$$

This proves that claim 3.3 also holds. □

To calculate the output current/voltage and incorporate the given voltage/current value of the module, the final two equations of the system are $V_M - V_{\text{out}} = 0$ and $I_M - I_{\text{out}} = 0$, where $V_M$ and $I_M$ can be expressed with the formulas seen in claim 3.3. In conclusion, we have $n$ equations for the base element behaviour: $F_i(V_i, I_i) = 0$. We'll define $\mathcal{F} = \left\{ F_i(V_i, I_i) \quad \text{for all } i \in \{1, 2, \ldots, n\} \right.$.

We have $n-1$ equations describing the interconnections as seen in claim 3.2 and its proof above. We'll define $\mathcal{H}$ to be the system of the left-hand sides of these $n-1$ equations. Note that the coefficients $\gamma$ and $\delta$ are defined per equation, so
$\mathcal{H} = \left\{ \quad \sum_{i=1}^{n} \gamma_{k,i} V_i + \delta_{k,i} I_i \quad \text{for all } k \in \{1, 2, \ldots, n-1\} \right.$,
where for each $k$ we have either $\gamma_{k,i} \in \{-1, 0, 1\}, \delta_{k,i} = 0\ \forall i \in \{1, \ldots, n\}$ or $\delta_{k,i} \in \{-1, 0, 1\}, \gamma_{k,i} = 0\ \forall i \in \{1, \ldots, n\}$.

Finally, we define system $\mathcal{K}$ to be the two formulas that include the output voltage and current formula from claim 3.3, and the given and unknown values of $V_{\text{out}}$ and $I_{\text{out}}$. W.l.o.g. the given value will be $\nu$ for the output voltage and $I_{\text{out}}$ is the unknown variable from here on out. Then we have $\mathcal{K} = \begin{cases} \sum_{i=1}^{n} \alpha_i V_i - \nu, \text{ with } \alpha_i \in \{0, 1\}\ \forall i \in \{1, \ldots, n\} \\ \sum_{i=1}^{n} \beta_i I_i - I_{\text{out}}, \text{ with } \beta_i \in \{0, 1\}\ \forall i \in \{1, \ldots, n\} \end{cases}$
Let $\mathcal{G}$ be the complete system $(\mathcal{F}, \mathcal{H}, \mathcal{K})$. Then to calculate module's (I-V) point $\mathcal{G} = \mathbf{0}$ needs to be solved. This system has $n + (n-1) + 2 = 2n + 1$ equations and $2n + 1$ unknown variables, therefore it is a square system and has a unique solution.

Let us illustrate the system of equations with an example. As seen in the description of $\mathcal{G}$ each PV cell and bypass diode gets assigned a number. As a convention we number the sets and base elements inside a (sub-)module from left to right and top to bottom, see Figure 31.

If we assume that the output voltage is given, $V_{\text{out}} = \nu$. Then this module has the 13 unknown variables:
$V_1, V_2, \ldots, V_6, I_1, I_2, \ldots, I_6, I_{\text{out}}$. The $\mathcal{F}$ part of the system of equations consists of $F_i(V_i, I_i)$, $i \in 1, \ldots, 6$. For the equations describing the interconnections we work from the inside out.

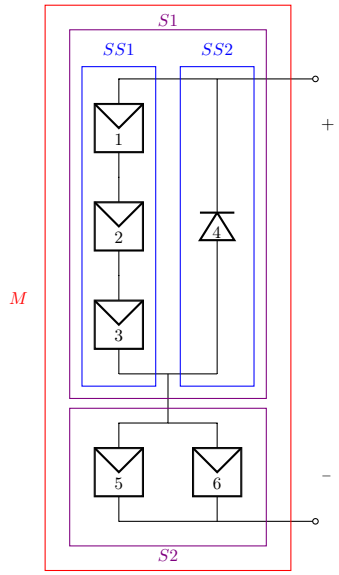


Figure 31: Example of a (non-realistic) module, divided into sub-modules and numbered base elements

$$\mathcal{H} = \begin{cases} \text{string } SS1: \begin{cases} I_2 - I_1 \\ I_3 - I_1 \end{cases} \\ \text{string } SS2: \ / \\ \text{parallel set } S1: \ V_{SS2} - V_{SS1} \\ \text{parallel set } S2: \ V_6 - V_5 \\ \text{string } M: \ I_{S2} - I_{S1} \end{cases}$$

Note that this gives us 5 equations, as required. And building up from the sub-modules with only base elements we get: $V_{SS2} = V_4, V_{SS1} = V_1 + V_2 + V_3, I_{S2} = I_5 + I_6$ and $I_{S1} = I_{SS1} + I_{SS2} = I_1 + I_4$. We get

$$\mathcal{H} = \begin{cases} I_2 - I_1 \\ I_3 - I_1 \\ V_4 - V_1 - V_2 - V_3 \\ V_6 - V_5 \\ I_5 + I_6 - I_1 - I_4 \end{cases}$$

Lastly, we get the two equations for the output voltage and current of the entire module.

$$\mathcal{K} = \begin{cases} V_M - \nu \\ I_M - I_{\text{out}} \end{cases}$$

For $V_M$ we can write $V_{S1} + V_{S2} = V_{SS1} + V_5 = V_1 + V_2 + V_3 + V_5$, and for $I_M$ we can write $I_{S1} = I_{SS1} + I_{SS2} = I_1 + I_4$. Hence,

$$\mathcal{K} = \begin{cases} V_1 + V_2 + V_3 + V_5 - \nu \\ I_1 + I_4 - I_{\text{out}} \end{cases}$$

In conclusion, the total system $\mathcal{G} = \begin{cases} \mathcal{F} \\ \mathcal{H} \\ \mathcal{K} \end{cases} = \mathbf{0}$
describes the PV module $M$ with 13 equations and 13 unknown variables.

# 4 MATLAB model

For the purpose of this research, understanding the electrical behaviour of SP and TCT configurations under partial shading, a generic model was developed in MATLAB to calculate maximum power points and entire P-V and I-V curves of nonhomogeneous modules. The model takes into account the users choice of irradiance, ambient temperature, number of cells, interconnection topology, type of bypass diode, number of bypass diodes and type of cells in the PV module. Also, the model can be used to observe what is happening internally in the module, by calculating the operating points for all the individual cells, at a specific operating point of the entire PV module. Though the model is not limited to thin-film PV modules, the simulated results generated with the model in the next chapters will be specifically for thin-film since that is the objective of this research.

The theoretical framework that is described in the previous chapters is the basis that the MATLAB model is built on. However, there are some (numerical) methods applied in the model that deserve some additional elaboration. But let's first discuss the general structure of the model.

## 4.1 Structure of the model

The structure of the model in MATLAB is based on definition of classes. The module components PV cell, PV set and bypass diodes are all defined as classes with certain properties and methods. For an instance of the `PVcell` class, the properties given by the manufacturer and ambient conditions are user-defined, and then the corresponding parameters of the I-V characteristic are calculated, as discussed in Section 2.4. An instance of the `BypassDiode` class has the properties $I_0, n$ and $T$ defined by the user. An instance of the `PVset` class is a set of `PVcell`-type objects, `BypassDiode`-type objects, and/or more `PVset`-type objects. The configuration, 'parallel' or 'series', and array of the sub-modules are given by the user. So in the same way as described in the theory in Section 5.1, a PV module is inductively defined as a `PVset`-type object consisting of other PV sets or base elements. For example, let `c0` be a `PVcell`-type object, then we can make a $2 \times 3$ TCT module (without bypass diodes) with the constructor `PVset('series', [PVset('parallel', [c0, c0, c0]), PVset('parallel', [c0, c0, c0])])`.

All of the three defined classes have a `Current(obj,V)` method, which calculates the current(s) of an object `obj` for a voltage value `V` or an array of voltage values `V`. Similarly, `Voltage(obj, I)` calculates the output voltage(s) of `obj` corresponding to a current value `I` or an array of current values `I`. For a PV cell the current and voltage are calculated with the Lambert $W$ function as in Equation 2.3 and 2.4. For a bypass diode, the current as function of voltage is calculated with the Shockley diode equation, see Equation 1.1, except with the voltage multiplied with a factor $-1$ because of the reversed polarity as explained in Section 3.3. The inverse of that equation,

$$V = -\frac{nkT}{q} \ln\left(\frac{I}{I_0} + 1\right),$$

is used to calculate the voltage as function of the current for the bypass diode. For a PV set the current and voltage are calculated with the system of equations as described in Section 3.5. Each of the classes have methods that, given a vector of unknown variables and an array of index number(s) of base element(s), calculates the system of equations for an object of the class. The system of equations of a `PVset` object is then inductively constructed from the base up: each base element gets assigned a number, this is saved in a property of the `PVset` object called `Layout`, then for each of the sub-modules the method is called which constructs the system of equations for the sub-module, given

the unknown variables of the total module and the index numbers of the base elements in that sub-module. For example, let's say we have a module with 5 base elements and vector of unknown variables $\mathbf{x} = (V_1, V_2, V_3, V_4, V_5, I_1, I_2, I_3, I_4, I_5, I_{\text{out}})$. Then a `PVcell`-type object in the module with assigned index number 4, will have a method that, given the index number '4' and the vector of variables $\mathbf{x}$, returns its system of equations: the equation $F_{\text{cell}_4}(\mathbf{x}_4, \mathbf{x}_9) = 0$. Note that $\mathbf{x}_4 = V_4$ and $\mathbf{x}_9 = I_4$. In the `PVset` method, the system of equations of the sub-modules will be combined with the equations for the interconnection between the sub-modules and with the equations for the module's voltage output and current output to form the total system of equations (as described in Section 3.5). Then in the `Current` or `Voltage` method of a `PVset` object, the system of equations is solved for a given output voltage or current of the module. We'll elaborate on the solving of the system in the next section.

The function `plotIV` is defined to plot the I-V (and P-V) curve of a module or cell, using the `Current` method to calculate (I-V) points which are then linearly interpolated. The methods `Current` and `Voltage` can return not only the module's operating point at a given voltage or current, but also the operating points of each individual base element at that point. This way the internal workings of a module can be better understood. Another practical function in the model is `makeModule`. This allows for the user to easily make a TCT or SP module with or without bypass diodes, instead of having to define the module inductively as a PV set of sets, as shown before. The function `makeModule` can make a module, as a `PVset` type, based on a given matrix of cells, possibly a bypass diode, and the configuration 'TCT' or 'SP'. Note that the ambient temperature and irradiance are known, because they are defined as properties of the `PVcell` object. The function `makeModule` is adapted for CIGS modules, so the `BypassDiode` object is connected per two cells, or per two parallel sets of cells in case of the TCT configuration. If there is an uneven number of rows in the matrix of cells, then the last cells in a string, or the last parallel set, are also connected to one bypass diode. When there is no `BypassDiode` object given to the function `makeModule`, then a module without bypass diodes is created. Another option of input for the `makeModule` is to enter, instead of a matrix of cells, an irradiance matrix, ambient temperature and `PVcell` object. In that case, the function defines a module based on the irradiance matrix: an $N_s \times N_p$ irradiance matrix defines an $N_s \times N_p$ PV module where the cells are the given `PVcell` object but with the given ambient temperature and with for each cell the irradiance value of the corresponding entry in the given irradiance matrix. The `PVcell` method `changeGandTambient` will be called to change the ambient temperature and the irradiance of the `PVcell` object, and this method will also change the dependent parameters $I_0, I_{\text{ph}}$ and $T_{\text{cell}}$ of the cell accordingly. It is important to note here that a matrix, either irradiance matrix or matrix of cells, always defines the same interconnection layout as a shading pattern would (see Section 3.4).

## 4.2 Solving the system of equations

The system of equations of a PV module is solved in MATLAB using the trust-region method. This is the most suitable method considering that an initial guess for an I-V point of a module, which needs to be supplied to the numerical method, is hard to estimate. The trust-region method turns out to be the fastest gradient method compared with other numerical methods, and the trust-region method can guarantee stability regardless of the initial conditions[33,27]. The MATLAB function used to solve the system of equations is called `fsolve`. This function can be chosen with a trust-region method option. We can also supply the Jacobian matrix of the system of equations to `fsolve`. This decreases the computing time vastly, since the Jacobian matrix is sparse for our system, which isn't recognised automatically. So if the Jacobian matrix isn't

supplied, then at each iteration of the solving steps in `fsolve` the Jacobian is calculated for all entries, even the zero-entries.

### 4.2.1 Jacobian matrix of the system of equations

Let $\mathcal{G} = \mathbf{0}$ be the system of equations for a PV module $M$ with $n$ base elements, as seen in Section 3.5. W.l.o.g. we can assume that the output voltage is the given value and the vector of unknown variables is $\mathbf{x} = (V_1, V_2, \ldots, V_n, I_1, I_2, \ldots, I_n, I_{\text{out}}) \in \mathbb{R}^{2n+1}$. The system $\mathcal{G}$ consists of three parts $\mathcal{F}, \mathcal{H}$ and $\mathcal{K}$.
Part $\mathcal{F}$:
This part consists of the functions $F_i(V_i, I_i)$ for all base elements $i \in \{1, 2, \ldots, n\}$. The derivative of $F_i$ with respect to $\mathbf{x}$ is

$$\frac{dF_i(V_i, I_i)}{d\mathbf{x}} = [0, \ldots, 0, \underset{\substack{\uparrow \\ i\text{-th entry}}}{\frac{\partial F_i(V_i, I_i)}{\partial V_i}}, 0, \ldots, 0, \underset{\substack{\uparrow \\ (n+i)\text{-th entry}}}{\frac{\partial F_i(V_i, I_i)}{\partial I_i}}, 0, \ldots, 0].$$

Using Definition 2.1, we get for a PV cell:

$$\frac{\partial F_{\text{cell}}(V, I)}{\partial V} = -I_0 \cdot \frac{q}{nkT} \exp\left(\frac{q(V + IR_{\text{s}})}{nkT}\right) - \frac{1}{R_{\text{sh}}} \quad \text{and}$$
$$\frac{\partial F_{\text{cell}}(V, I)}{\partial I} = -I_0 \cdot \frac{qR_{\text{s}}}{nkT} \exp\left(\frac{q(V + IR_{\text{s}})}{nkT}\right) - \frac{R_{\text{s}}}{R_{\text{sh}}} - 1.$$

Using Definition 3.1, we get for a bypass diode:

$$\frac{\partial F_{\text{bd}}(V, I)}{\partial V} = -I_0 \cdot \frac{q}{nkT} \exp\left(\frac{-qV}{nkT}\right) \quad \text{and}$$
$$\frac{\partial F_{\text{bd}}(V, I)}{\partial I} = -1.$$

In conclusion, we get

$$\nabla\mathcal{F} = (a_{ij}) \in \mathbb{R}^{n \times (2n+1)}, \text{ where } a_{ij} = \begin{cases} \frac{\partial F_i(\mathbf{x}_i, \mathbf{x}_{i+n})}{\partial \mathbf{x}_j} & \text{if } j \in \{i, i+n\} \\ 0 & \text{otherwise} \end{cases}.$$

Note that this is a sparse matrix.
Part $\mathcal{H}$:
This part of the system consists of the $n-1$ formulas describing the interconnections in the module. In Section 3.5 we saw that

$$\mathcal{H} = \Big\{ \quad \sum_{i=1}^{n} \gamma_{k,i} V_i + \delta_{k,i} I_i \quad \text{for all } k \in \{1, 2, \ldots, n-1\}$$

where for each $k$ we have either $\gamma_{k,i} \in \{-1, 0, 1\}, \delta_{k,i} = 0 \ \forall i \in \{1, \ldots, n\}$ or $\delta_{k,i} \in \{-1, 0, 1\}, \gamma_{k,i} = 0 \ \forall i \in \{1, \ldots, n\}$. We get

$$\nabla\mathcal{H} = \frac{d\mathcal{H}}{d\mathbf{x}} = \begin{pmatrix} \gamma_{1,1} & \cdots & \gamma_{1,n} & \delta_{1,1} & \cdots & \delta_{1,n} & 0 \\ \vdots & \ddots & & & & & \\ \gamma_{n-1,1} & \cdots & \gamma_{n-1,n} & \delta_{n-1,1} & \cdots & \delta_{n-1,n} & 0 \end{pmatrix} \in \{-1, 0, 1\}^{(n-1) \times (2n+1)}$$

Since in each row either all $\delta$ or all $\gamma$ are zero, $\nabla\mathcal{H}$ will also be sparse.
Part $\mathcal{K}$:

This part contains the formulas considering the module's output voltage and current. As seen in Section 3.5, we have $\mathcal{K} = \begin{cases} \sum_{i=1}^{n} \alpha_i V_i - \nu, \text{ with } \alpha_i \in \{0,1\} \ \forall i \in \{1,\dots,n\} \\ \sum_{i=1}^{n} \beta_i I_i - I_{\text{out}}, \text{ with } \beta_i \in \{0,1\} \ \forall i \in \{1,\dots,n\} \end{cases}$.
So,

$$\nabla\mathcal{K} = \begin{pmatrix} \alpha_1 & \dots & \alpha_n & 0 & \dots & 0 & 0 \\ 0 & \dots & 0 & \beta_1 & \dots & \beta_n & -1 \end{pmatrix} \in \{-1,0,1\}^{2\times(2n+1)}.$$

In conclusion, the Jacobian of system $\mathcal{G}$ is

$$\nabla\mathcal{G} = \begin{pmatrix} \nabla\mathcal{F} \\ \nabla\mathcal{H} \\ \nabla\mathcal{K} \end{pmatrix},$$

which is a sparse $(2n+1)\times(2n+1)$ matrix.

### 4.2.2 Euler's method

The MATLAB method `fsolve` finds the solution of the vector of unknown variables $\mathbf{x} = (V_1, V_2, \dots, V_n, I_1, I_2, \dots, I_n, I_{\text{out}}) \in \mathbb{R}^{2n+1}$ for the system of equations $\mathcal{G} = \mathbf{0}$. Note that the formulas in $\mathcal{G}$ are functions of $\mathbf{x}$. The method `fsolve` requires an initial guess for $\mathbf{x}$ to be able to solve the system. Since the trust-region method is used as system solver in `fzero`, the zero-vector is a good enough initial guess to ensure convergence to the solution. However, the closer the initial guess is to the actual value of $\mathbf{x}$, the fewer iteration steps are needed to converge to the solution of the system and thereby, less computation time will be needed. For the calculation of the I-V curve the `Current` method is used for an array of voltages ranging from before 0 to after $V_{\text{oc}}$ with small voltage increments in between. This means that we can base the initial guess for the solution of $\mathbf{x}$ at a voltage $\nu_t$ on the solution for the previous voltage $\nu_{t-1}$ in the array. The way we estimate the initial guess based on the previous solution is with the explicit Euler method.

Let $G : \mathbb{R}^n \to \mathbb{R}^m$ be given, and $x : \mathbb{R} \to \mathbb{R}^{n-1}$, $t \mapsto \mathbf{x} = (x_1, x_2, \dots, x_{n-1})$ is an unknown function. Suppose that we have the following system of equations;

$$G(x(t), t) = \mathbf{0}, \text{ with initial point } G(\mathbf{x_0}, t_0) = \mathbf{0} \text{ where } \mathbf{x_0} = x(t_0),$$

and we want to find an approximation for the solution at a next time step $t_1$. In other words we want to find $x(t_1)$ for which $G(x(t_1), t_1) = 0$.

We know $\frac{dG}{dt} = \mathbf{0} \in \mathbb{R}^m$, since $G(\mathbf{x}, t) = 0$. We also know that $\frac{dG}{dt} = \frac{\partial G}{\partial \mathbf{x}} \cdot \frac{d\mathbf{x}}{dt} + \frac{\partial G}{\partial t}$ because of the chain rule for total derivatives. So,

$$\frac{\partial G}{\partial \mathbf{x}} \cdot \frac{d\mathbf{x}}{dt} = -\frac{\partial G}{\partial t}.$$

Let $J$ bet the Jacobian, i.e., $J = \nabla G$, then $\frac{\partial G}{\partial \mathbf{x}} = J[1,2,\dots,m; 1,2,\dots,n-1]$, the submatrix of $J$ consisting of rows 1 to $m$ and columns 1 to $n-1$. We define $G_x := \frac{\partial G}{\partial \mathbf{x}}$. Similarly, we have $G_t := \frac{\partial G}{\partial t} = J[1,2,\dots,m; n]$. Thus everything combined we get for $t_0$:

$$G_x(x(t_0), t_0) \cdot x'(t_0) = -G_t(x(t_0), t_0).$$

Assuming that the Jacobian $J$ is known, we can get $x'(t_0) \in \mathbb{R}^{n-1}$ by solving that equation. Finally, we get an approximation for the solution at next time step $t_1$ with Euler's estimation:

$$x(t_1) \approx x(t_0) + x'(t_0) \cdot \Delta t,$$

where $\Delta t = t_1 - t_0$ must be sufficiently small.

Now let's apply Euler's method to the system of equations of a PV module. Instead of time steps $\Delta t$ we have voltage steps $\Delta v$. Let $G$ be the system $\mathcal{G}$ from Section 3.5, but with the module's output voltage seen as a variable $v$ instead of as a given value $\nu$. Clearly, the vector of unknown variables $\mathbf{x} = (V_1, \ldots, V_n, I_1, \ldots, I_n, I_{\text{out}})$ depends on the choice of $v$. Let $x : \mathbb{R} \to \mathbb{R}^{2n+1}$ be the function that maps $v$ to the corresponding vector of variables $\mathbf{x} = (V_1(v), V_2(v), \ldots, V_n(v), I_1(v), I_2(v), \ldots, I_n(v), I_{\text{out}}(v))$. Then we get the system of equations $G(x(v), v) = \mathbf{0}$. Note that $G : \mathbb{R}^{2n+2} \to \mathbb{R}^{2n+1}$. Given an initial solution $(\mathbf{x_0}, v_0)$ with $\mathbf{x_0} = x(v_0)$, we want to find an approximation of $\mathbf{x_1} = x(v_1)$ such that $G(\mathbf{x_1}, v_1) = 0$. Since $\mathcal{G}$ is the system $G$ restricted to its first $2n + 1$ variables, we see that $G_x = \nabla\mathcal{G}$. In all the functions of $\mathcal{G}$, $\nu$ only occurs in the first function of part $\mathcal{K}$, which describes the output voltage of the module as $\sum_{i=1}^{n} \alpha_i V_i - \nu$. Thus, because $\nu$ is replaced with variable $v$ in $G$ and the first function of part $\mathcal{K}$ corresponds to the $2n$-th function of $G$, we conclude that $G_v = \begin{pmatrix} 0 \\ \vdots \\ 0 \\ -1 \\ 0 \end{pmatrix} \in \mathbb{R}^{2n+1}$.

Therefore, we can find $x'(v_0)$ by solving

$$\nabla\mathcal{G}(x(v_0), v_0) \cdot x'(v_0) = -(0, \ldots, 0, -1, 0),$$

as is shown above. Then, we get the Euler estimation:

$$x(v_1) \approx x(v_0) + x'(t_0) \cdot \Delta v.$$

In the MATLAB model, if the `Current` method is called for a `PVset` object and an array of voltages $V = [v_0, v_1, \ldots]$, then the used method `fsolve` is given the zero-vector as initial guess for $v_0$, but for the succeeding voltages the described Euler method is used to determine the initial guess which is given to `fsolve`. Analogously, the Euler method will be used in the `PVset`'s `Voltage` method for an array of currents.

## 4.3 Computing time

It was found that constructing the Jacobian and giving this as input to the `fsolve` method along with the system of equations, improves the computing time drastically (compared with only giving the system of equations as input an not the Jacobian). For example, plotting the I-V curve of four $4\times3$ modules, namely SP and TCT both with and without bypass diodes, for a certain random shading pattern took 626 seconds (over 10 minutes) before including the Jacobian matrix. After including the Jacobian this took only 15 seconds. It was also found that including Euler's method had an improving effect of about $30 - 40\%$ on the computing time, compared with just using the solution of the previous voltage (or current) as initial guess.

Overall, the computing time depends on the size of the module, the shading pattern and whether or not there are bypass diodes. Calculating the I-V curve of small modules can be done in a matter of seconds. Whereas the I-V curves of the largest modules simulated in this research, $24 \times 4$, took between 2 and 6 minutes to plot.

# 5 Verification of the model

In the following experiment we measured I-V curves of four different PV modules for partial shading scenarios. The results were compared with the simulated I-V curves in order to verify the accuracy of our model.

## 5.1 The PV modules and shading patterns

To try different cell and module sizes, one of the module types is a $12 \times 4$ module built with 'half' CIGS MiaSolé cells, and the other module is a $24 \times 4$ module built with 'quarter' CIGS MiaSolé cells. A SP and TCT configuration with bypass diodes was made for both module sizes. So in total there are 4 modules to measure. The 'half' CIGS cell is a MiaSolé cell cut to a length of 130mm instead of the full length of 312mm (so technically less than half). This results in a reduced cell output current of 130/312 times the original current output. The output voltage is, in theory, not affected by cutting the cell. The 'quarter' CIGS cell is cut to a length of 65mm, and therefore has a (65/312)-th part of the original current.

The modules are fairly large, which makes it possible to measure multiple interesting shading patterns. The shading patterns and naming of the patterns can be found in Appendices III and IV.

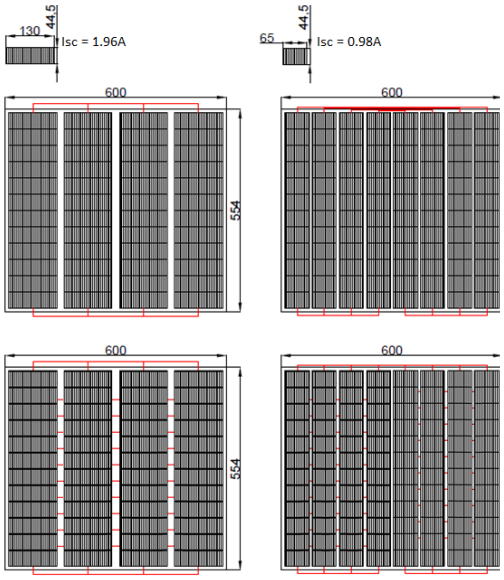


Figure 32: Schematic layout of, from left to right and top to bottom, the SP $12 \times 4$, SP $24 \times 4$, TCT $12 \times 4$ and TCT $24 \times 4$ modules. Dimensions are in milimeters.

In the figure above we see the layout of the modules, where the strings are split in half and placed side by side for the $24 \times 4$ modules to get practical dimensions. The short circuit current and open circuit voltage for the $12 \times 4$ modules will be approximately 8A and 8V respectively. The $24 \times 4$ modules will approximately have $I_{\text{sc}} = 4\text{A}$ and $V_{\text{oc}} = 16\text{V}$.

In the lamination step of the modules some creasing of the top layer occurred for the TCT $12 \times 4$, SP $12 \times 4$ and TCT $24 \times 4$ modules. Despite this all the modules reasonably worked as expected, except for the SP $12 \times 4$ module. More about this later.

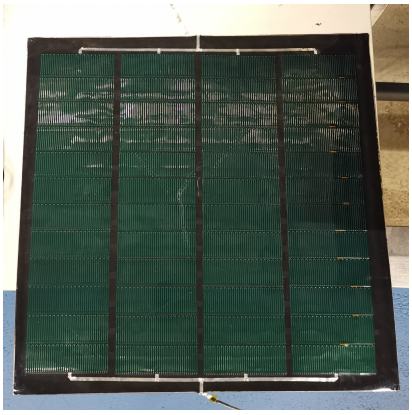

TCT $12 \times 4$

SP $12 \times 4$

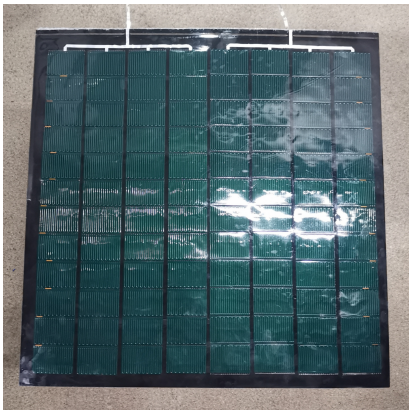

TCT $24 \times 4$

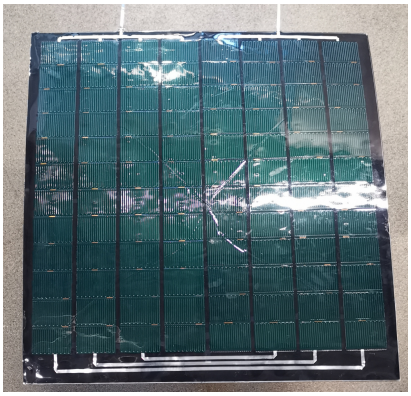

SP $24 \times 4$

Figure 33: PV modules. For the $12 \times 4$ modules the positive terminal is oriented at the top of the pictures, and for the $24 \times 4$ modules the positive terminal is at the top right, while the negative terminal is at the top left of the picture.

## 5.2 Solar simulator and irradiance

Solar simulators are devices that illuminate a certain area, simulating the light of the sun. At the Solliance lab there are two sun simulators for which the PV modules can be mounted on a vertical rack. This makes it possible to easily stick shapes on the module to create various shading patterns, without having to take the module out of the simulator each time. Of the two solar simulators one is made with LED lights and one is a made with gas-discharge and halogen lamps. The LED solar simulator has the largest illumination surface. The size of our modules is approximately 60cm by 60cm and they would fit in both simulators. However, using a reference cell the irradiance on the module area was measured and it was found that the irradiance in the LED solar simulator was most homogeneous and higher than in the smaller gas-discharge and halogen lamp solar simulator (see Figure 34). Therefore the LED solar simulator was the one used for this experiment. This solar simulator consists of colored LED lights and is surrounded by a climate chamber. This means that we can set and maintain a constant ambient temperature of 20°C ($\pm$0.4).

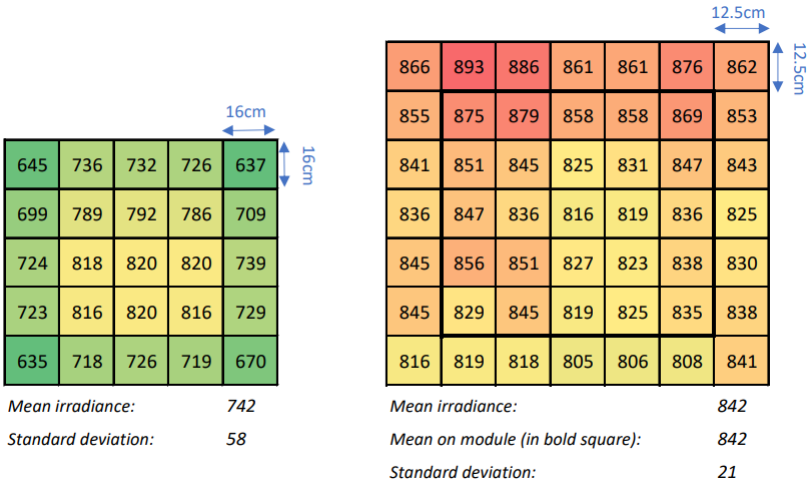


Figure 34: Measured irradiances in W/m$^2$ for both the small solar simulator (on the left) and the large solar simulator (on the right).

LED solar simulator and climate chamber

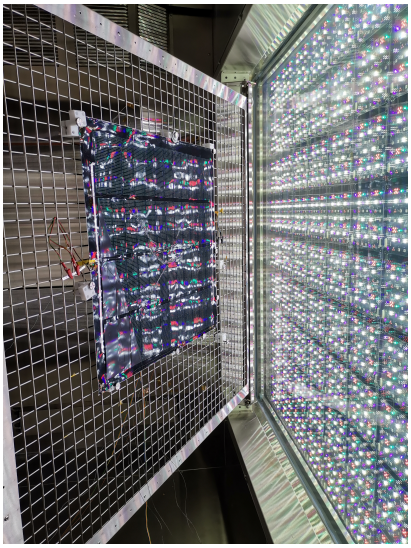

One of the 24 × 4 PV modules mounted on the solar simulator rack. Note that this rack will be closed during measurements, so that the module is parallel to the light source.

For the modelling purpose we take the mean of the measurements in Figure 34, 842W/m$^2$, for the irradiance level of an unshaded cell. Then I-V measurements of the modules without shading was used as a baseline. It was found that if an irradiance of 842W/m$^2$ was used in modelling the unshaded module I-V curves, the short circuit current was underestimated. The short circuit current of the measured module was 0.3A higher, which is unexpected. Checking with also the other unshaded modules it turned out that the model is systematically underestimating the short circuit current. The only cause for this can be an error in estimated irradiance, since increasing efficiency doesn't

help the short circuit current being higher. Neither does changing the cell temperature, as the temperature coefficient of short circuit current isn't significant enough to validate such a big simulating error. So the only reason for a higher than estimated short circuit current is that the actual irradiance is larger than 842W/m$^2$. To get a good fit for an unshaded TCT $12 \times 4$ module, it turned out that an irradiance of 875W/m$^2$ resulted in the smallest difference, 0.02A, in measured and simulated short circuit currents. A confirmation of this choice was found by checking the difference in simulated short circuits for the other modules. With the irradiance correction we found $\Delta$0.01A, $\Delta$0.13A, $\Delta$0.03A in measured and simulated $I_{sc}$ for the unshaded modules of $24 \times 4$ TCT, $12 \times 4$ SP and $24 \times 4$ SP, respectively. The difference for the $12 \times 4$ SP module is relatively large, the model overestimates the short circuit current, but this is probably because the module was damaged by some creasing in the top lamination layer.

The irradiance was measured with a reference cell, which was small (about 3 by 2 cm), and encapsulated in a box. This might block light coming in from the sides. Since a PV module is much larger and might catch more reflected light, this can explain why the irradiance on the modules is higher than measured with the reference cell.

## 5.3 Cell temperature and efficiency

When we take an NOCT of 48 degrees celsius, as prescribed by the MiaSolé datasheet, we systematically overestimate the open circuit voltage, as we can see for the $12 \times 4$ TCT module in the figure below.

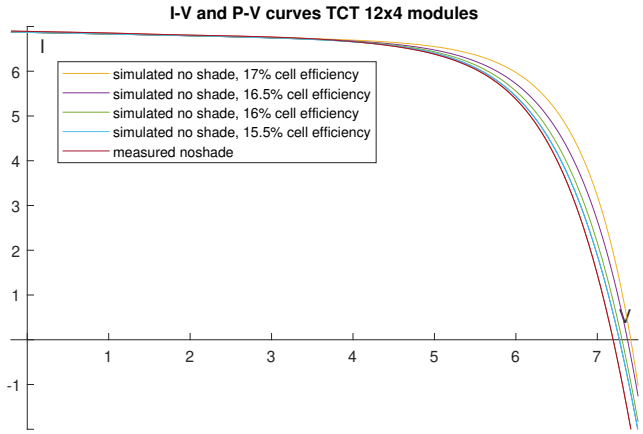


Figure 35: Simulated unshaded TCT $12 \times 4$ module with a NOCT of 48°C and various efficiencies compared with the measured I-V curve

The cell temperature has a high impact on the open circuit voltage. Secondly, in the datasheet and in the figure we can see that the open circuit voltage also depends on the efficiency of the cell. So in order to choose the right open circuit voltage, we need to find the correct NOCT and cell efficiency. Unfortunately, the efficiency of the used cells in particular is not known. It is not likely that the efficiency of a module in practice is 17%. Therefore, in order to approximate the module efficiency better, it is more realistic that the cell efficiency is 16% or 15.5%.

The NOCT that is given in the datasheet is for a MiaSolé FLEX-02 module. This does have a black back-sheet, like our module, but it has a different stack of the cells, and might use other adhesives and layer materials. So to determine the NOCT for

our modules, we measured the cell temperature with thermocouples at four different locations on the front surface, whilst the module was fully illuminated. For an ambient temperature of 20 degrees two measurements were done and for 25 degrees one measurement was done. Assuming that all modules have the same temperature behaviour since they consist of the same materials, cell temperatures were only measured for the $12 \times 4$ TCT module.

| $T_{\text{amb}}$ | 20°C | 20°C | 25°C |
|---|---|---|---|
| T1 | 56.7 | 59.0 | 61.5 |
| T2 | 57.2 | 58.8 | 62.5 |
| T3 | 54.1 | 55.3 | 58.8 |
| T4 | 39.0 | 39.0 | 43.6 |

Table 2: Cell temperature measurements in degrees Celsius at four points on the module

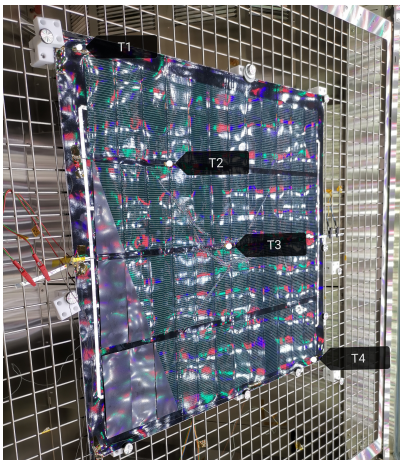


Figure 36: Locations of the thermocouples

The differences in cell temperatures across the module can have multiple causes, especially the temperature at T4 is very low. The cooling and heating system in the solar simulator chamber may cause cold or hot air fluctuation, and the air temperature of 20°C is measured at one point in the chamber so we don't know how the heat is distributed across the chamber. Also the irradiance at the measurement locations varies slightly.

Comparing the locations of the reference cell irradiance measurements in Figure 34 and the locations of the thermocouples we get that the irradiance at T1 is 875, at T2 is 845, at T3 is 816, and at T4 is 835 W/m$^2$. We can calculate the NOCT with the following equation, derived from equation (2.10).

$$\text{NOCT} = \frac{T_{\text{cell}} - T_{\text{amb}}}{G} \cdot 800 + 20$$

With the local irradiance and the cell temperature we calculated the NOCT for each measurement.

| $T_{\text{amb}}$ | 20°C | 20°C | 25°C |
|---|---|---|---|
| T1 | 53.6 | 55.7 | 53.4 |
| T2 | 55.2 | 56.7 | 55.5 |
| T3 | 53.4 | 54.6 | 53.1 |
| T4 | 38.2 | 38.2 | 37.8 |

Table 3: Corresponding calculated NOCT values for the measured cell temperatures

On average the NOCT was 50.5°C. However, if we use this value to simulate the unshaded modules for TCT $12 \times 4$, SP $12 \times 4$, TCT $24 \times 4$ and SP $24 \times 4$ then either the simulated open circuit voltage is too high (for higher cell efficiency choice) or the simulated maximum power is too low (for lower cell efficiency choice) for every module, except TCT $12 \times 4$. So a second option is to assume that measurements at T4 are

outliers, and that the cell temperature is only this low at that one corner. If we neglect the T4 measurements, then we get an average NOCT of 54.6°C. Using this NOCT, we can get smallest deviations from measured maximum power points and open circuit voltages with a cell efficiency of 16%. Only TCT $12 \times 4$ showed less deviation for the combination of NOCT = 50.5°C and efficiency = 16%. Thereby, we set the NOCT at 54.6°C and pick cell with an efficiency of 16% for the further simulations.

## 5.4 Cell ideality factor and resistances

As described in Section 2.4 the best way to find cell intrinsic ideality factor and resistances is to first find $R_{\text{sh}}$ based on the measurements around $I_{\text{sc}}$ and then fit $n$ and $R_{\text{s}}$ to the manufacturer's given nominal power point. The measurements around $I_{\text{sc}}$ are only available for entire modules, but cell measurements can be derived by dividing voltage by 12 or 24 and the current by 4. For the $12 \times 4$ modules measured points around $-0.19$V and 0.7V and for the $24 \times 4$ modules measured points around $-0.19$V and 1.4V were taken. For each module separately, $\Delta V$ and $\Delta I$ of the single cell were calculated with these measurements around the short circuit point. Then we know that $R_{\text{sh}} = -\Delta V/\Delta I$ is a good estimation, and we can use the fitting method for $n$ and $R_{\text{s}}$ for each cell. An advantage of using module measurements for determining cell resistances is that the series resistance of tabbing material gets included in the model via the cell's calculated series resistance.

In conclusion, based on the parameters discussed in the previous sections, the following properties for the cells were obtained.

Single cell of the TCT $12 \times 4$ module.

```
PVcell with properties:
Tambient:           20 °C
Irradiance:         875 W/m^2
NOCT:               54.6 °C
TempCoefIshort:     0.008 %
TempCoefVopen:      -0.28 %
RefIshort:          1.958 A
RefVopen:           0.664 V
RefImpp:            1.713 A
RefVmpp:            0.531 V
RefPmpp:            0.909 W
IdealityFactor:     2
Rseries:            0.006 Ohm
Rshunt:             9.106 Ohm
Tcell:              57.844 °C
Photocurrent:       1.719 A
ReverseSatcurrent:  0 A
```

Single cell of the SP $12 \times 4$ module.

```
PVcell with properties:
Tambient:           20 °C
Irradiance:         875 W/m^2
NOCT:               54.6 °C
TempCoefIshort:     0.008 %
TempCoefVopen:      -0.28 %
RefIshort:          1.958 A
RefVopen:           0.664 V
RefImpp:            1.713 A
RefVmpp:            0.531 V
RefPmpp:            0.909 W
IdealityFactor:     2
Rseries:            0.007 Ohm
Rshunt:             15.929 Ohm
Tcell:              57.844 °C
Photocurrent:       1.719 A
ReverseSatcurrent:  0 A
```

Single cell of the TCT 24 × 4 module.

| PVcell with properties: | |
|---|---|
| Tambient: | 20 °C |
| Irradiance: | 875 W/m$^2$ |
| NOCT: | 54.6 °C |
| TempCoefIshort: | 0.008 % |
| TempCoefVopen: | -0.28 % |
| RefIshort: | 0.979 A |
| RefVopen: | 0.664 V |
| RefImpp: | 0.856 A |
| RefVmpp: | 0.531 V |
| RefPmpp: | 0.455 W |
| IdealityFactor: | 1.954 |
| Rseries: | 0.01 Ohm |
| Rshunt: | 11.813 Ohm |
| Tcell: | 57.844 °C |
| Photocurrent: | 0.86 A |
| ReverseSatcurrent: | 0 A |

Single cell of the SP 24 × 4 module.

| PVcell with properties: | |
|---|---|
| Tambient: | 20 °C |
| Irradiance: | 875 W/m$^2$ |
| NOCT: | 54.6 °C |
| TempCoefIshort: | 0.008 % |
| TempCoefVopen: | -0.28 % |
| RefIshort: | 0.979 A |
| RefVopen: | 0.664 V |
| RefImpp: | 0.856 A |
| RefVmpp: | 0.531 V |
| RefPmpp: | 0.455 W |
| IdealityFactor: | 1.915 |
| Rseries: | 0 Ohm |
| Rshunt: | 8.504 Ohm |
| Tcell: | 57.844 °C |
| Photocurrent: | 0.859 A |
| ReverseSatcurrent: | 0 A |

## 5.5 Determining bypass diode parameters

The earlier mentioned Flex Schottky diode is used as bypass diode in the modules. We know for these bypass diodes that $I_0 = 0.4 \cdot 10^{-3}$A, and we know that the bypass diodes are located inside layers of the modules, which had a mean temperature of about 55°C (this is not the exact mean of the module temperature, but small diode temperature differences didn't seem to impact the I-V output). However, we don't know ideality factor $n$. With the values for $T$ and $I_0$ set, and with keeping in mind that the diode should 'turn on' between 0.2V and 0.3V, we tried to estimate the best ideality factor. This was done by trying increments of 0.1 between 1 and 2, and comparing the resulting simulated I-V curves with the measured I-V curves for the various shading patterns in this experiment. It turned out that the best fitting ideality factor is 1.4. In Figure 38 we see the I-V curve of the bypass diode in forward bias, for both module temperature and room temperature. For the room temperature we can clearly see that the forward voltage is between 0.2V and 0.3V.

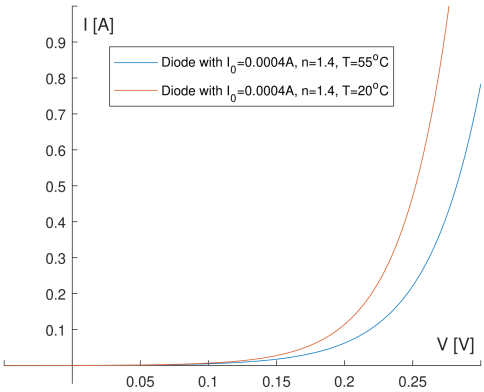


Figure 37: Simulated I-V curve of Schotkky bypass diode for two temperatures

## 5.6 Results

Let's first look at the baseline measurements: the unshaded modules. Since we fitted cell parameters to these measurements, the simulated I-V curves are good estimations, except for the SP 12 × 4 module. The I-V curve of this module already shows some current drops although there is no shading. This indicates that this module has some

defects. There most likely are some shunted cells, because of the crease in the lamination layer.

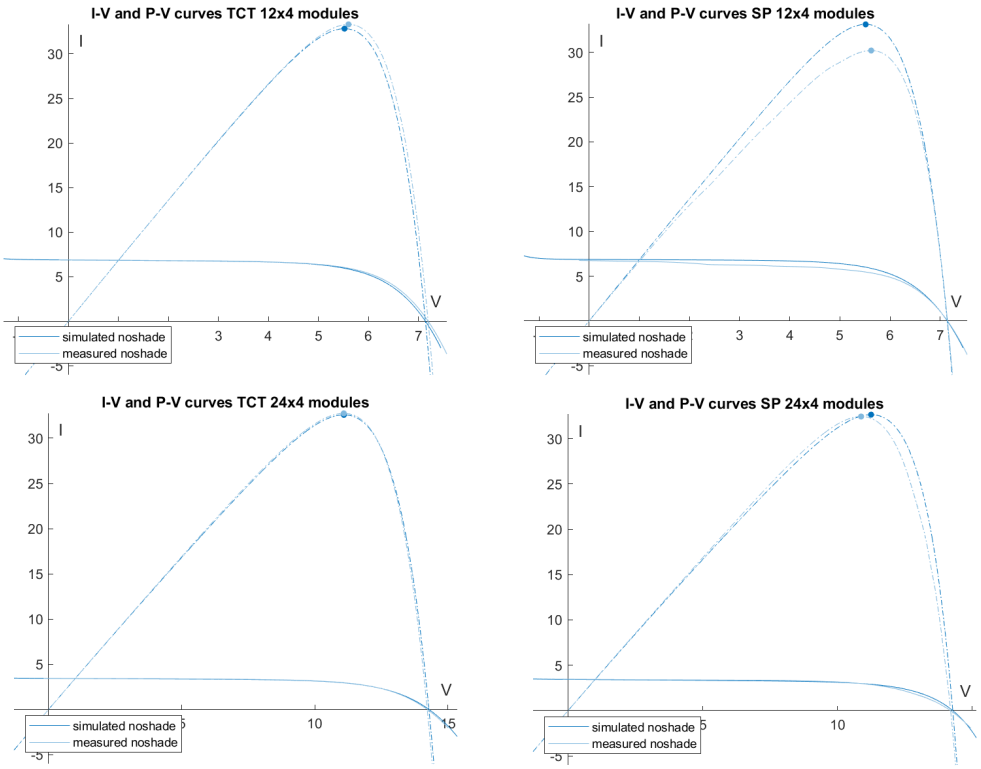


Figure 38: Baseline measured and simulated I-V curves (no shade). On the y-axis we have current [in A] and power [in W], and the x-axis is voltage [in V]

Secondly, we apply some horizontal and vertical shades. For all modules left half, right half, top half and bottom half shading is measured. Theoretically the bottom half shading is equivalent to top half shaded, and left half shading is equivalent to right half shading. So with these measurements we can detect if there are defects in the module and where they are located.

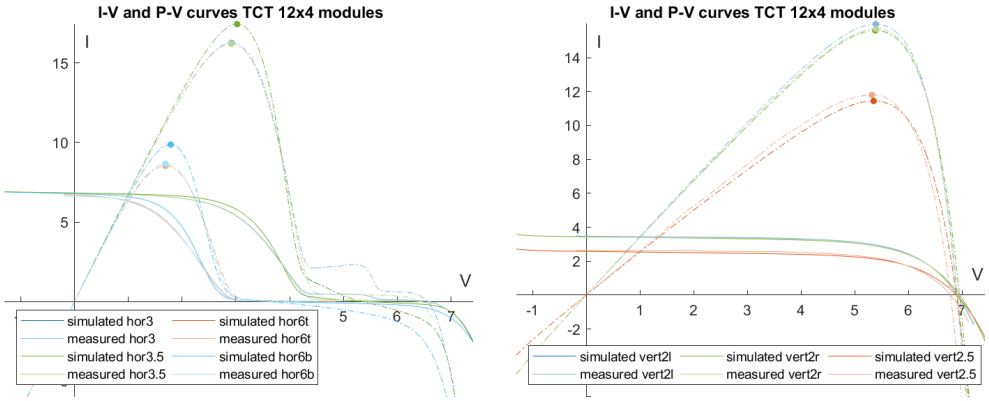


We can see in the figure on the left that even though the model overestimates the

measurements, at least top and bottom shading patterns overlap for the measurements. On the right we see that the left and right side of the module also behave the same.

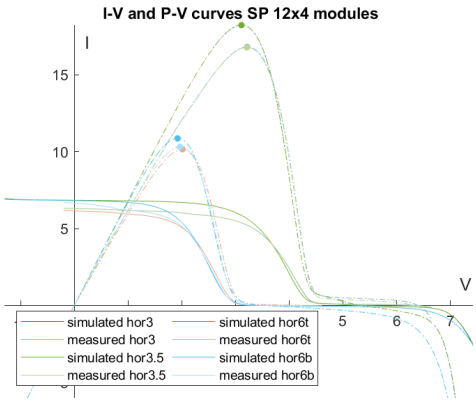


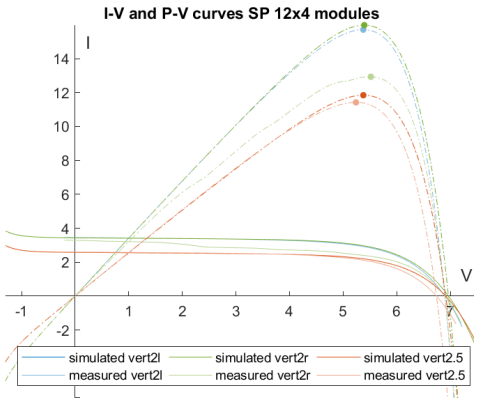


The top half and bottom half seem to behave the same for this module, though for the bottom half shaded we can see a current drop after the short circuit point. For both halfs the simulated maximum power point is a bit higher than the measured one. The shading of three and three and a half rows also results in a lower than simulated maximum power output. In the figure on the right, it becomes clear that the right half of the module behaves approximately as expected, but the left half performs worse. So there are some defects in the left half of the module.

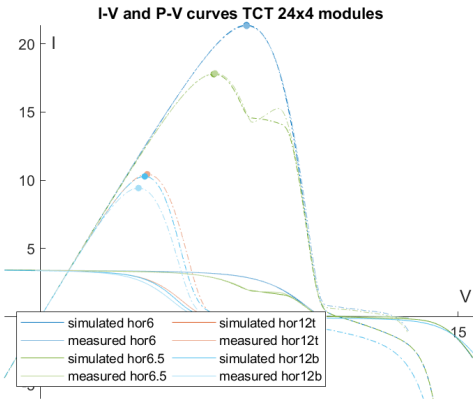


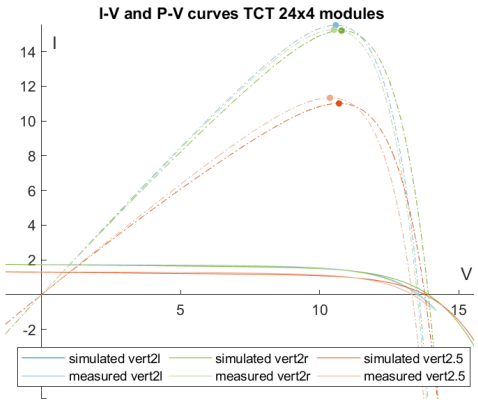


For the shading of the bottom half of the TCT $24 \times 4$ module, the power output is a bit lower than expected, so there are some irregularities in the top half of this module. Besides this, the left and right half of the module are approximately behaving the same as the model predicts.

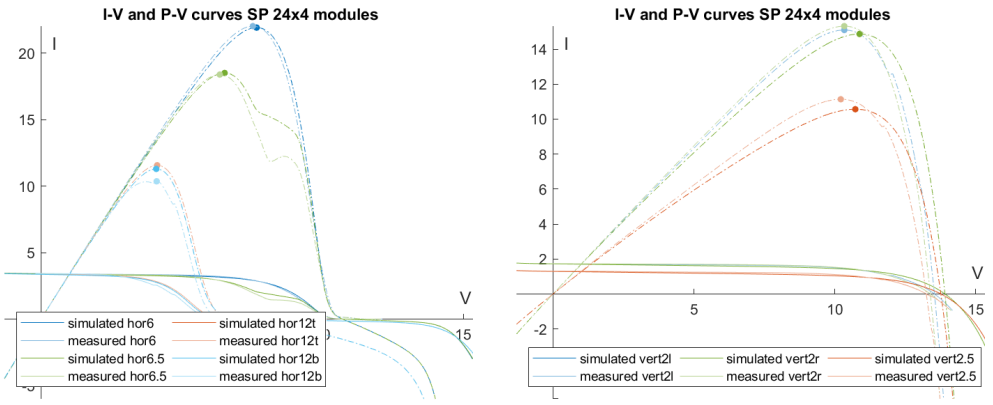


For the SP $24 \times 4$ module, the top half of the module is also performing a bit worse than simulated. The left and right half of this module behave the same, though the $V_{\text{MPP}}$ for all vertical shading scenarios seem to deviate more from the simulated value than for the other modules. We saw this also for the unshaded module, so this is probably caused by resistances in the module or less efficient cells.

Finally, the I-V and P-V curves for the more interesting shading scenarios are measured and simulated. These results can be found in Appendix V. Note that we have one missing measurement for SP $24 \times 4$, namely slopeB1, and that diagB is not the same pattern for TCT $12 \times 4$ as for SP $12 \times 4$. Apart from SP $12 \times 4$ the simulation I-V and P-V curves are really close to the measured curves.

In the tables in Appendix V, the maximum power, short circuit current and open circuit voltage of all shading scenarios and modules are compared. The absolute error and relative error in the simulation results of these parameters are calculated. The relative error for a parameter is the absolute difference of the measured and simulated value, divided by the measured baseline value (measured value of the parameter for unshaded scenario). This relative error is in percentage. We find that, ignoring SP $12 \times 4$ module, the relative error in $P_{\text{MPP}}$ and $I_{\text{sc}}$ is less than 1.6%. The relative error for $V_{\text{oc}}$ is a bit bigger, about 5%, but still relatively small. The errors for the SP $12 \times 4$ module are much larger. It is unclear why this module is performing so much worse than expected. Looking at the horizontal and vertical shading results, we see some decrease in current and voltage compared with Simulated values, but this doesn't explain why in the other, not semi-homogeneous, shading scenarios the module is behaving so poorly. Both the short circuit currents and the open circuit voltages (and as a consequence of course the maximum power output also) are a lot lower than expected in these scenarios. Supposedly, there are a number of cells or bypass diodes that are damaged in this module.

## 5.7 Electroluminescence measurements

After the partial shading experiment, we did electroluminescence (EL) measurements of the modules. For EL measurements, a small current (in this case 20% of the short circuit current) is fed into the PV modules. Then instead of absorbing light, the PV modules will emit some light. This can be captured by a photograph in a dark room using special filters. EL measurements show a qualitative picture of the defects and irregularities in a PV cell or module: the more light that is emitted, the better the cell. If a cell shows up black, then it is completely shunted, which means that it is short circuited.

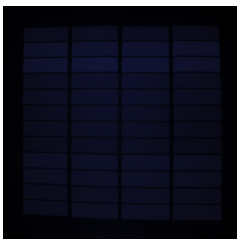

Figure 39: EL measurement of TCT $12 \times 4$

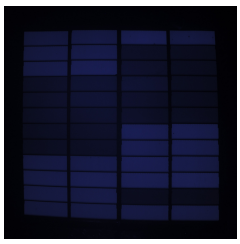

Figure 40: EL measurement of SP $12 \times 4$

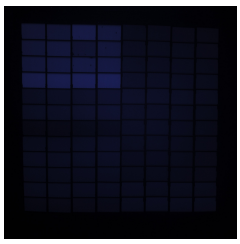

Figure 41: EL measurement of TCT $24 \times 4$

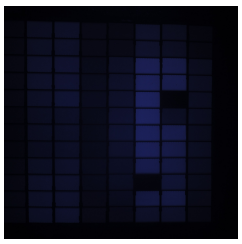

Figure 42: EL measurement of SP $24 \times 4$

In these figures the orientation of the modules is the same as in the pictures and schematic layout in Section 5.1. So for the $12 \times 4$ modules the positive terminal is at the top, and the negative terminal is at the bottom. And for the $24 \times 4$ modules the positive terminal is located at the top right half, while the negative terminal is located at the top left half. Note that because of the module layout, when we talk about the top half of a $24 \times 4$ in a shading pattern, this is the right half of the module in the real-life layout. Similarly, the left half in a shading pattern, are outer four columns of cells in the real-life module, and the right half in a shading pattern, are the inner four columns in the real-life $24 \times 4$ module.

The TCT $12 \times 4$ EL measurement looks reasonably uniform. This agrees with the results of vertical and horizontal shading in the previous section. In the EL measurement of SP $12 \times 4$ we can see what might be the cause for the irregular behaviour of this module: the emitted light is far from uniform.

For SP $12 \times 4$ the location of the darker cells somewhat coincides with the location of the crease in the lamination layer (see Figure 33). In the vertical shade I-V curves of this module, we saw that the left half of the module has lower output currents than the right half. This can not be explained with the EL measurement.

For the TCT $24 \times 4$ module, the left upper cells in the picture emit more light. These cells are the bottom four rows of the module when considering the shading pattern layout. In the horizontal shade measurements of this module, we indeed obtained that the bottom half of the module had a higher power output than the top half.

The SP $24x4$ module has two completely shunted cells on the right (i.e., in the top half of the module in terms of shading pattern layout). This was also seen in the horizontal shade I-V measurements: the bottom half of the module has a higher power output than the top half.

Unfortunately, EL measurements were only done after the partial shading measurements. So it is unknown whether the defects are caused by the module manufacturing phase, for example by the creases in the lamination layer, or because the bypass diodes didn't fully protect the cells during the partial shading scenarios. However, from the above mentioned consistency in EL measurements and vertical/horizontal shade I-V measurements, which were taken before the other partial shading measurements, it seems like the defects in the modules were already there at the beginning of the partial shading I-V measurements. All the modules were still working at the end of the I-V measurements, so assuming that the defects formed in the lamination phase, the bypass diodes did their job in protecting the cells from negative voltages, negative currents and too much power dissipation.

# 6 Findings

Finally, we can use our verified model to generate some data in order to compare TCT with SP for various shading patterns. For all the following measurements we modelled the cells after MiaSolé CIGS PV cells with an efficiency of 17%, unless otherwise mentioned. The used method for determining the resistances and ideality factor, is prefixing the ideality factor at 1.5 as given in Table 1. The bypass diodes are modelled as Schotkky diodes as before with $I_0 = 0.4 \cdot 10^{-3}$A, $n = 1.4$, $T = 328$K (i.e., 55 degrees Celsius). The standard full irradiance is 1000W/m$^2$, and the ambient temperature is set at 20 degrees Celsius.

| | |
|---|---|
| PVcell with properties: | |
| Tambient: | 20 °C |
| Irradiance: | 1000 W/m$^2$ |
| NOCT: | 48 °C |
| TempCoefIshort: | 0.008 % |
| TempCoefVopen: | -0.28 % |
| RefIshort: | 4.7 A |
| RefVopen: | 0.673 V |
| RefImpp: | 4.25 A |
| RefVmpp: | 0.545 V |
| RefPmpp: | 2.316 W |
| IdealityFactor: | 1.5 |
| Rseries: | 0.006 Ohm |
| Rshunt: | 3.711 Ohm |
| Tcell: | 55 °C |
| Photocurrent: | 4.718 A |
| ReverseSatcurrent: | 0 A |

Table 4: Properties of a CIGS cell with an efficiency of 17% at the given ambient conditions.

## 6.1 Effect of bypass diodes

### 6.1.1 Modules with and without bypass diodes

We generated I-V curves for SP and TCT $4 \times 4$ modules with and without bypass diodes. The used shading patterns and the results can be found in Appendix VI. We use the abbreviations *BDs* for modules with bypass diodes in these results. Table 5 gives an overview of the maximum power outputs for the various shading patterns and results. From here on out we define the difference in power outputs for TCT and SP, $\Delta P_{\text{MPP}}$, to be $P_{\text{MPP, TCT}} - P_{\text{MPP, SP}}$. This difference results in a negative value if TCT has a lower power output than SP, since we are looking for a configuration that is more shadow tolerant than the traditional SP configuration. The relative error, *relative* $\Delta P_{\text{MPP}}$, will also be in terms of improving or decreasing with respect to SP. So the relative error is defined as *relative* $\Delta P_{\text{MPP}} = (P_{\text{MPP, TCT}} - P_{\text{MPP, SP}})/P_{\text{MPP, SP}} \cdot 100\%$.

| | without bypass diodes | | with bypass diodes | |
|---|---|---|---|---|
| | $\Delta P_{\text{MPP}}$ [W] | *rel.* $\Delta P_{\text{MPP}}$ [%] | $\Delta P_{\text{MPP}}$ [W] | *rel.* $\Delta P_{\text{MPP}}$ [%] |
| Vertical | 0.000 | 0.000 | 0.002 | 0.010 |
| Horizontal | 0.000 | 0.000 | -0.867 | -8.328 |
| Vertical fading | 1.944 | 7.927 | 1.947 | 7.938 |
| Horizontal fading | 0.517 | 3.757 | 0.519 | 3.776 |
| Diagonal | 23.364 | 2570.279 | 13.861 | 133.145 |
| Diagonal fading | 12.713 | 92.403 | 12.715 | 92.444 |
| Corner | 2.557 | 15.832 | 2.560 | 15.848 |
| Corner fading | 1.585 | 10.665 | 1.587 | 10.684 |
| Vertical large | 0.000 | 0.000 | 0.002 | 0.017 |
| Horizontal large | 0.000 | 0.000 | -0.456 | -7.367 |

Table 5: Power output results from shading patterns on $4 \times 4$ SP and TCT modules, with and without bypass diodes (see Appendix VI).

We see that the first four shading patterns (vertical, horizontal, vertical large, horizontal large) are semi-homogeneous shades. Therefore, the I-V curves of the SP and TCT modules without bypass diodes coincide, as can be seen in the figures in the Appendix. However, with the bypass diodes this is no longer the case, but we can see that the differences, especially for vertical shading, are very small. This is because the differences are only caused by the different layout and number of the bypass diodes. We see for the horizontal semi-homogeneous shading patterns, that SP slightly outperforms TCT (by less than 8%).

We can also note that sometimes including the bypass diodes doesn't significantly change the maximum power points (all 'vertical shades', 'corner shades', 'horizontal fading' and 'diagonal fading'), the small differences we see in the table might even be accounted to inaccuracies of the used numerical methods. And in other cases including the bypass diodes only increased the power output of the SP module ('diagonal'), or it increased the power output for both modules ('horizontal' and 'horizontal large').

It is also important to note that we can see in Table 5 for the modules with bypass diodes, that in two cases the SP outperforms the TCT by 8%. However, for some of the other cases the TCT outperforms the SP with even up to a 133% increase in power output (so the TCT's power output is more than twice as much as the SP's). It is really hard to predict what configuration is going to have the higher power output, the horizontally shaped shading patterns have a different outcomes, but it does seem like the advantages of TCT might outweigh its disadvantages. We will try to verify this later on with more shading patterns on different sized modules.

### 6.1.2 Individual cell operating points

To see if there is any dangerous negative voltages, powers or currents in the module, we looked at all the module's operating points between 0V and the open circuit voltage for the 'diagonal fading' pattern from Appendix VI. For all these operating points the model calculated the corresponding operating points for each cell and gave the minimal voltage, current and power that was found in the individual cells.

For the SP module without bypass diodes the minimal voltage level that was found in a cell was $-1.83$V at the module's short circuit point. This is lower than the breakdown voltage, so the cell might be damaged. At this point the minimum power point at a cell was also found: $-6.04$W. The maximum negative power that a cell can withstand is considered to be $-2$ times its nominal power point, which is 2.32W in this case. So there is a cell in the module that exceeds the negative power output that should be the

limit. In Figure 43 we can see all the individual voltages and power points in the cells. The layout of these matrices correspond to the module layout in the same way that the shading patterns do.

The lowest current that was found in the SP module was $-0.48$A at the open circuit point of the module. The individual cell currents can be found in Figure 44. It is not really known what effect negative currents have on the cell.

| | | | |
|---|---|---|---|
| -1.53 | 0.56 | 0.59 | 0.61 |
| 0.51 | -1.68 | 0.59 | 0.61 |
| 0.51 | 0.56 | -1.76 | 0.61 |
| 0.51 | 0.56 | 0.59 | -1.83 |

| | | | |
|---|---|---|---|
| -6.04 | 1.57 | 0.97 | 0.30 |
| 2.01 | -4.71 | 0.97 | 0.30 |
| 2.01 | 1.57 | -2.91 | 0.30 |
| 2.01 | 1.57 | 0.97 | -0.90 |

Figure 43: Cell voltages [V] and power points [W] at the short circuit point of the $4 \times 4$ SP module under shading pattern 'Diagonal fading' (Appendix VI)

| | | | |
|---|---|---|---|
| 0.24 | 0.21 | 0.02 | -0.48 |
| 0.24 | 0.21 | 0.02 | -0.48 |
| 0.24 | 0.21 | 0.02 | -0.48 |
| 0.24 | 0.21 | 0.02 | -0.48 |

Figure 44: Cell currents [A] at the open circuit point of the $4 \times 4$ SP module under shading pattern 'Diagonal fading' (Appendix VI)

If we do the same for the SP module with bypass diodes we see that the cells don't exceed the breakdown voltage and negative power limit anymore. The lowest negative voltage is still found at the module's short circuit point, and so is the lowest cell power, but these minimum values are now $-0.98$V and $-3.11$W, respectively. We can find the corresponding voltages and powers at the short circuit point in Figure 45. The larger rectangles represent the bypass diodes connected to the two cells left of the bypass diode.

The minimum current in a cell is found at the module's open circuit point and is $-0.48$A. Note that this value did not increase.

| | | | | | | | |
|---|---|---|---|---|---|---|---|
| -0.83 | -0.31 | 0.57 | -0.34 | 0.18 | 0.36 | 0.18 | 0.37 |
| 0.52 | | -0.90 | | 0.18 | | 0.18 | |
| 0.15 | 0.31 | 0.17 | 0.34 | -0.95 | -0.36 | 0.61 | -0.37 |
| 0.15 | | 0.17 | | 0.59 | | -0.98 | |

| | | | | | | | |
|---|---|---|---|---|---|---|---|
| -3.11 | -0.28 | 1.47 | -0.70 | 0.83 | 0.00 | 0.86 | 0.00 |
| 1.96 | | -2.35 | | 0.83 | | 0.86 | |
| 0.71 | 0.00 | 0.79 | 0.00 | -1.36 | -1.15 | 0.16 | -1.62 |
| 0.71 | | 0.79 | | 0.85 | | -0.26 | |

Figure 45: Cell voltages [V] and power points [W] at the short circuit point of the $4 \times 4$ SP module with bypass diodes under shading pattern 'Diagonal fading' (Appendix VI)

| | | | | | | | |
|---|---|---|---|---|---|---|---|
| 0.24 | 0.00 | 0.21 | 0.00 | 0.03 | 0.00 | -0.48 | 0.00 |
| 0.24 | | 0.21 | | 0.03 | | -0.48 | |
| 0.24 | 0.00 | 0.21 | 0.00 | 0.03 | 0.00 | -0.48 | 0.00 |
| 0.24 | | 0.21 | | 0.03 | | -0.48 | |

Figure 46: Cell currents [A] at the open circuit point of the $4 \times 4$ SP module with bypass diodes under shading pattern 'Diagonal fading' (Appendix VI)

In the same way we find a minimum cell voltage and power of $-1.03$V and $-5.14$W for the TCT module, at its short circuit point. This voltage level does not exceed the breakdown voltage, but the power does exceed the negative power limit. The minimal current was found at the open circuit voltage and has a value of $-0.80$A.

With the bypass diodes, the minima were found at the same operating points as before, but they are now at the safe levels of $-0.69$V, $-3.36$W and $-0.80$A instead.

In conclusion, we can see that the bypass diodes do protect the cells from exceeding the breakdown voltage and from dissipating too much power (and possibly becoming a hot spot).

### 6.1.3 Other bypass diodes

To see if the choice of bypass diode has an effect on the maximum power output we generated the I-V curves of the 'horizontal' shading pattern and 'corner fading' shading pattern for two other (theoretical) types of bypass diode. Bypass diode 1 has a forward voltage between 0 and 0.1V and has parameters $I_0 = 0.4 \cdot 10^{-1}$A, $n = 1.4$, $T = 328$K. Bypass diode 2 has a forward voltage between 0.6 and 0.7V and has parameters $I_0 = 0.4 \cdot 10^{-8}$A, $n = 1.4$, $T = 328$K.

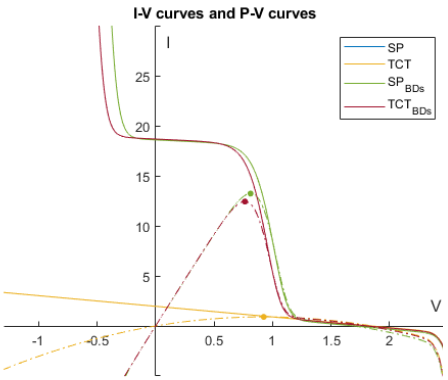


Figure 47: 'Horizontal' shading pattern (see Appendix VI) for $4 \times 4$ SP and TCT modules with bypass diode 1

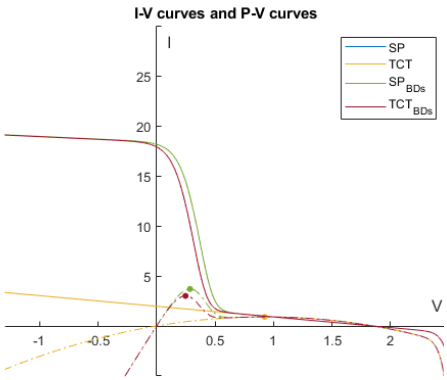


Figure 48: 'Horizontal' shading pattern for $4 \times 4$ SP and TCT modules with bypass diode 2

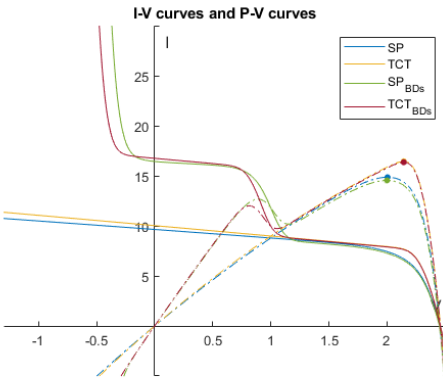


Figure 49: 'Corner fading' shading pattern (see Appendix VI) for $4 \times 4$ SP and TCT modules with bypass diode 1

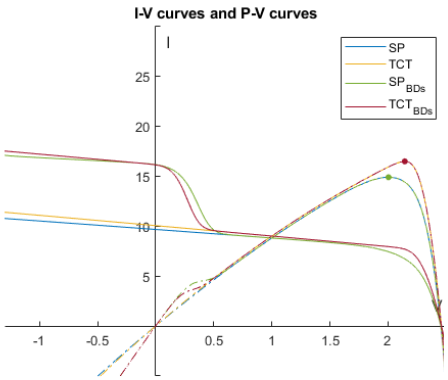


Figure 50: 'Corner fading' shading pattern for $4 \times 4$ SP and TCT modules with bypass diode 2

It can be seen that, in case the power output increases because of the bypass diodes, then a bypass diode with a lower forward voltage can allow the modules to have a much higher power output. Though we do see in Figure 49 that the power output of the SP module decreases a bit with the bypass diode 1.

Of course, the bypass diodes should be chosen so that they protect the cells and not purely in order to get the highest maximum power output. However, if there are safe multiple options for the bypass diodes, the bypass diode with the lowest forward voltage has an advantage.

## 6.2 Random patterns

In order to obtain a larger amount of data, we generated random patterns. Six module sizes were tried, each with 48 cell in total: $16 \times 3, 12 \times 4, 8 \times 6, 6 \times 8, 4 \times 12$ and $3 \times 16$. For all of these module sizes we generated 40 (pseudo-)random discrete irradiance matrices. The irradiance matrices can be split into two groups:
Group 1: matrices where entries can be $400, 500$ and $600\text{W}/\text{m}^2$
Group 2: matrices where entries of the matrices can be $0, 100, 200, \ldots, 900$ or $1000\text{W}/\text{m}^2$.

| | | | |
|---|---|---|---|
| 600 | 400 | 600 | 400 |
| 500 | 600 | 500 | 500 |
| 400 | 400 | 600 | 500 |
| 400 | 400 | 500 | 500 |
| 600 | 500 | 500 | 500 |
| 400 | 400 | 600 | 500 |
| 500 | 600 | 400 | 400 |
| 400 | 600 | 400 | 500 |
| 600 | 600 | 400 | 400 |
| 600 | 400 | 500 | 600 |
| 500 | 500 | 600 | 400 |
| 500 | 500 | 600 | 400 |

| | | | | | | | |
|---|---|---|---|---|---|---|---|
| 0 | 500 | 500 | 400 | 100 | 100 | 900 | 500 |
| 200 | 600 | 200 | 1000 | 200 | 700 | 300 | 500 |
| 800 | 200 | 500 | 0 | 300 | 500 | 700 | 900 |
| 0 | 500 | 600 | 900 | 700 | 800 | 200 | 600 |
| 1000 | 1000 | 700 | 1000 | 100 | 700 | 0 | 600 |
| 800 | 600 | 400 | 800 | 700 | 900 | 800 | 900 |

Figure 51: Example of two random irradiance matrices. On the left a matrix from group 1 for a $12 \times 4$ module, and on the right a matrix from group 2 for a $6 \times 8$ module.

For each of the groups 20 random matrices were generated, per module size. Then the maximum power points for both the TCT and SP module (with bypass diodes) are calculated for all these irradiance matrices and module sizes. This gives us in total $6 \cdot 40 = 240$ data points for $\Delta P_{\text{MPP}}$ and *relative* $\Delta P_{\text{MPP}}$, as defined before.

Since all of the modules have the same number of cells, namely 48, and a single cell for 20 degrees and full irradiance has a maximum power output of 2.0479W, we get a maximum power of 98W for the unshaded modules.

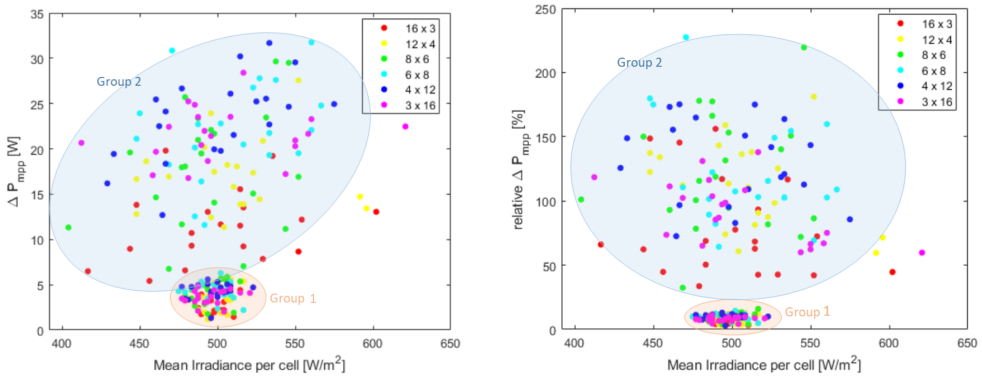


Figure 52: Absolute and relative power output differences between SP and TCT for random shading patterns, compared to the mean irradiance per cell.

In Figure 52 we see that all the difference values are positive, which means that the in all the generated scenarios TCT performs better. Even up to about 230% better (i.e., the maximum power output of TCT is more than 3 times the maximum power of SP).

Also, in this figure we can see that the power difference for irradiance matrices of group 1 is much lower, even though the mean irradiance is also located around $500\text{W}/\text{m}^2$ (i.e., total irradiance is about the same). So the mean or total irradiance level does not correlate with the relative difference in power output between SP and TCT. We do see that for the absolute power difference there is a slight positive trend of higher difference for a higher mean irradiance. However, this can be attributed to the fact that higher

irradiance gives higher power output levels, so the differences in power output can also be larger.

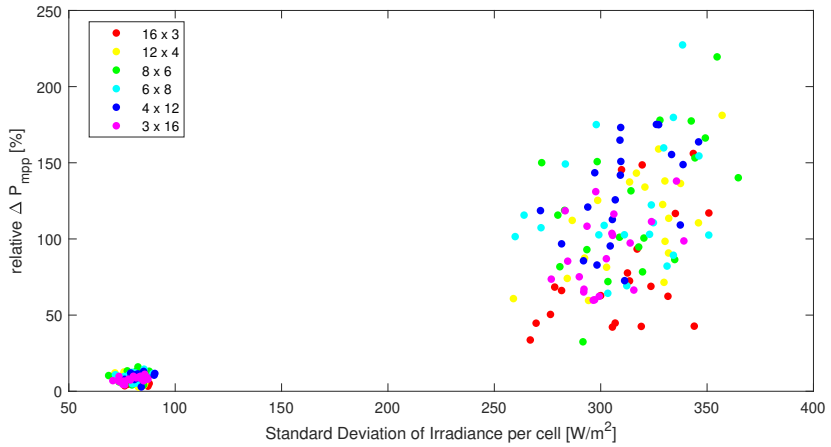


Figure 53: Relative difference in maximum power points compared with the standard deviation of irradiance per cell.

The data in Figure 53 that is grouped together on the left is from irradiance matrix group 1, and on the right we see the data from irradiance matrix group 2. The standard deviation of irradiance per cell is calculated as the standard deviation of all the values in the corresponding irradiance matrix. The irradiance levels can vary more for group 2, so that is why the deviation range for this group is wider. In general, we see an increasing trend: the larger the standard deviation of irradiance across the module, the more TCT can relatively improve compared with SP. For group 1 we see relative differences between zero and 20%, while for group 2 we see relative differences ranging from 25 to 250%. So if large differences in irradiance are expected, then the benefits of picking TCT over SP can also be high. But you only expect this large standard deviation if something is completely covering some part of you module. Also, on sunny days the differences in irradiance between shade and no shade can be more intense. Still the advantages with less irradiance deviation can still be about 5-25% improvement over SP.

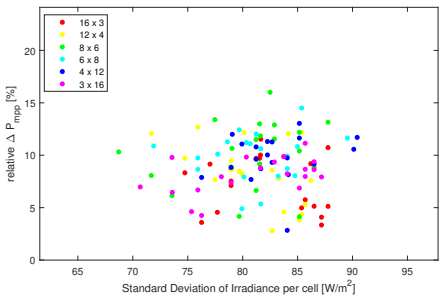


Figure 54: *Relative* $\Delta P_{\text{MPP}}$ w.r.t. the standard deviation of irradiance per cell for group 1

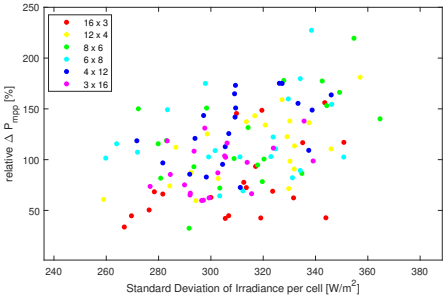


Figure 55: *Relative* $\Delta P_{\text{MPP}}$ w.r.t. the standard deviation of irradiance per cell for group 2

Within group 1 we don't really see a positive correlation between the relative error and standard deviation of irradiance, but then the standard deviation doesn't have a

larger range in Figure 54. In Figure 55 we do see that within group 2 there is a slight positive correlation with standard deviation of the irradiance.

To see if the dimensions of the module matter for random shading we calculated the mean relative difference in maximum power output per module size.

| module size | mean *relative* $\Delta P_{\text{MPP}}$ |
|---|---|
| $16 \times 3$ | 42.6 |
| $12 \times 4$ | 60.1 |
| $8 \times 6$ | 66.1 |
| $6 \times 8$ | 65.7 |
| $4 \times 12$ | 70.2 |
| $3 \times 16$ | 49.7 |

It seems like the wider the module the more advantage of TCT over SP, but there is a limit to this as at the $3 \times 16$ module the mean was decreasing. Though this isn't conclusive proof.

A final note on random patterns is that they might not be very realistic scenarios, we might expect more regular shapes because of nearby objects that cast a shade on the PV module. However, the irradiance matrices with lower deviation (group 1) could represent shading caused by trees, by dirt on the module, or shading caused by traffic as could occur, for example, on a pavement made with solar panels. The irradiance matrices with higher deviation (group 2), can occur on a bright day when the light is not diffused.

## 6.3 Impact of module dimensions

The next question is; does the difference between the power output of SP and TCT depend on the module dimensions. Modules of size $16 \times 4$, $8 \times 8$, $4 \times 16$ were tested with four different shading pattern shapes. These module sizes were picked so that the following shading patterns could be scaled nicely, without creating half shaded cells, according to the module size.

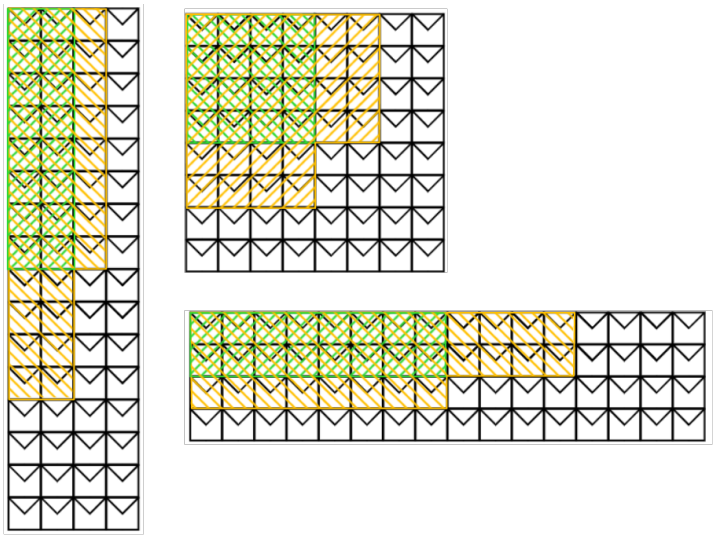

Figure 56: Green and orange shading patterns, scaled according to the module size.

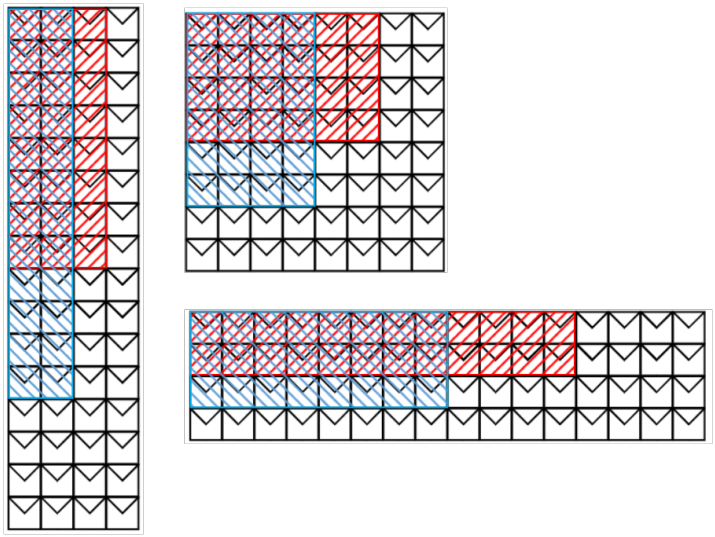

Figure 57: Red and blue shading patterns, scaled according to the module size.

The coloured cells are fully shaded ($0\text{W}/\text{m}^2$) in the corresponding colour shading pattern. So for example, in the pattern 'red' all cells have irradiance $1000\text{W}/\text{m}^2$, except for the red filled cells, those are fully shaded. Then we also define a 'red inverse' shading pattern, this has the irradiance matrix of 'red' but inverted: cells that are coloured red are now the fully illuminated and the empty cells are fully shaded. This is also applied for the other colours, therefore we get eight shading patterns that are scaled with the module size.

| | | $P_{\text{MPP}}$ TCT [W] | $P_{\text{MPP}}$ SP [W] | $\Delta P_{\text{MPP}}$ [W] | *rel.* $\Delta P_{\text{MPP}}$ [%] |
|---|---|---|---|---|---|
| Green | 16 x 4 | 70.652 | 64.040 | 6.612 | 10.325 |
| | 8 x 8 | 70.653 | 64.040 | 6.614 | 10.328 |
| | 4 x 16 | 70.654 | 64.040 | 6.615 | 10.329 |
| Green inverse | 16 x 4 | 19.070 | 20.522 | -1.452 | -7.077 |
| | 8 x 8 | 18.228 | 20.522 | -2.295 | -11.181 |
| | 4 x 16 | 17.391 | 20.522 | -3.131 | -15.259 |
| Red | 16 x 4 | 38.929 | 43.550 | -4.621 | -10.611 |
| | 8 x 8 | 37.210 | 43.550 | -6.340 | -14.558 |
| | 4 x 16 | 35.503 | 43.550 | -8.047 | -18.479 |
| Red inverse | 16 x 4 | 28.654 | 31.012 | -2.359 | -7.606 |
| | 8 x 8 | 27.371 | 31.012 | -3.641 | -11.742 |
| | 4 x 16 | 26.097 | 31.012 | -4.916 | -15.850 |
| Blue | 16 x 4 | 66.611 | 63.569 | 3.042 | 4.785 |
| | 8 x 8 | 66.612 | 63.569 | 3.043 | 4.787 |
| | 4 x 16 | 66.613 | 63.569 | 3.044 | 4.789 |
| Blue inverse | 16 x 4 | 40.982 | 42.121 | -1.139 | -2.705 |
| | 8 x 8 | 40.541 | 42.121 | -1.581 | -3.752 |
| | 4 x 16 | 17.543 | 20.591 | -3.048 | -14.801 |
| Orange | 16 x 4 | 33.539 | 30.138 | 3.401 | 11.285 |
| | 8 x 8 | 33.541 | 30.138 | 3.403 | 11.290 |
| | 4 x 16 | 33.542 | 30.138 | 3.403 | 11.293 |
| Orange inverse | 16 x 4 | 46.929 | 42.532 | 4.397 | 10.339 |
| | 8 x 8 | 46.456 | 42.532 | 3.924 | 9.226 |
| | 4 x 16 | 26.246 | 31.082 | -4.836 | -15.557 |

Table 6: Results of the shading patterns for the different modules sizes.

What we can see in Table 6 is that even though the shading patterns are scaled with the module's size and shade the exact same amount for the three modules, there is still a difference in power output between the modules sizes and a difference in (*relative*) $\Delta P_{\text{MPP}}$. For the shading patterns 'green', 'blue' and 'orange', TCT has a higher maximum power output and also the (relative) $\Delta P_{\text{MPP}}$ are almost the same for the different module sizes. We have a larger deviation in (relative) $\Delta P_{\text{MPP}}$ for the other shading patterns. Overall, the TCT's power output mostly decreases relatively to the SP's power output when the module is wider and shorter. This effect can be explained by the bypass diode layout; for the size $4 \times 16$ there is more mismatching between the pairs of cells (or parallel sets) that are connected to a bypass diode, because the shading patterns can have uneven number of rows for this size. Why this effect doesn't influence the 'green', 'blue' and 'orange' patterns is unclear. In conclusion, the effects of scaling and different sizing are complicated. Without any specific information about the expected shading patterns, cell type, and bypass diode, there can be no recommendation given for the best module dimensions.

We can also look into the possibility of rotating the layout of the interconnections between the cells. Rotating the interconnections means that for a SP the cells in a row get connection in a string instead of the cells in a column, and those horizontal strings then get connected in parallel. For a TCT module we mean by 'rotating the interconnection layout' that instead of the rows, the cells in columns will be connected in parallel and then these vertical parallel sets get connected in series. Bypass diodes will be changed accordingly. Then we see that if a certain shading pattern is excepted, rotating the layout interconnection can by very beneficial. For example, the 'blue' $4 \times 16$ module is the rotation of the 'red' $16 \times 4$ module and vice versa. We see that the 'blue' shading pattern has much higher power outputs than the 'red' shading patterns, about 20W higher. So if we would expect the 'red' shading pattern on a $16 \times 4$ module, it

will be beneficial for the power output to rotate the connection layout. And the same for the other two modules: rotating the connection layout in case 'red' horizontal shade is expected gives higher power output. We could also see this effect in the previous simulations in Appendices V and VI: vertical shades have higher power outputs than the same amount of shade horizontally, for both SP and TCT. Further research would be needed into this effect to determine in exactly which cases rotating interconnection layout would be beneficial and possible.

## 6.4 More patterns

We defined some more shading patterns but now for $12 \times 4$ modules of half CIGS cells that have an efficiency of 16% (see Figure 7), to get more variety on the cell types that we obtain the results for. The ambient temperature is again 20 degrees Celsius, and full irradiance is 1000W/m$^2$. The bypass diodes are Schottky diodes, modelled with same parameter values as before. The shading patterns can be found in Appendix VII. Note that if a cell has a shade across half of it, then we model this as half of the full irradiance on the cell, so 500W/m$^2$. Probably a cell will not have the same electrical behaviour for less irradiance or partial shade on the cell. But the effect of partly shading a cell is not exactly known. Therefore, by lack of a better method, if a cell has a ratio $x$ uncovered and the rest of it's surface is fully shaded, then we will model this as if the cell has an $x$ ratio of the full irradiance.

| PVcell with properties: | |
|---|---|
| Tambient: | 20 °C |
| Irradiance: | 1000 W/m$^2$ |
| NOCT: | 54.6 °C |
| TempCoefIshort: | 0.008 % |
| TempCoefVopen: | -0.28 % |
| RefIshort: | 2.35 A |
| RefVopen: | 0.664 V |
| RefImpp: | 2.055 A |
| RefVmpp: | 0.531 V |
| RefPmpp: | 1.091 W |
| IdealityFactor: | 1.5 |
| Rseries: | 0.014 Ohm |
| Rshunt: | 3.558 Ohm |
| Tcell: | 63.25 °C |
| Photocurrent: | 2.367 A |
| ReverseSatcurrent: | 0 A |

Table 7: Parameters of half a CIGS cell of 16% at shown ambient conditions.

We can conclude from Table 8 that even though sometimes the SP has a higher maximum power output, the relative difference with the TCT power output stays under 10% in these cases. The mean relative difference in power outputs of the cases where SP performs better is $-5.0\%$. On the other hand, when the TCT configuration has a larger power output, then it can be up to a 77% improvement of power output over SP. The mean relative difference of the cases where TCT performs better than SP is 17.0%. So statistically the TCT performs better, but again like for the other simulations, for specific cases it is hard to predict what to expect. For example, 'Diag3a' and 'Diag4a' are the same shades but just shifted one row downwards for 'Diag4a'. Despite that, because of a difference in shading pattern with respect to the bypass diodes, the TCT and SP almost have the same power output for 'Diag3a' but have a large relative difference of 41% for 'Diag4a'. Also among the same category of shades (diagonal, corner, spot), sometimes SP is better and sometimes TCT is better.

A final measurement is that based on the results in Table 8 it might seem that the TCT configuration more often has the same power output. This however is not necessarily true, because if we look at the 24x4 simulation measurements from the verification experiment (tables in Appendix V), then amongst those measurements the SP comes out on top most often. The baseline of the SP 24x4 does have a 0.1W higher power point, but this can not bridge the gap between the other SP and TCT power output simulations. Since simulated shading patterns will never cover all the possible

| Pattern | $P_{\mathrm{MPP}}$ TCT [W] | $P_{\mathrm{MPP}}$ SP [W] | $\Delta P_{\mathrm{MPP}}$ [W] | *rel.* $\Delta P_{\mathrm{MPP}}$ [%] |
|---|---|---|---|---|
| Diag1a | 36.902 | 34.622 | 2.280 | 6.585 |
| Diag1b | 26.095 | 24.849 | 1.246 | 5.013 |
| Diag2a | 25.488 | 26.684 | -1.196 | -4.483 |
| Diag2b | 18.546 | 20.391 | -1.845 | -9.046 |
| Diag3a | 34.617 | 34.586 | 0.031 | 0.089 |
| Diag3b | 24.089 | 14.719 | 9.370 | 63.658 |
| Diag4a | 34.617 | 24.506 | 10.111 | 41.259 |
| Diag4b | 24.095 | 21.287 | 2.808 | 13.189 |
| Diag5a | 34.617 | 26.684 | 7.933 | 29.731 |
| Diag5b | 26.406 | 14.915 | 11.491 | 77.045 |
| Corner1a | 34.730 | 37.299 | -2.570 | -6.889 |
| Corner1b | 26.079 | 26.855 | -0.776 | -2.890 |
| Corner2a | 32.300 | 31.887 | 0.414 | 1.297 |
| Corner2b | 23.623 | 23.261 | 0.361 | 1.554 |
| Corner3a | 34.315 | 34.871 | -0.557 | -1.596 |
| Corner3b | 30.244 | 27.896 | 2.349 | 8.419 |
| Corner4a | 29.295 | 29.200 | 0.096 | 0.328 |
| Corner4b | 19.180 | 19.582 | -0.402 | -2.052 |
| Spot1 | 39.543 | 39.424 | 0.118 | 0.300 |
| Spot2 | 30.369 | 29.086 | 1.284 | 4.413 |
| Spot3 | 24.120 | 25.771 | -1.651 | -6.405 |
| Spot4 | 29.441 | 29.037 | 0.404 | 1.391 |
| Spot5 | 23.985 | 25.606 | -1.621 | -6.329 |

Table 8: Results of the shading patterns in Appendix VII on $12 \times 4$ TCT and SP modules of half CIGS cell with an efficiency of 16%.

shading patterns, it is impossible to derive a quantitative conclusion from just these simulations.

# Conclusion

There is no conclusive answer on which configuration has the highest power output in general, because there are too many variables. Among the factors that influence the difference in maximum power output between a TCT and SP configuration, are the number and type of bypass diodes, dimensions of the module, the ambient conditions and the shading pattern. Not only does the shape of the shading pattern matter, but also the location on the module with respect to the bypass diodes; shifting a shade one row can make a big difference for the power output. It was found for 240 random shading patterns that the TCT configuration always had a higher power output than the SP configuration in those cases. The data showed a positive correlation between the relative difference of both configurations' maximum power outputs, and the standard deviation of the irradiance levels on the module. In other words, the more the irradiance levels between cells of the module deviated, the relatively better TCT was compared with SP. The relative maximum power difference between TCT and SP can range from about 2% to 230%, which means that TCT can even have more that 3 times the power output of SP (for high deviation in irradiance of about 350W/m$^2$). For non-random, more regular, shading patterns it was found that the SP configuration could have a higher maximum power output than the SP configuration. However, the maximum power output of TCT was at most 5% worse than the maximum power output of SP. Whereas, when TCT had a higher maximum power output, then it could be an improvement of up to 77% compared to SP. Therefore, if no more specific information is known about the expected shading patterns, TCT can be a safer option, because it could increase the power output by a lot or otherwise have almost the same power output as the SP configuration.

# Discussion and outlook

It is known that there are some inaccuracies in the model. First of all, in reality $n$, $R_\mathrm{s}$, and $R_\mathrm{sh}$ are temperature dependent, instead of constant as assumed in this research. Secondly, there are multiple diode models which are more accurate than the single diode model. However, considering the verification experiment showed that the model is quite accurate (ca. 2% error in maximum power output estimations), improvement on those areas might not be significant.

Since there are a limited amount of simulated shading patterns and it will never be possible to cover all the potential shading patterns, it is impossible to obtain a definite conclusion from just the simulations done in this research. Also, the results were only generated for MiaSol'e CIGS cells, and not yet for other thin-film cell types. It is possible to use the developed model for other type of cells, not even necessarily thin-film, and this can be an interesting subject for further research. What can also be done, is modifying the model to be used for other parameter differences of the cells: for example to research what happens for the I-V and P-V curves in case of cells with different shunt resistances in a module.

Most importantly, combining the developed model with a tool that predicts the shading patterns, could be very useful for determining which configuration is the best option for a specific situation.

As a final note, the configurations explored in this research aren't the only possible ones. Besides the TCT and the SP configuration, there are the so-called honey-comb and bridge-link. They could have some potential [3], and could be an interesting subject for further research into shadow tolerant design for thin-film modules.

# References


[1] Solliance, "Scaled perovskite solar modules pass three critical stability tests." Press release, 2020.

[2] Solliance, "About us." Page on `www.solliance.eu`, 2020.

[3] R. Ramaphrabha and B. Mathur, "A comprehensive review and analysis of solar photovoltaic array configurations under partial shaded conditions," *International Journal of Photoenergy*, 2012.

[4] J. Jewett and R. Serway, *Physics for Scientists and Engineers with Modern Physics, Eigth Edition.* BROOKS/COLE Cengage Learning, 2010.

[5] C. Honsberg and S. Bowden, "Solar cell structure." Page on `www.pveducation.org`, 2019.

[6] NREL, "Best research-cell efficiency chart." Page on `www.nrel.gov`, 2019.

[7] M. Kibria *et al.*, "A review: Comparative studies on different generation solar cells technology," *Proceedings of 5th International Conference on Environmental Aspects of Bangladesh*, 2014.

[8] M. T. Hörantner *et al.*, "The potential of multijunction perovskite solar cells," *ACS Energy Letters*, vol. 2, no. 10, pp. 2506–2513, 2017.

[9] F. Dimroth and S. Kurtz, "High-efficiency multijunction solar cells.," *MRS Bulletin*, vol. 32, no. 3, pp. 230–235, 2007.

[10] C. Honsberg and S. Bowden, "Ideality factor." Page on `www.pveducation.org`, 2019.

[11] C. Honsberg and S. Bowden, "Measuring ideality factor." Page on `www.pveducation.org`, 2019.

[12] M. A. Green, *Solar Cells Operating Principles.* Englewood Cliffs: Prentice-Hall, 1982.

[13] P. EE, "Diodes." Page on `www.practicalee.com`, 2020.

[14] J. Soon, K.-S. Low, and S. Goh, "Multi-dimension diode photovoltaic (pv) model for different pv cell technologies," *Institute of Electrical and Electronics Engineers*, 2014.

[15] M. Villalva, J. Gazoli, and E. Filho, "Comprehensive approach to modeling and simulation of photovoltaic arrays," *IEEE TRANSACTIONS ON POWER ELECTRONICS*, vol. 25, no. 5, pp. 1198–1208, 2009.

[16] H. Tsai, C. Tu, and Y. Su, "Development of generalized photovoltaic model using matlab/simulink," *Proceedings of the World Congress on Engineering and Computer Science*, 2008.

[17] O. Dupré and M. A. Green, *Thermal Behavior of Photovoltaic Devices.* Springer, 2017.

[18] C. Honsberg and S. Bowden, "Nominal operating cell temperature." Page on `www.pveducation.org`, 2019.

[19] D. Cotfas, P. Cotfas, and O. Machidon, "Study of temperature coefficients for parameters of photovoltaic cells," *Hindawi, International Journal of Photoenergy*, 2018.

[20] A.Virtuani, D. Pavanello, and G. Friesen, "Overview of temperature coefficients of different thin film photovoltaic technologies," *5th World Conference on Photovoltaic Energy Conversion*, 2010.

[21] A. Parisi *et al.*, "Thin film cigs solar cells, photovoltaic modules, and the problems of modeling," *Hindawi, International Journal of Photoenergy*, 2013.

[22] P. Dash and N. Gupta, "Variation of temperature coefficient of different technology photovoltaic modules with respect to irradiance," *Inpressco, International Journal of Current Engineering and Technology*, vol. 5, no. 1, 2015.

[23] C. Honsberg and S. Bowden, "Effect of temperature." Page on `www.pveducation.org`, 2019.

[24] J. Phang, D. Chan, and J. Phillips, "Accurate analytical method for the extraction of solar cell model parameters," *Electronics Letters*, vol. 20, no. May, pp. 406–408, 1984.

[25] W. D. Soto, S. Klein, and W. Beckman, "Improvement and validation of a model for photovoltaic array performance," *Elsevier, Solar Energy*, vol. 80, pp. 78–88, 2006.

[26] E. Karatepe, M. Boztepe, and M. Colak, "Development of a suitable model for characterizing photovoltaic arrays with shaded solar cells," *Elsevier, Solar Energy*, vol. 81, pp. 977–992, 2007.

[27] E. Karatepe, M. Boztepe, and M. Colak, "Neural network based solar cell model," *Elsevier, Energy Conversion and Management*, vol. 47, pp. 1159–1178, 2006.

[28] W. Xiao, W. Dunford, and A. Capel, "A novel modeling method for photovoltaic cells," *Institute of Electrical and Electronics Engineers*, 2004.

[29] C. Honsberg and S. Bowden, "Inverters." Page on `www.pveducation.org`, 2019.

[30] C. Honsberg and S. Bowden, "Bypass diodes." Page on `www.pveducation.org`, 2019.

[31] I. Poole, "Schottky diode: Schottky barrier diode." Page on `www.electronics-notes.com`, 2020.

[32] S. Mortazavi, K. Bakker, *et al.*, "Effect of reverse bias voltages on small scale gridded cigs solar cells," *IEEE PVSEC*, vol. 44, 2017.

[33] B. McCartin, "A model-trust region algorithm utilizing a quadratic interpolant," *Journal of Computational and Applied Mathematics*, vol. 91, pp. 249–259, 1998.

# Appendices

## I Best Research-Cell Efficiencies Chart

[6]

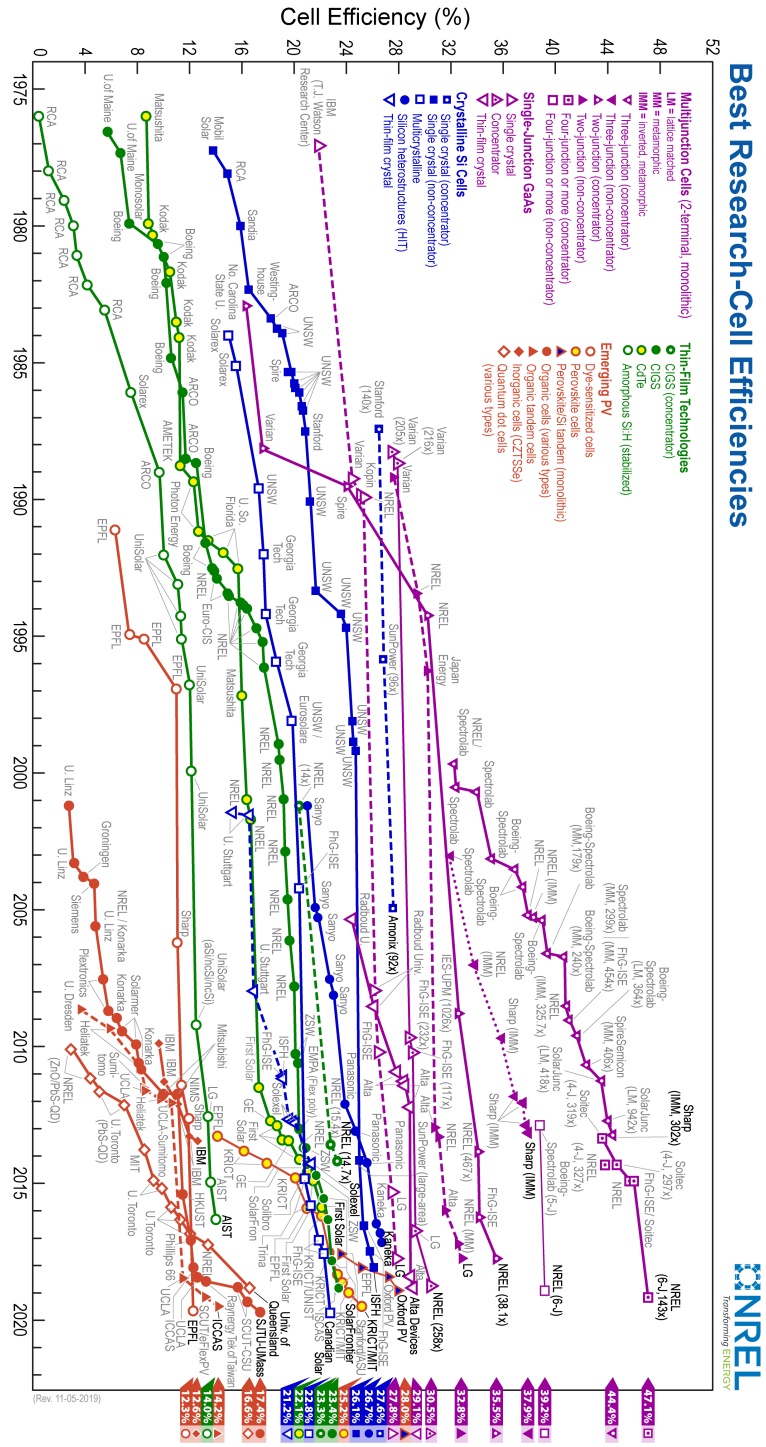

# II Datasheet MiaSolé CIGS Solar Cell

MiaSolé

# CIGS SOLAR CELL

## Copper Indium Gallium Diselenide (CIGS) Solar Cells: High Power Density in a Flexible Form Factor

MiaSolé thin–film CIGS solar cells on stainless steel substrate have high efficiency levels and provide significant advantages over conventional, rigid solar cells.

### KEY FEATURES

- Aperture efficiency of up to 17% in a flexible form factor.
- Thin—0.33mm
- Lightweight—7.5 gm
- Ideal for many specialized uses. Versatile cell architecture means the size can be modified to suit various applications.
- Bendable and shatter–proof

### HANDLING AND STORAGE NOTES

- Cells are sensitive to temperature and humidity. They must be stored either in vacuum–sealed containers or in a dry box with ≤5% relative humidity. Cells should be kept between 20–25 ° C.
- Cells require encapsulation before use to protect against moisture and the environment.

MiaSolé
A Hanergy Company

MiaSolé

# CIGS SOLAR CELL

## ELECTRICAL PERFORMANCE BY 0.5% EFFICIENCY BINS

| Cell Efficiency | | | 15.5% | 16.0% | 16.5% | 17% |
|---|---|---|---|---|---|---|
| Nominal Power | $P_{MPP}$ | [W] | 2.12 | 2.18 | 2.25 | 2.32 |
| Power Output Tolerance | | [W] | +0.1/-0 | +0.1/-0 | +0.1/-0 | +0.1/-0 |
| Maximum Power Voltage | $V_{MPP}$ | [V] | 0.526 | 0.531 | 0.538 | 0.545 |
| Maximum Power Current | $I_{MPP}$ | [A] | 4.04 | 4.11 | 4.17 | 4.25 |
| Open Circuit Voltage | $V_{OC}$ | [V] | 0.661 | 0.664 | 0.670 | 0.673 |
| Short Circuit Current | $I_{SC}$ | [A] | 4.70 | 4.70 | 4.70 | 4.70 |

## THERMAL CHARACTERISTICS*

| | | |
|---|---|---|
| NOCT | [℃] | 48 |
| Temperature Coefficient of $P_{MPP}$ | [%/℃] | -0.38 |
| Temperature Coefficient of $V_{OC}$ | [%/℃] | -0.28 |
| Temperature Coefficient of $I_{SC}$ | [%/℃] | 0.008 |

*based on MiaSole FLEX-02 module measurements

## PHYSICAL AND MECHANICAL SPECIFICATIONS

| | |
|---|---|
| Length | 312 mm +2/-4 mm |
| Width | 43.75 mm ± .005 mm |
| Thickness | 0.33 mm ± 0.1 mm |
| Weight | 7.5 gm ± 0.1 gm |
| Cell Type | Copper Indium Gallium Diselenide (CIGS) |

## CELL DIAGRAM

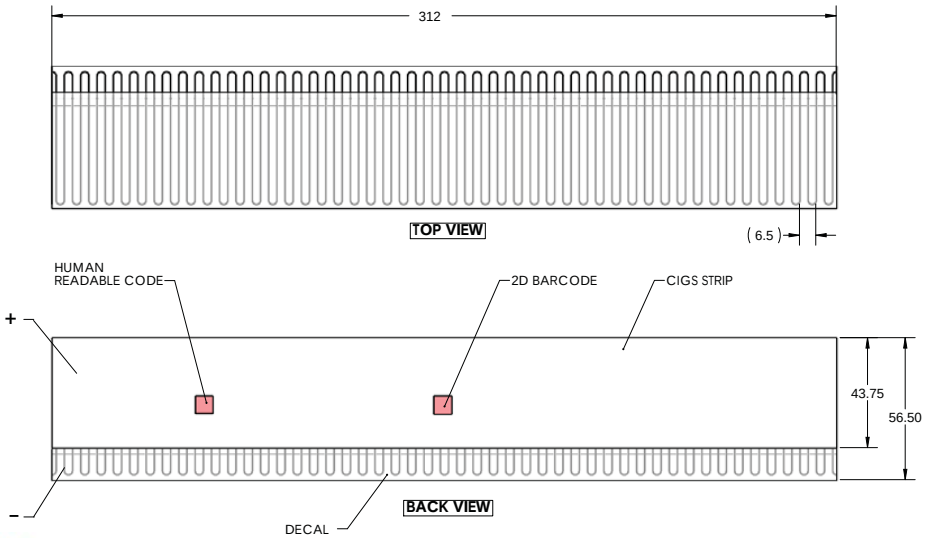


MiaSolé A Hanergy Company

2590 Walsh Avenue, Santa Clara, California 95051, USA
1.408.919.5700 info@miasole.com www.miasole.com

# III Shading patterns 12x4

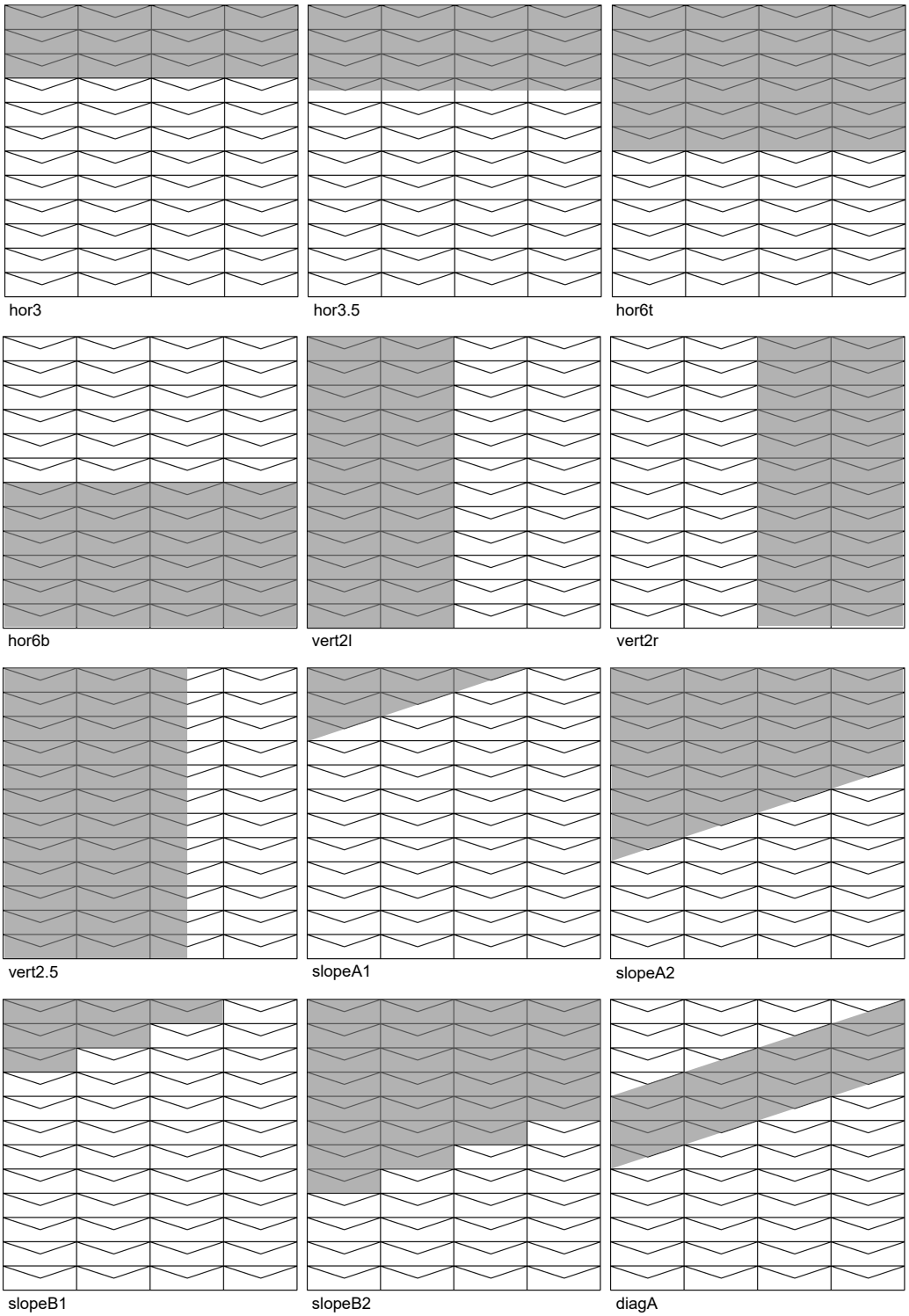

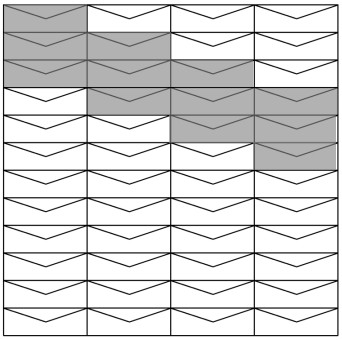

diagB

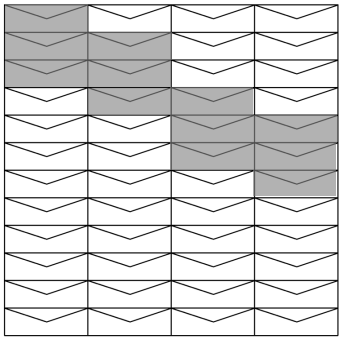

diagB for TCT*

* The shading pattern for the 12x4 TCT module was accidentally applied wrongly. This was actually found out because the simulation curve had such differently located current drops. Luckily, there was a picture taken of the originally applied shade.

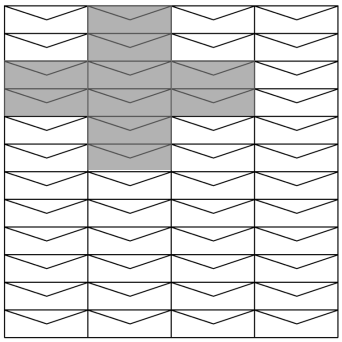

spotA

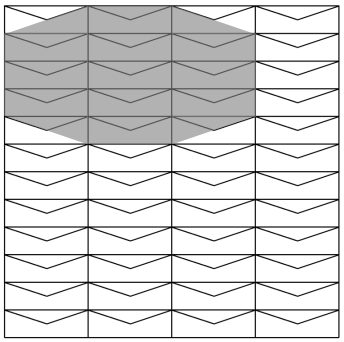

spotB

# IV Shading patterns 24x4

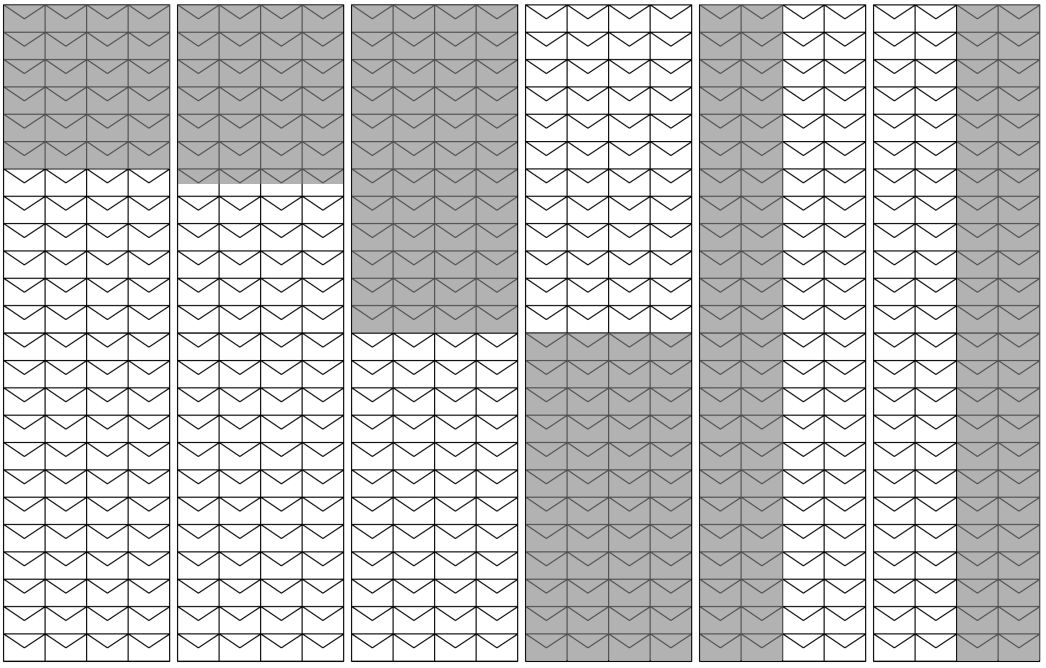


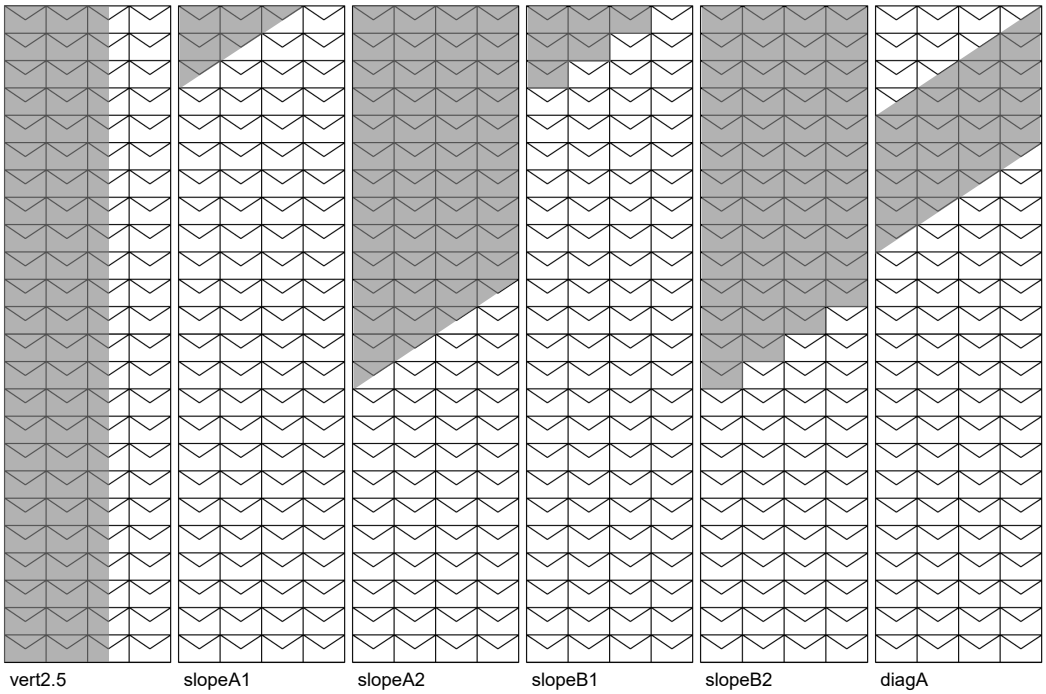

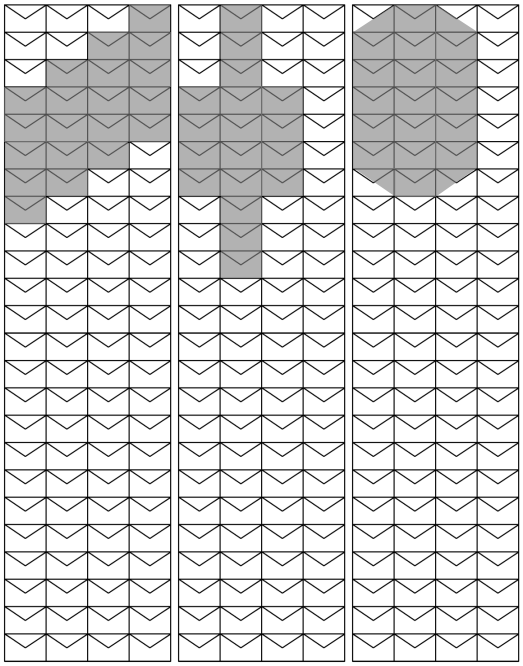
diagB
spotA
spotB

# V Results verification experiment

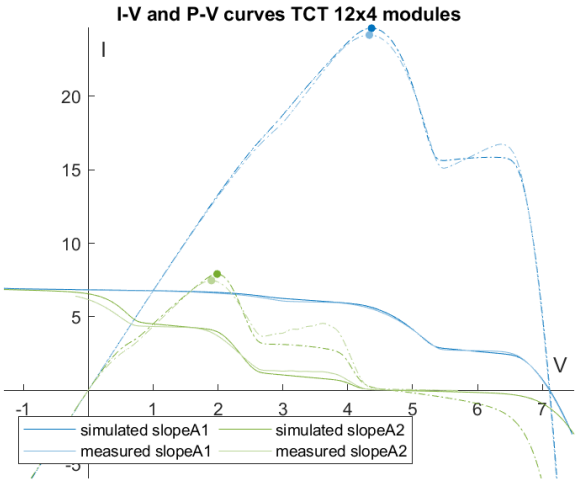


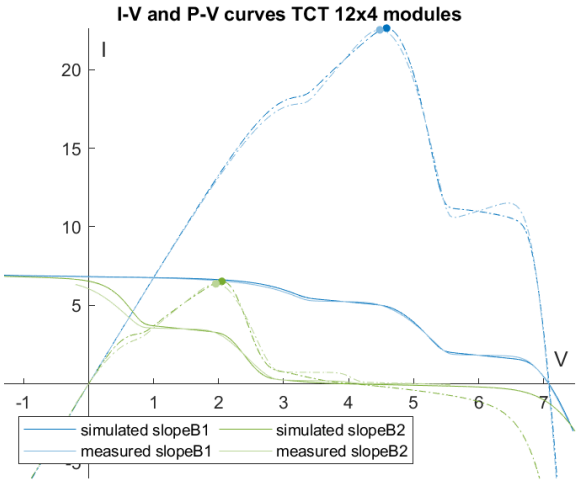


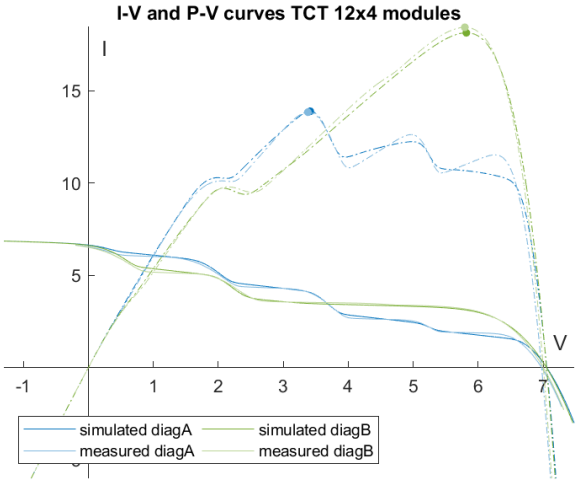


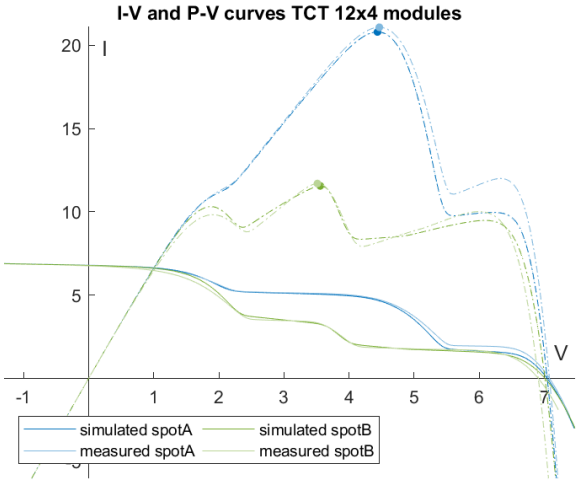


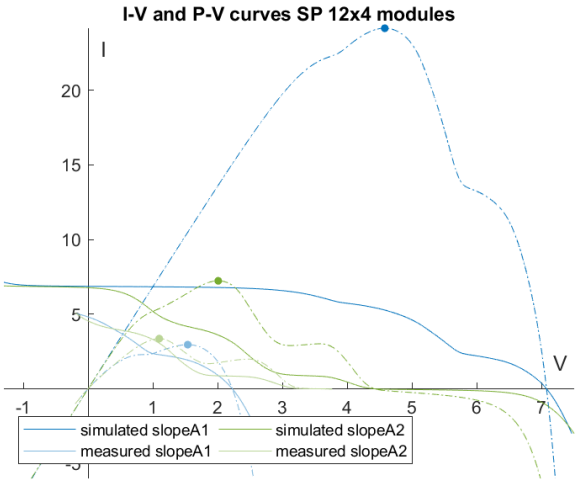


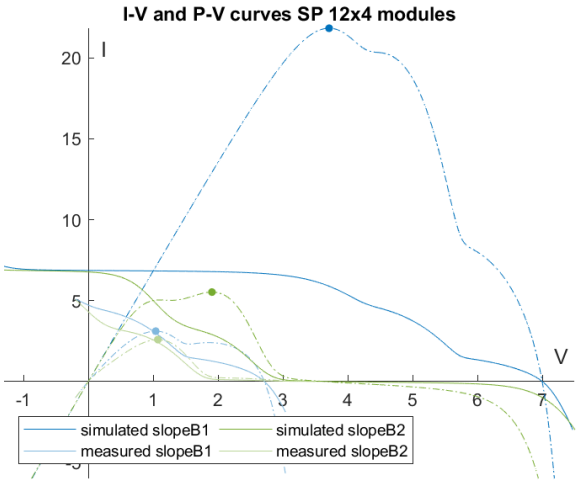

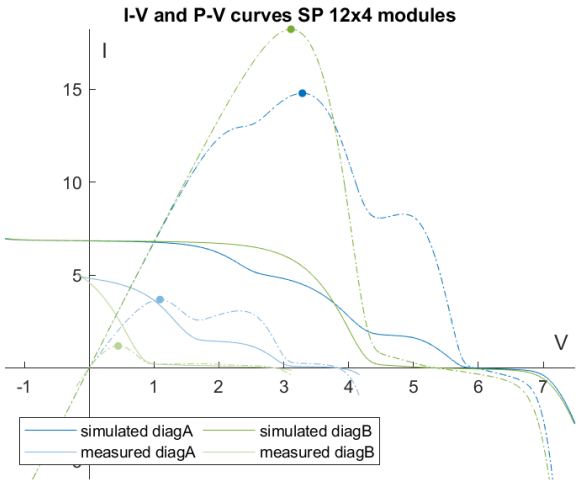
I-V and P-V curves SP 12x4 modules
I
V
simulated diagA
simulated diagB
measured diagA
measured diagB

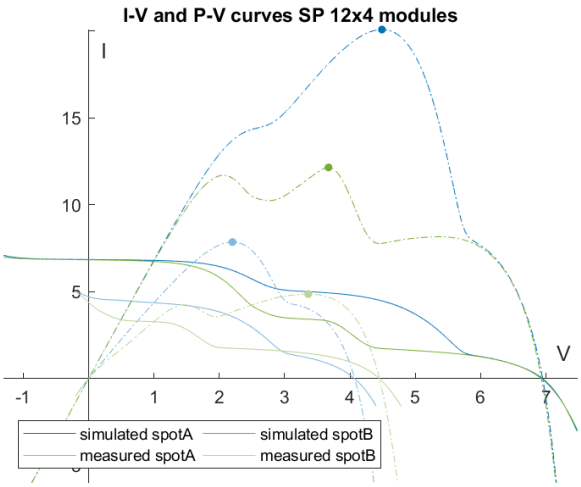
I-V and P-V curves SP 12x4 modules
I
V
simulated spotA
simulated spotB
measured spotA
measured spotB

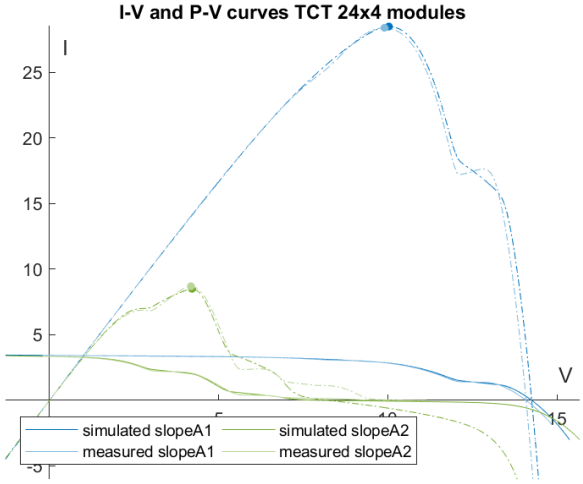
I-V and P-V curves TCT 24x4 modules
I
V
simulated slopeA1
simulated slopeA2
measured slopeA1
measured slopeA2

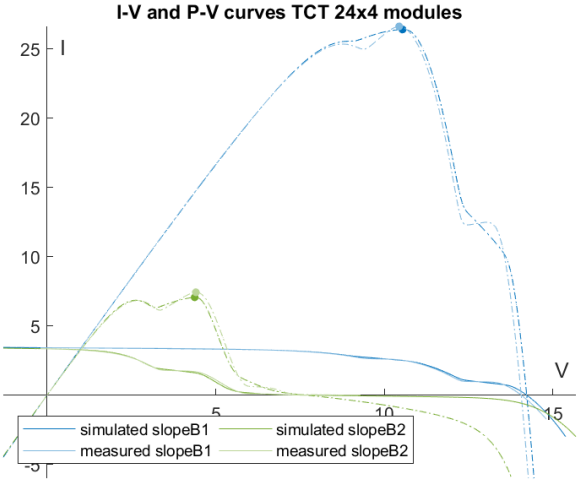
I-V and P-V curves TCT 24x4 modules
I
V
simulated slopeB1
simulated slopeB2
measured slopeB1
measured slopeB2

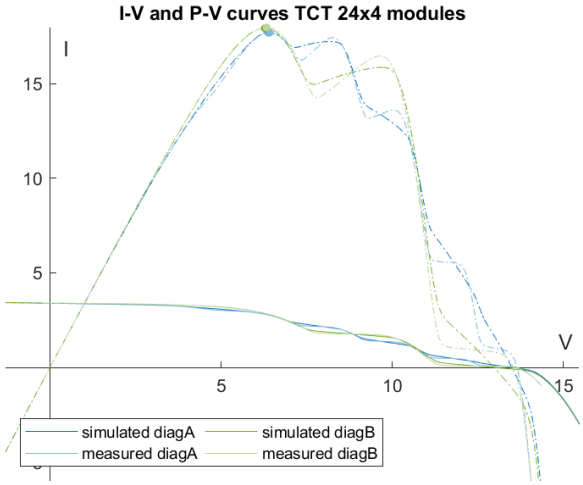
I-V and P-V curves TCT 24x4 modules
I
V
simulated diagA
simulated diagB
measured diagA
measured diagB

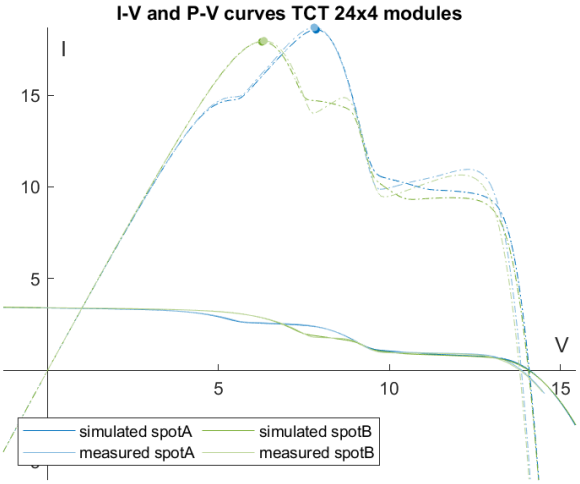
I-V and P-V curves TCT 24x4 modules
I
V
simulated spotA
simulated spotB
measured spotA
measured spotB

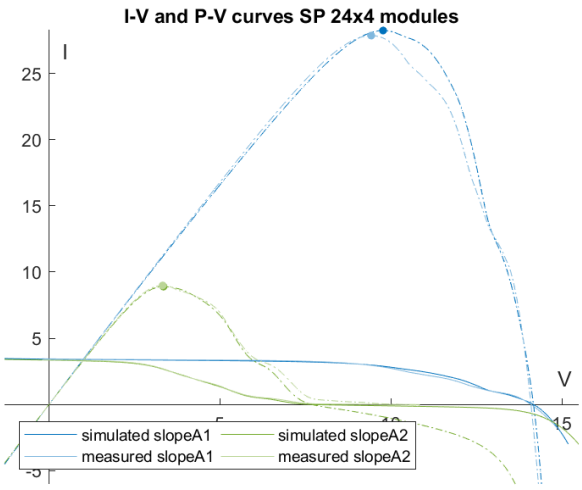
I-V and P-V curves SP 24x4 modules
I
V
simulated slopeA1
simulated slopeA2
measured slopeA1
measured slopeA2

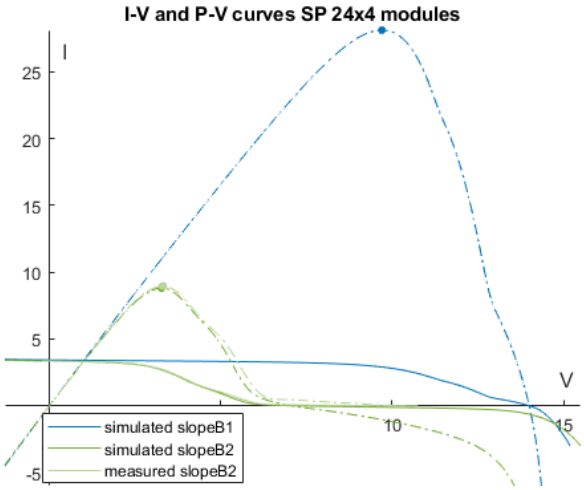
I-V and P-V curves SP 24x4 modules
I
V
simulated slopeB1
simulated slopeB2
measured slopeB2

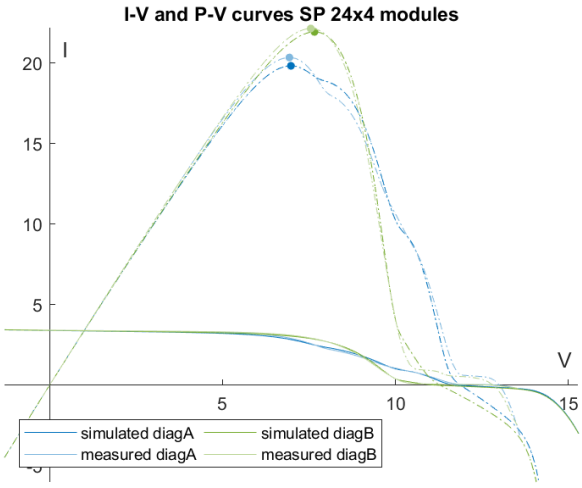
I-V and P-V curves SP 24x4 modules
I
V
simulated diagA
simulated diagB
measured diagA
measured diagB

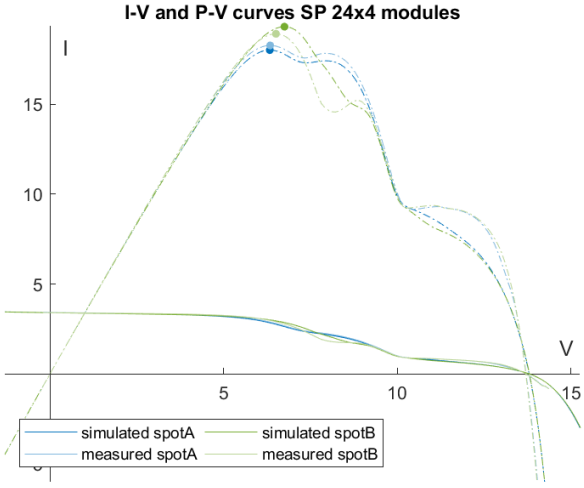
I-V and P-V curves SP 24x4 modules
I
V
simulated spotA
simulated spotB
measured spotA
measured spotB

| **TCT 12x4** | $P_{\mathrm{MPP}}$ | | | | $I_{\mathrm{sc}}$ | | | | $V_{\mathrm{oc}}$ | | | |
|---|---|---|---|---|---|---|---|---|---|---|---|---|
| | *measured* | *simulated* | *abs. error* | *rel. error* | *measured* | *simulated* | *abs. error* | *rel. error* | *measured* | *simulated* | *abs. error* | *rel. error* |
| noshade | 33.302 | 32.824 | 0.478 | 1.437 | 6.890 | 6.872 | 0.018 | 0.261 | 7.192 | 7.141 | 0.051 | 0.706 |
| hor3 | 16.278 | 17.451 | 1.172 | 3.521 | 6.795 | 6.829 | 0.033 | 0.483 | 6.352 | 5.355 | 0.997 | 13.870 |
| hor3.5 | 16.209 | 17.451 | 1.242 | 3.729 | 6.795 | 6.829 | 0.034 | 0.495 | 6.087 | 5.351 | 0.736 | 10.240 |
| hor6t | 8.539 | 9.875 | 1.336 | 4.012 | 6.708 | 6.781 | 0.073 | 1.060 | 4.216 | 3.570 | 0.646 | 8.983 |
| hor6b | 8.665 | 9.875 | 1.210 | 3.633 | 6.633 | 6.781 | 0.148 | 2.146 | 3.994 | 3.570 | 0.423 | 5.884 |
| vert2l | 15.974 | 15.600 | 0.375 | 1.125 | 3.474 | 3.436 | 0.038 | 0.553 | 6.904 | 6.956 | 0.052 | 0.717 |
| vert2r | 15.697 | 15.600 | 0.097 | 0.293 | 3.420 | 3.436 | 0.016 | 0.228 | 6.919 | 6.956 | 0.036 | 0.504 |
| vert2.5 | 11.801 | 11.444 | 0.357 | 1.072 | 2.642 | 2.576 | 0.066 | 0.960 | 6.781 | 6.897 | 0.116 | 1.612 |
| slopeA1 | 24.169 | 24.630 | 0.461 | 1.383 | 6.810 | 6.836 | 0.026 | 0.373 | 7.098 | 7.113 | 0.014 | 0.196 |
| slopeA2 | 7.464 | 7.908 | 0.444 | 1.334 | 6.140 | 6.559 | 0.419 | 6.081 | 5.184 | 4.670 | 0.514 | 7.146 |
| slopeB1 | 22.522 | 22.626 | 0.104 | 0.312 | 6.807 | 6.833 | 0.026 | 0.382 | 7.066 | 7.082 | 0.016 | 0.221 |
| slopeB2 | 6.380 | 6.529 | 0.150 | 0.450 | 6.045 | 6.544 | 0.499 | 7.242 | 4.924 | 4.106 | 0.818 | 11.376 |
| diagA | 13.850 | 13.898 | 0.047 | 0.142 | 6.506 | 6.645 | 0.140 | 2.029 | 6.965 | 7.056 | 0.091 | 1.267 |
| diagB | 18.449 | 18.154 | 0.296 | 0.888 | 6.533 | 6.626 | 0.093 | 1.345 | 6.998 | 7.052 | 0.055 | 0.760 |
| spotA | 21.083 | 20.805 | 0.278 | 0.835 | 6.805 | 6.792 | 0.013 | 0.192 | 7.067 | 7.043 | 0.024 | 0.334 |
| spotB | 11.702 | 11.560 | 0.142 | 0.427 | 6.767 | 6.786 | 0.019 | 0.277 | 6.888 | 7.008 | 0.120 | 1.675 |
| **Mean** | | | **0.512** | **1.537** | | | **0.104** | **1.507** | | | **0.294** | **4.093** |

| **SP 12x4** | $P_{\mathrm{MPP}}$ | | | | $I_{\mathrm{sc}}$ | | | | $V_{\mathrm{oc}}$ | | | |
|---|---|---|---|---|---|---|---|---|---|---|---|---|
| | *measured* | *simulated* | *abs. error* | *rel. error* | *measured* | *simulated* | *abs. error* | *rel. error* | *measured* | *simulated* | *abs. error* | *rel. error* |
| noshade | 30.209 | 33.125 | 2.916 | 9.652 | 6.742 | 6.872 | 0.131 | 1.937 | 7.143 | 7.142 | 0.001 | 0.009 |
| hor3 | 16.818 | 18.231 | 1.413 | 4.677 | 6.315 | 6.849 | 0.535 | 7.929 | 6.129 | 5.350 | 0.778 | 10.899 |
| hor3.5 | 16.786 | 18.231 | 1.445 | 4.784 | 6.308 | 6.849 | 0.541 | 8.023 | 6.014 | 5.347 | 0.667 | 9.333 |
| hor6t | 10.161 | 10.868 | 0.707 | 2.340 | 6.160 | 6.825 | 0.664 | 9.856 | 4.089 | 3.571 | 0.518 | 7.258 |
| hor6b | 10.312 | 10.868 | 0.555 | 1.838 | 6.659 | 6.825 | 0.166 | 2.467 | 3.817 | 3.571 | 0.246 | 3.439 |
| vert2l | 15.710 | 15.974 | 0.264 | 0.874 | 3.452 | 3.436 | 0.016 | 0.232 | 6.896 | 6.966 | 0.070 | 0.979 |
| vert2r | 12.929 | 15.974 | 3.045 | 10.080 | 3.286 | 3.436 | 0.150 | 2.227 | 6.894 | 6.966 | 0.072 | 1.008 |
| vert2.5 | 11.420 | 11.841 | 0.421 | 1.394 | 2.598 | 2.576 | 0.022 | 0.325 | 6.740 | 6.915 | 0.175 | 2.457 |
| slopeA1 | 2.955 | 24.142 | 21.187 | 70.136 | 4.782 | 6.862 | 2.080 | 30.847 | 2.219 | 7.079 | 4.860 | 68.039 |
| slopeA2 | 3.358 | 7.229 | 3.871 | 12.815 | 4.598 | 6.771 | 2.172 | 32.220 | 3.495 | 4.431 | 0.936 | 13.106 |
| slopeB1 | 3.107 | 21.840 | 18.733 | 62.012 | 4.751 | 6.862 | 2.111 | 31.306 | 2.680 | 6.994 | 4.314 | 60.397 |
| slopeB2 | 2.585 | 5.521 | 2.937 | 9.722 | 4.338 | 6.767 | 2.429 | 36.033 | 3.086 | 3.613 | 0.526 | 7.371 |
| diagA | 3.681 | 14.787 | 11.107 | 36.767 | 4.848 | 6.839 | 1.990 | 29.525 | 3.652 | 5.941 | 2.288 | 32.038 |
| diagB | 1.185 | 18.231 | 17.046 | 56.427 | 4.528 | 6.849 | 2.322 | 34.437 | 2.695 | 5.350 | 2.655 | 37.170 |
| spotA | 7.861 | 20.088 | 12.226 | 40.473 | 4.767 | 6.855 | 2.088 | 30.977 | 4.043 | 6.947 | 2.904 | 40.663 |
| spotB | 4.867 | 12.154 | 7.287 | 24.123 | 4.406 | 6.838 | 2.432 | 36.071 | 4.429 | 6.928 | 2.499 | 34.989 |
| **Mean** | | | **6.573** | **21.757** | | | **1.241** | **18.401** | | | **1.469** | **20.572** |

| **TCT 24x4** | $P_{\mathrm{MPP}}$ | | | | $I_{\mathrm{sc}}$ | | | | $V_{\mathrm{oc}}$ | | | |
|---|---|---|---|---|---|---|---|---|---|---|---|---|
| | *measured* | *simulated* | *abs. error* | *rel. error* | *measured* | *simulated* | *abs. error* | *rel. error* | *measured* | *simulated* | *abs. error* | *rel. error* |
| noshade | 32.750 | 32.584 | 0.167 | 0.509 | 3.445 | 3.436 | 0.009 | 0.252 | 14.212 | 14.282 | 0.070 | 0.494 |
| hor6 | 21.314 | 21.367 | 0.053 | 0.162 | 3.413 | 3.415 | 0.002 | 0.069 | 12.357 | 10.712 | 1.645 | 11.573 |
| hor6.5 | 17.832 | 17.782 | 0.050 | 0.153 | 3.407 | 3.406 | 0.001 | 0.038 | 12.167 | 10.708 | 1.459 | 10.267 |
| hor12t | 10.448 | 10.288 | 0.160 | 0.488 | 3.383 | 3.373 | 0.009 | 0.274 | 8.004 | 7.141 | 0.863 | 6.071 |
| hor12b | 9.435 | 10.288 | 0.853 | 2.606 | 3.380 | 3.373 | 0.007 | 0.210 | 8.658 | 7.141 | 1.517 | 10.672 |
| vert2l | 15.515 | 15.205 | 0.311 | 0.949 | 1.733 | 1.718 | 0.015 | 0.429 | 13.551 | 13.901 | 0.350 | 2.463 |
| vert2r | 15.254 | 15.205 | 0.049 | 0.151 | 1.725 | 1.718 | 0.007 | 0.195 | 13.493 | 13.901 | 0.408 | 2.871 |
| vert2.5 | 11.332 | 11.009 | 0.323 | 0.987 | 1.304 | 1.288 | 0.016 | 0.475 | 13.313 | 13.774 | 0.460 | 3.239 |
| slopeA1 | 28.387 | 28.487 | 0.100 | 0.305 | 3.424 | 3.426 | 0.002 | 0.061 | 14.079 | 14.253 | 0.174 | 1.223 |
| slopeA2 | 8.688 | 8.489 | 0.199 | 0.609 | 3.356 | 3.346 | 0.009 | 0.275 | 10.112 | 8.232 | 1.880 | 13.227 |
| slopeB1 | 26.639 | 26.415 | 0.224 | 0.684 | 3.424 | 3.425 | 0.001 | 0.025 | 14.046 | 14.221 | 0.175 | 1.232 |
| slopeB2 | 7.432 | 7.066 | 0.366 | 1.116 | 3.350 | 3.345 | 0.004 | 0.130 | 8.302 | 7.674 | 0.629 | 4.424 |
| diagA | 17.700 | 17.703 | 0.004 | 0.011 | 3.405 | 3.397 | 0.009 | 0.252 | 13.222 | 13.488 | 0.266 | 1.872 |
| diagB | 17.971 | 17.932 | 0.040 | 0.121 | 3.408 | 3.407 | 0.002 | 0.045 | 12.801 | 12.967 | 0.166 | 1.165 |
| spotA | 18.701 | 18.583 | 0.118 | 0.361 | 3.405 | 3.396 | 0.010 | 0.282 | 13.828 | 14.088 | 0.260 | 1.828 |
| spotB | 17.969 | 17.920 | 0.049 | 0.149 | 3.409 | 3.407 | 0.002 | 0.059 | 13.776 | 14.063 | 0.287 | 2.016 |
| **Mean** | | | **0.192** | **0.585** | | | **0.007** | **0.192** | | | **0.663** | **4.665** |

| **SP 24x4** | $P_{\mathrm{MPP}}$ | | | | $I_{\mathrm{sc}}$ | | | | $V_{\mathrm{oc}}$ | | | |
|---|---|---|---|---|---|---|---|---|---|---|---|---|
| | *measured* | *simulated* | *abs. error* | *rel. error* | *measured* | *simulated* | *abs. error* | *rel. error* | *measured* | *simulated* | *abs. error* | *rel. error* |
| noshade | 32.437 | 32.643 | 0.206 | 0.635 | 3.462 | 3.436 | 0.026 | 0.762 | 14.189 | 14.282 | 0.093 | 0.653 |
| hor6 | 22.034 | 21.924 | 0.110 | 0.338 | 3.418 | 3.411 | 0.007 | 0.200 | 11.478 | 10.711 | 0.766 | 5.400 |
| hor6.5 | 18.394 | 18.511 | 0.117 | 0.361 | 3.402 | 3.400 | 0.002 | 0.059 | 11.436 | 10.707 | 0.729 | 5.138 |
| hor12t | 11.568 | 11.296 | 0.271 | 0.836 | 3.365 | 3.363 | 0.003 | 0.082 | 7.942 | 7.141 | 0.801 | 5.645 |
| hor12b | 10.362 | 11.296 | 0.934 | 2.880 | 3.434 | 3.363 | 0.071 | 2.050 | 8.084 | 7.141 | 0.943 | 6.646 |
| vert2l | 15.094 | 14.867 | 0.227 | 0.700 | 1.727 | 1.718 | 0.009 | 0.261 | 13.525 | 13.907 | 0.382 | 2.696 |
| vert2r | 15.316 | 14.867 | 0.449 | 1.384 | 1.734 | 1.718 | 0.016 | 0.473 | 13.380 | 13.907 | 0.527 | 3.713 |
| vert2.5 | 11.134 | 10.565 | 0.569 | 1.754 | 1.308 | 1.288 | 0.020 | 0.579 | 13.249 | 13.762 | 0.514 | 3.619 |
| slopeA1 | 27.858 | 28.238 | 0.380 | 1.171 | 3.448 | 3.429 | 0.019 | 0.558 | 14.078 | 14.168 | 0.090 | 0.638 |
| slopeA2 | 8.991 | 8.906 | 0.085 | 0.261 | 3.361 | 3.349 | 0.013 | 0.369 | 9.684 | 7.691 | 1.993 | 14.047 |
| slopeB1 | - | 28.112 | - | - | - | 3.429 | - | - | - | 14.000 | - | - |
| slopeB2 | 8.944 | 8.801 | 0.144 | 0.442 | 3.356 | 3.348 | 0.008 | 0.233 | 9.552 | 7.044 | 2.509 | 17.679 |
| diagA | 20.349 | 19.831 | 0.518 | 1.597 | 3.423 | 3.406 | 0.017 | 0.495 | 12.701 | 11.889 | 0.811 | 5.719 |
| diagB | 22.148 | 21.939 | 0.208 | 0.642 | 3.425 | 3.411 | 0.015 | 0.421 | 12.341 | 11.303 | 1.038 | 7.318 |
| spotA | 18.279 | 18.022 | 0.257 | 0.793 | 3.423 | 3.410 | 0.013 | 0.365 | 13.634 | 13.802 | 0.168 | 1.187 |
| spotB | 18.927 | 19.323 | 0.396 | 1.220 | 3.412 | 3.409 | 0.003 | 0.096 | 13.645 | 13.808 | 0.163 | 1.148 |
| **Mean** | | | **0.325** | **1.001** | | | **0.016** | **0.467** | | | **0.769** | **5.416** |

# VI Effect of bypass diodes: results

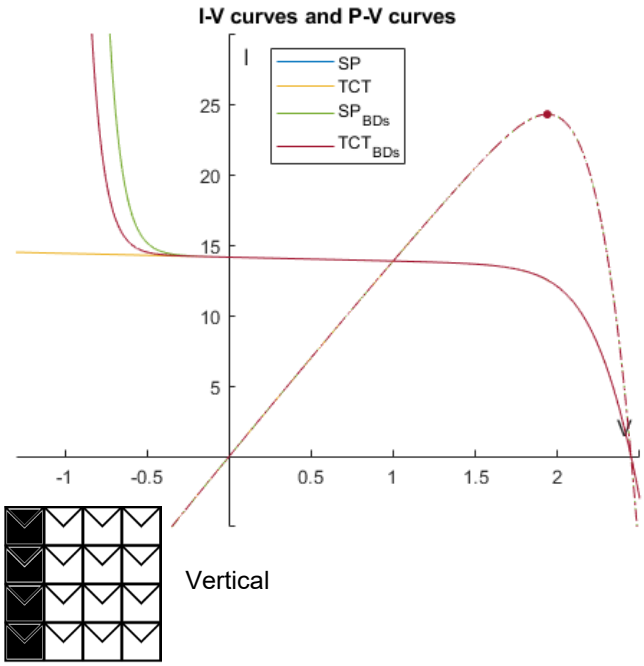


Vertical

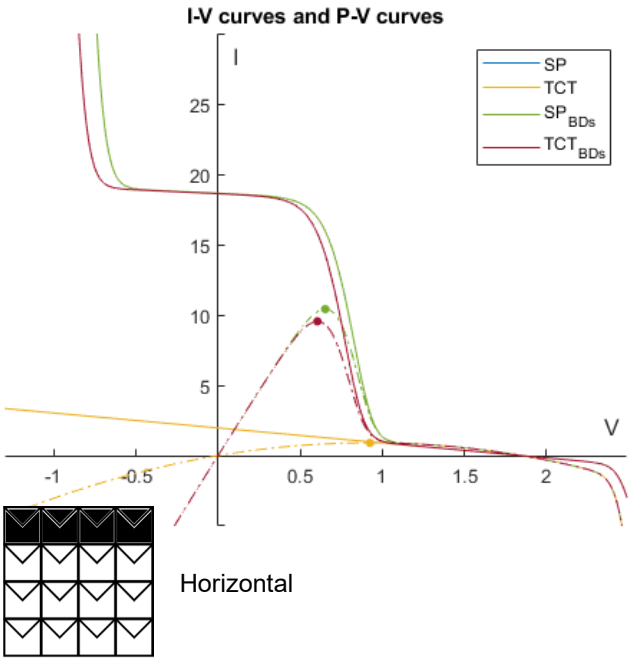


Horizontal

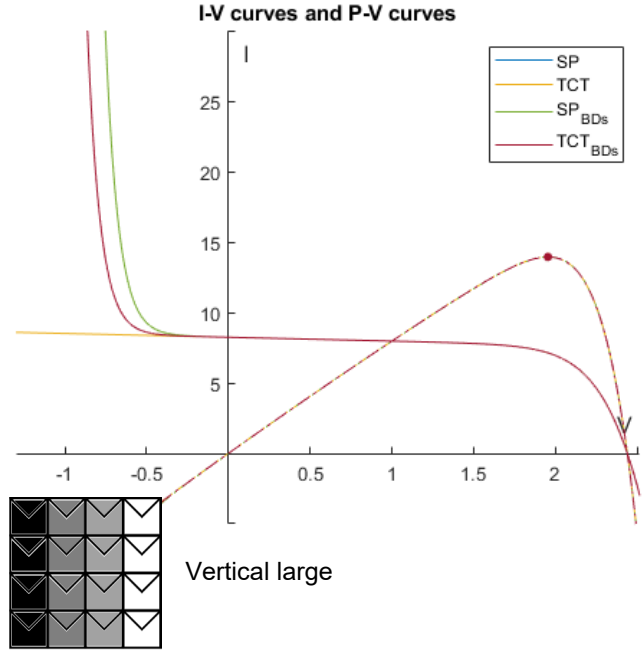


Vertical large

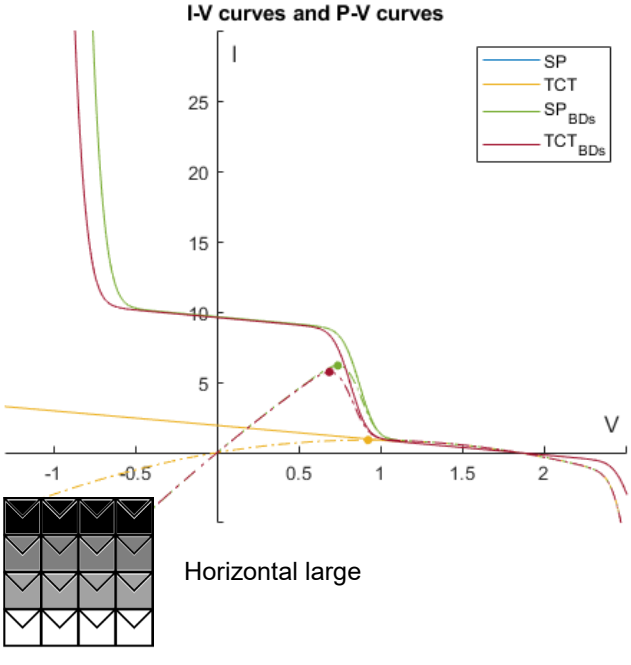


Horizontal large

= 1000 W/m²

= 250 W/m²

= 750 W/m²

= 0 W/m²

= 500 W/m²

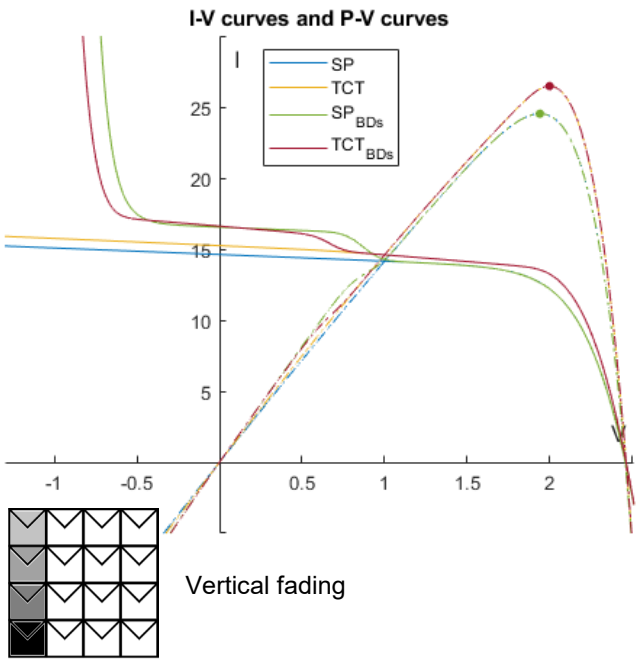




Vertical fading

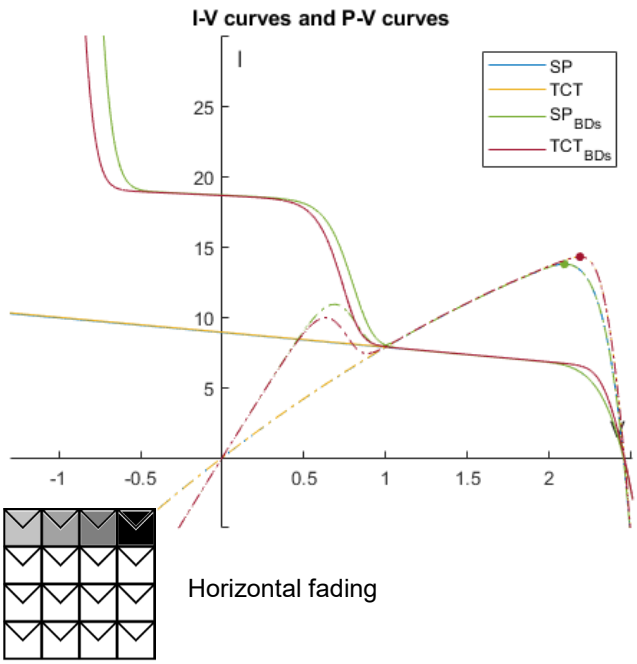




Horizontal fading

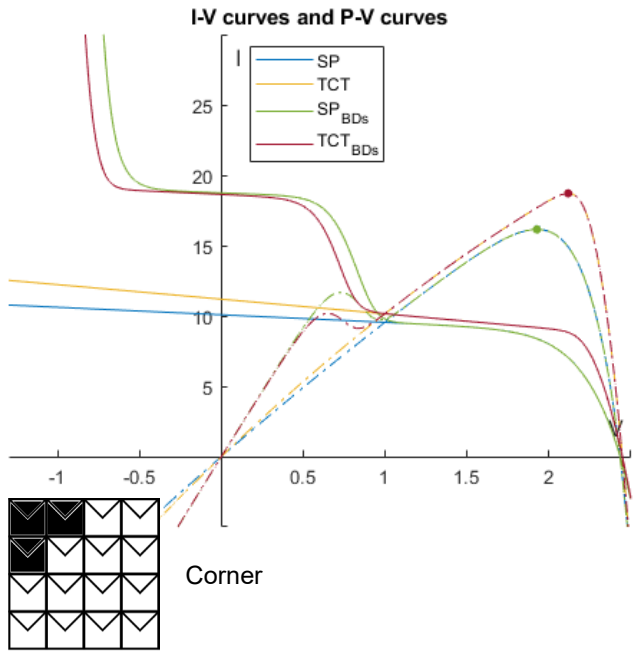




Corner

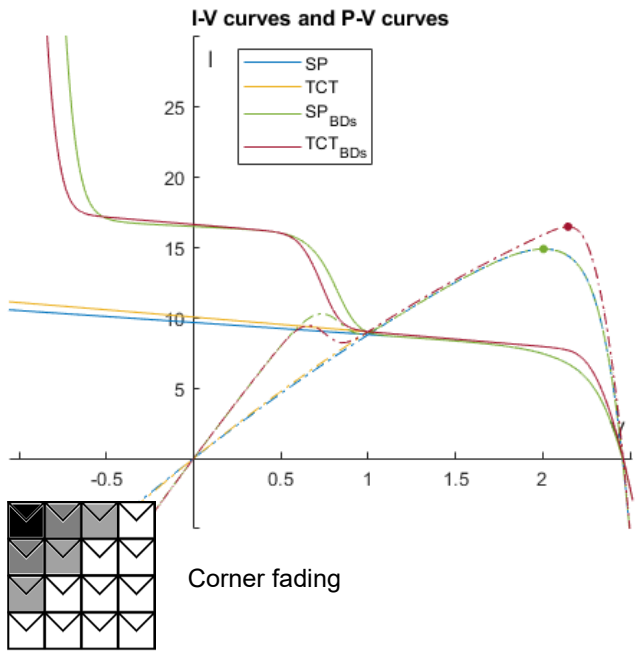




Corner fading

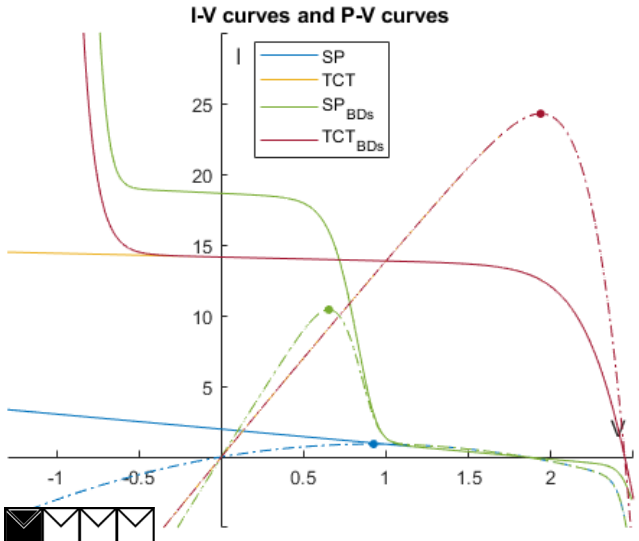


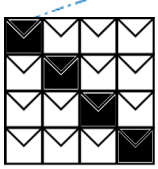

Diagonal

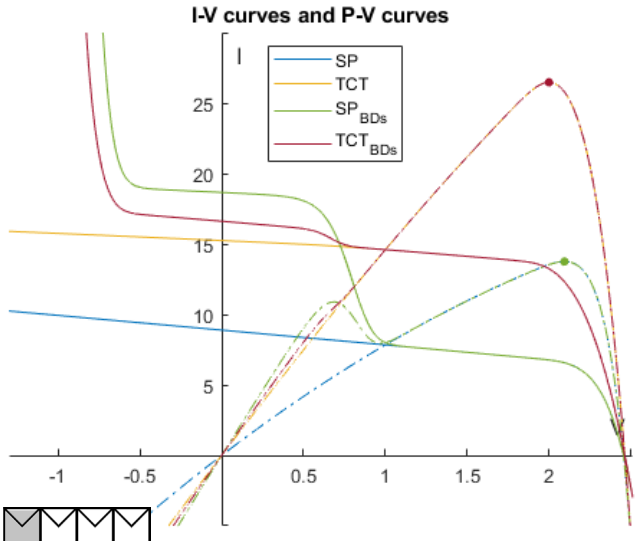


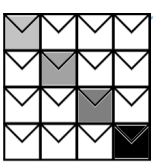

Diagonal fading

# VII More patterns

**Diag**

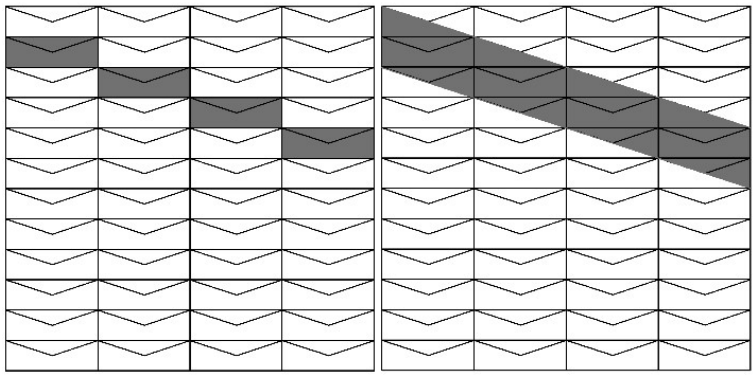

1a, 1b

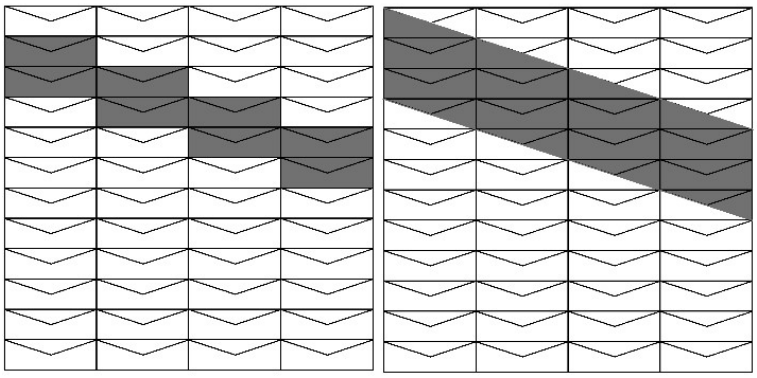

2a, 2b

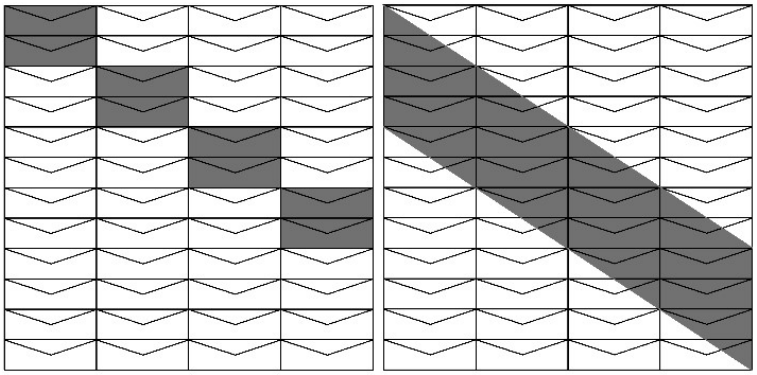

3a, 3b

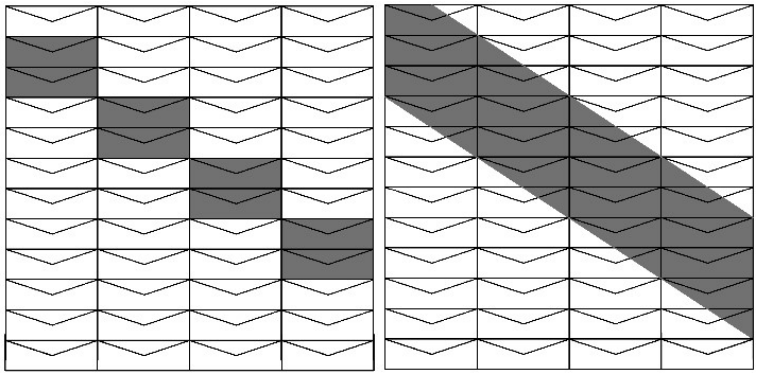

4a, 4b

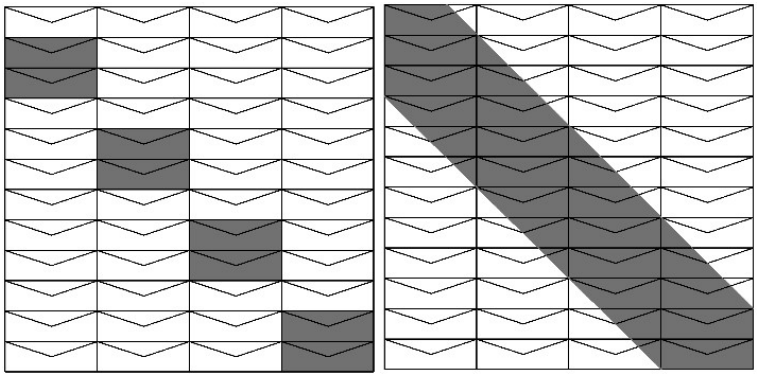

5a, 5b

**Spot**

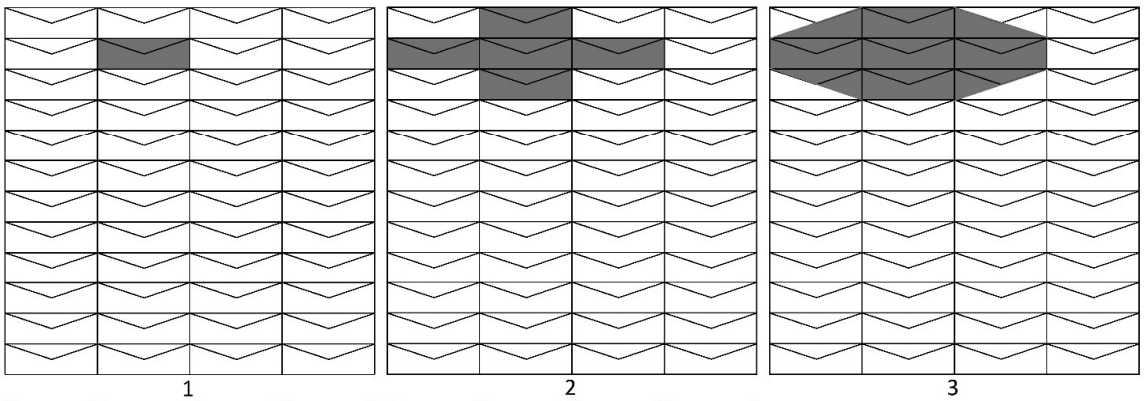

1 2 3

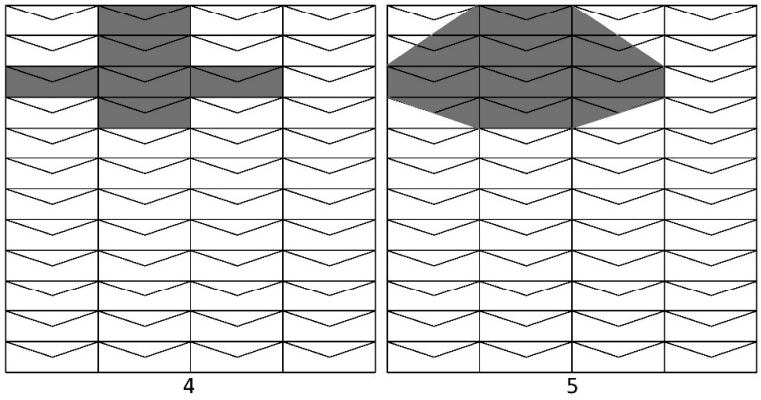

4 5

**Corner**